



Universitätsklinikum
Hamburg-Eppendorf



Fachbereich Biologie

Universität Hamburg

DER FORSCHUNG | DER LEHRE | DER BILDUNG



Calcium microdomains during T lymphocyte activation – role of second messengers and calcium channels

Dissertation

Zur Erlangung der Würde des Doktors der Naturwissenschaften des Fachbereichs
Biologie der Fakultät für Mathematik, Informatik und Naturwissenschaften der
Universität Hamburg

vorgelegt von

Björn-Philipp Diercks

Hamburg, 2016

Folgende Gutachter empfehlen die Annahme der Dissertation:

Prof. Dr. rer. nat. Dr. med. habil. Andreas H. Guse

Prof. Dr. rer. nat. Arp Schnittger

Datum der Disputation: 13.01.2017

Contents

| | |
|--|-------------|
| Contents | II |
| Abbreviations | IV |
| Abstract | VI |
| Zusammenfassung | VIII |
| 1 Introduction | 1 |
| 1.1 Role of T lymphocytes in the immune system | 1 |
| 1.1.1 Activation of T lymphocytes..... | 1 |
| 1.2 Calcium - an universal messenger in signal transduction | 3 |
| 1.2.1 Release of Ca ²⁺ from intracellular Ca ²⁺ stores | 4 |
| 1.2.2 Ca ²⁺ entry from extracellular space..... | 6 |
| 1.2.2.1 CRAC and SOCE in T lymphocyte activation..... | 8 |
| 1.3 Nicotinic acid adenine dinucleotide phosphate (NAADP)..... | 9 |
| 1.3.1 Metabolism of NAADP | 11 |
| 1.3.2 Proposed target receptors of NAADP | 11 |
| 1.3.2.1 Ryanodine receptors (RyRs) | 12 |
| 1.3.2.2 Two pore channels (TPCs)..... | 14 |
| 1.3.2.3 Transient receptor potential channel, subfamily melastatin, member 2 (TRPM2) | 16 |
| 1.3.2.4 Transient receptor potential channel, subfamily mucolipin, member 1 (TRP- ML1) | 18 |
| 1.4 Imaging subcellular Ca ²⁺ signals..... | 19 |
| 1.4.1 Classification of different subcellular Ca ²⁺ signals..... | 21 |
| 1.5 Study objective | 22 |
| 2 Publications | 23 |
| 2.1 Publication I | 23 |
| 2.1.1 Contribution to publication I..... | 24 |
| 2.2 Publication II | 25 |
| 2.2.1 Contribution to publication II | 26 |
| 3 Discussion | 27 |
| 3.1 Establishing a method to detect subcellular, initial Ca ²⁺ release events in T lymphocytes | 27 |
| 3.1.1 Single-wavelength Ca ²⁺ indicators..... | 28 |
| 3.1.2 Dual wavelength dyes | 29 |
| 3.1.3 Combining Fluo-4 and Fura Red for subcellular Ca ²⁺ imaging..... | 30 |

| | | |
|---------|--|-----------|
| 3.1.4 | Activation of T lymphocytes <i>in vitro</i> | 33 |
| 3.1.5 | Discrimination between signal and noise..... | 35 |
| 3.2 | Automation of the post-processing workflow | 36 |
| 3.2.1 | Comparison of different deconvolution algorithms | 38 |
| 3.2.2 | Evaluation of bleaching correction strategies | 40 |
| 3.3 | Analyzing the fundamental Ca ²⁺ network during T lymphocyte activation..... | 43 |
| 3.3.1 | Initial Ca ²⁺ microdomains in T lymphocytes | 43 |
| 3.3.1.1 | Initial bi-phasic Ca ²⁺ response in T lymphocytes | 45 |
| 3.3.1.2 | Comparison of initial Ca ²⁺ microdomains in T lymphocytes to previously described Ca ²⁺ sparks and quarks | 48 |
| 3.3.2 | Using knockouts to decode the fundamental Ca ²⁺ network T lymphocytes | 49 |
| 3.3.2.1 | Involvement of RyRs in the formation of initial Ca ²⁺ signals in T lymphocytes | 50 |
| 3.3.2.2 | TRPM2 is not linked to the formation of initial Ca ²⁺ signals in primary T lymphocytes | 52 |
| 3.3.3 | NAADP and initial, localized Ca ²⁺ signals | 52 |
| 3.3.4 | Strengths and limitations of the presented method | 55 |
| 3.3.5 | Working model and open questions..... | 56 |
| | References | 60 |
| | Figure Index..... | 85 |
| | Publications, awards, talks and poster presentations | 86 |
| | Eidesstattliche Versicherung..... | 89 |
| | Acknowledgment | 90 |

Abbreviations

| | |
|---------------|---|
| ADPR | adenosine diphosphoribose |
| AM | acetoxymethyl ester |
| AMP | adenosine monophosphate |
| ACR-1 | Asante Calcium Red-1 |
| ATP | adenosine triphosphate |
| $[Ca^{2+}]_i$ | free cytoplasmic calcium concentration |
| cADPR | cyclic adenosine diphosphoribose |
| CAM | calmodulin |
| cAMP | cyclic adenosine monophosphate |
| CCD | charge-coupled device |
| CD | cluster of differentiation |
| CDI | Ca^{2+} -dependent inactivation |
| CFP | cyan fluorescent protein |
| CICR | calcium induced calcium release |
| CRAC | calcium release activated channels |
| cSMAC | central supramolecular activation cluster |
| CTL | $CD8^+$ cytotoxic T lymphocyte |
| DAG | diacylglycerol |
| DMSO | dimethyl sulfoxide |
| dSMAC | distal supramolecular activation cluster |
| Epac1 | exchange protein activated by cAMP 1 |
| ER | endoplasmic reticulum |
| FITC | fluorescein isothiocyanate |
| FRET | fluorescence resonance energy transfer |
| FWHM | full width at half maximum |
| ICAM-1 | intercellular adhesion molecule-1 |
| ITAMs | immuno-receptor tyrosine-based activation motifs |
| IP_3 | <i>D-myo</i> -inositol-1,4,5-trisphosphate |
| IP_3R | <i>D-myo</i> -inositol-1,4,5-trisphosphate receptor |
| kDa | kilodalton |
| KO | knockout |
| Lat | linker of activated T cells |

| | |
|--------|--|
| Lck | lymphocyte-specific protein tyrosine kinase |
| LPC2 | lymphocyte cytosolic protein 2 |
| LR | Lucy-Richardson deconvolution |
| mAb | monoclonal antibody |
| MHC | major histocompatibility complex |
| NAAD | nicotinic acid adenine dinucleotide |
| NAADP | nicotinic acid adenine dinucleotide 2'-phosphate |
| NAD | nicotinamid adenine dinucleotide |
| NADP | nicotinamid adenine dinucleotide 2'-phosphate |
| NCX | Na ⁺ /Ca ²⁺ exchanger |
| Orai1 | Calcium release-activated calcium channel protein 1 |
| OVA | ovalbumin |
| PBS | phosphate – buffered salt solution |
| PMCA | plasma membrane Ca ²⁺ ATPase |
| PSF | point-spread-function |
| pSMAC | peripheral supramolecular activation cluster |
| RT | room temperature |
| RyR | ryanodine receptors |
| SEM | standard error of mean |
| SERCA | sarcoplasmic/endoplasmic reticulum Ca ²⁺ -ATPase |
| SLP-76 | lymphocyte cytosolic protein 2 |
| SNR | signal-to-noise ratio |
| SOAR | STIM-Orai activating region |
| SOCE | store-operated Ca ²⁺ entry |
| STIM | stromal interaction molecule |
| TCR | T cell receptor |
| TIRF | total internal reflection fluorescence |
| TPC | two pore channel |
| TRP | transient receptor potential channels |
| TRPM | melastatin subfamily of TRP channels |
| TRPM2 | transient receptor potential channel, subfamily melastatin, member 2 |
| TRP-ML | mucolipin subfamily of TRP channels |
| WNR | Wiener deconvolution |
| WT | wildtype |
| YFP | yellow fluorescent protein |

Abstract

Activation of T lymphocytes is the fundamental on-switch of the adaptive immune system. Calcium (Ca^{2+}) signaling is essential for T lymphocyte activation and is supposed to start by initial, localized Ca^{2+} microdomains. However, in contrast to excitable cells, in T lymphocytes such initial Ca^{2+} microdomains have not yet been characterized.

In this thesis, a new high resolution imaging method that allows for the first time to characterize initial Ca^{2+} microdomains in Jurkat T lymphocytes as well as primary murine T lymphocytes, was developed (2.2; Wolf et al., 2015). A combination of two Ca^{2+} sensitive dyes (Fluo-4 and Fura Red) enables the fast acquisition (approx. 40 frames/sec) of Ca^{2+} microdomains despite cellular movement and changes in cell shape. Further, the Ca^{2+} signaling method is technically limited by an amplitude differences as low as 18 nM (Jurkat T lymphocytes) or 32 nM (primary T lymphocytes) at a calculated spatial resolution of ~ 368 nm. Using antibody-coated beads, with the size of T lymphocytes, a cell-cell interaction could be mimicked and thus a directed activation of T lymphocytes was obtained. Directly after contact with an antibody-coated bead, Ca^{2+} microdomains were observed at the site of stimulation in Jurkat and primary wildtype (WT) T lymphocytes. Interestingly, the initial Ca^{2+} signals showed a bi-phasic pattern. In contrast, in ryanodine receptor (RyR) knockdown Jurkat and primary RyR1-knockout (KO) T lymphocytes the number of Ca^{2+} microdomains was significantly reduced and moreover, no bi-phasic pattern was detected.

Since in primary and Jurkat lymphocytes, initial Ca^{2+} microdomains were observed very close to the plasma membrane, an early Ca^{2+} entry component was considered to be involved. Since transient receptor potential channel, subfamily melastatin, member 2 (TRPM2) is a candidate channel for Ca^{2+} entry, primary murine TRPM2-KO T lymphocytes were analyzed. However, there was no significant difference in the number of Ca^{2+} microdomains per cell and Ca^{2+} amplitude compared to the primary murine WT T lymphocytes. Thus, TRPM2 seems not to be involved in the formation of initial Ca^{2+} microdomains in primary T cells.

To analyze the direct influence of NAADP on the initial localized Ca^{2+} signals, NAADP was directly microinjected in Jurkat T lymphocytes. In Jurkat T lymphocytes, initial Ca^{2+} signals after microinjection of NAADP were already observed after 20 msec fol-

lowing a global activation of the cell. In RyR-knockdown Jurkat T lymphocytes neither initial Ca^{2+} signals nor a global activation was observed. Thus, already the initial, very fast Ca^{2+} signals were depend on functional RyRs, suggesting that the RyRs are directly targeted by NAADP.

Furthermore, the well established but time-consuming analysis workflow was automated and implemented in MATLAB (MathWorks), resulting in a up to 24 times faster post processing time (2.1; Schetelig et al., 2015). During this process different deconvolution algorithms were compared and the bleach-correction of Fura Red was additionally optimized.

Taken together, the high resolution imaging method described here allowed for the first time to characterize initial Ca^{2+} microdomains in T lymphocytes and to obtain evidence for important roles of RyRs in such signals.

Zusammenfassung

Calcium (Ca^{2+}) ist essentiell für die Aktivierung von T-Lymphozyten und somit für die Mobilisierung des adaptiven Immunsystems. Es wird vermutet, dass globale Ca^{2+} Signale aus initialen, lokalen Ca^{2+} Mikrodomänen entstehen. Bisher konnten solche initialen, lokalen Ca^{2+} Mikrodomänen aber nur in erregbaren Zellen charakterisiert werden nicht aber in T-Lymphozyten.

In der vorliegenden Doktorarbeit, wurde eine hochauflösende Ca^{2+} Life-Cell-Imaging Methode entwickelt, mit der es zum ersten Mal möglich war initiale Ca^{2+} Mikrodomänen in Jurkat T-Lymphozyten und primären Maus T-Lymphozyten zu charakterisieren (2.2; Wolf et al., 2015). Eine Kombination aus zwei Ca^{2+} sensitiven Farbstoffen (Fluo-4 und Fura Red) ermöglichte die Aufnahme von ca. 40 Bildern/sec, und dies obwohl sich die T-Lymphozyten bewegten und ihre Zell-Form veränderten. Mit der neuen Ca^{2+} Life-Cell-Imaging Methode war es möglich noch Differenzen in der Ca^{2+} Amplitude von bis zu 18 nM bei Jurkat und 32 nM bei primäre T-Lymphozyten zu unterscheiden und dies bei einem berechneten Auflösungsvermögen von ~ 368 nm. Um die T-Lymphozyten gerichtet zu aktivieren und somit eine Zell-Zell-Interaktion zu imitieren, wurden Beads, welche die Größe von Jurkat T-Lymphozyten besitzen, mit aktivierenden Antikörpern beschichtet. Direkt nach dem Kontakt mit solchen Antikörper-beschichteten Beads, konnten sowohl in Jurkat als auch in primären Wild Typ (WT) T-Lymphozyten Ca^{2+} Mikrodomänen, direkt an der Kontaktstelle, detektiert werden. Interessanterweise, konnte hierbei ein bi-phasisches Ca^{2+} Signal beobachtet werden. Sowohl in Ryanodine Rezeptor (RyR) knockdown Jurkat und primären RyR1-KO T-Lymphozyten war dagegen die Anzahl der Ca^{2+} Mikrodomänen war signifikant reduziert und darüber hinaus konnte kein bi-phasisches Ca^{2+} Signal detektiert werden.

Da sowohl in den primären als auch in den Jurkat T-Lymphozyten die initialen Ca^{2+} Signale direkt an der Plasmamembran detektiert wurden, wurde vermutet, dass ein früher Ca^{2+} Einstrom an der Entstehung der Ca^{2+} Mikrodomänen beteiligt sein könnte. Daher wurde zusätzlich Transient Rezeptor Potential Kanal, Subfamilie M, Subtyp 2 (TRPM2) als ein möglicher Ca^{2+} Einstrom-Kanal in der Plasmamembran untersucht. Es konnte aber kein signifikanter Unterschied in der Anzahl der Ca^{2+} Mikrodomänen und der Ca^{2+} Amplitude zwischen TRPM2-KO und WT T-Lymphozyten detektiert werden.

TRPM2 scheint daher nicht an der Entstehung der initialen Ca^{2+} Mikrodomänen in T-Lymphozyten beteiligt zu sein.

Um den direkten Einfluss von NAADP auf die Entstehung der initialen Ca^{2+} Signale zu untersuchen, wurde NAADP direkt in Jurkat T-Lymphozyten mikroinjiziert. In Jurkat T-Lymphozyten konnten bereits nach 20 msec initiale Ca^{2+} Signale detektiert werden, welche nachfolgend zu einer globalen Aktivierung der Zelle führten. In RyR knock-down Jurkat T-Lymphozyten konnten weder initiale Ca^{2+} Signale noch eine globale Aktivierung der Zelle detektiert werden. Somit sind bereits die initialen Ca^{2+} Mikrodomänen abhängig von funktionalen RyR und NAADP scheint direkt auf die RyR zu wirken.

Zusätzlich wurde der etablierte, aber zeitlich gesehen sehr aufwendige, Analyse-Workflow automatisiert und in MATLAB implementiert (MathWorks), wodurch die Nachbearbeitungs-Zeit um das bis zu 24 fache beschleunigt werden konnte (2.1; Schetelig et al., 2015). Außerdem wurden noch verschiedene Dekonvolutions-Algorithmen miteinander verglichen und die Bleichkorrektur von Fura Red optimiert.

Zusammenfassend konnte mit der neu etablierten hochauflösenden Ca^{2+} Life-Cell-Imaging Methode zum ersten Male initiale Ca^{2+} Mikrodomänen in T-Lymphozyten charakterisiert werden und zusätzlich wurde der Einfluss der RyRs auf die Entstehung solcher Ca^{2+} Signale verdeutlicht.

1 Introduction

1.1 Role of T lymphocytes in the immune system

Every multicellular organism has to fight pathogens such as bacteria, viruses and unicellular and multicellular parasites as well as malignantly transformed cells. Therefore, during evolution the immune system was established, which is a complex network from a variety of effector cells and biomolecules (Kenneth Murphy, 2011).

The mammalian immune system can be differentiated in two main sections, the innate immunity, and the specific, adaptive immunity. T lymphocytes, together with B lymphocytes, form the adaptive immune response. There are two main subpopulations of T lymphocytes, the $CD8^+$ cytotoxic T lymphocytes (CTLs) and the $CD4^+$ T-helper-lymphocytes (T_h lymphocytes). CTLs kill infected and transformed cells. In contrast, T_h lymphocytes activate macrophages and B lymphocytes. $CD4^+$ T lymphocytes can be further subdivided by their cytokine profile and transcription factors into T_{h1} , T_{h2} , T_{h17} , T_{h9} lymphocytes and regulatory T lymphocytes (T_{regs}) (Broere et al., 2011; Kenneth Murphy, 2011). T_{regs} , opposed to all other T lymphocytes, exhibit immunosuppressive functions (reviewed in Safinia et al., 2015).

1.1.1 Activation of T lymphocytes

The activation of T lymphocytes is tightly coordinated in a temporal and spatial fashion and in the end leads to clonal expansion (reviewed in Feske, 2007; Samelson, 2002). The functional T cell receptor-complex is made up of a highly variable, antigen-binding T cell receptor (TCR) $\alpha:\beta$ heterodimer with four invariant signaling chains collectively called CD3 (Call et al., 2002; Exley et al., 1991). Every TCR recognizes one specific antigenic peptide bound to major histocompatibility complexes (MHC) presented on the surface of antigen-presenting cells (APCs). Signaling from the TCR is initiated, after TCR-MHC ligation (**Fig. 1**). Then Ca^{2+} releasing second messengers, e.g. D-myoinositol-1,4,5-trisphosphate (IP_3), cyclic ADP-ribose (cADPR) and nicotinic acid adenine dinucleotide phosphate (NAADP), are formed (Ernst et al., 2013). NAADP triggers

the initial release of Ca^{2+} that is amplified by cADPR and/or IP_3 through calcium induced calcium release (CICR; Ernst et al., 2013; Gasser et al., 2006; Guse et al., 2013). The CICR is mediated by ryanodine receptors (RyR) and IP_3 -receptors (IP_3R) on the endoplasmic reticulum (ER) membrane (Endo, 2009) subsequently leading to store-operated Ca^{2+} entry (SOCE) and a sustained global Ca^{2+} signal (Kummerow et al., 2009; Soboloff et al., 2012). These elevated Ca^{2+} concentrations induce proliferation and differentiation of the T lymphocytes via transcription factors like NFAT (nuclear factor of activated T cells), NF- κB (nuclear factor- κB) and CREB (cyclic-AMP- responsive-element-binding protein) (Fig. 1; Feske, 2007).

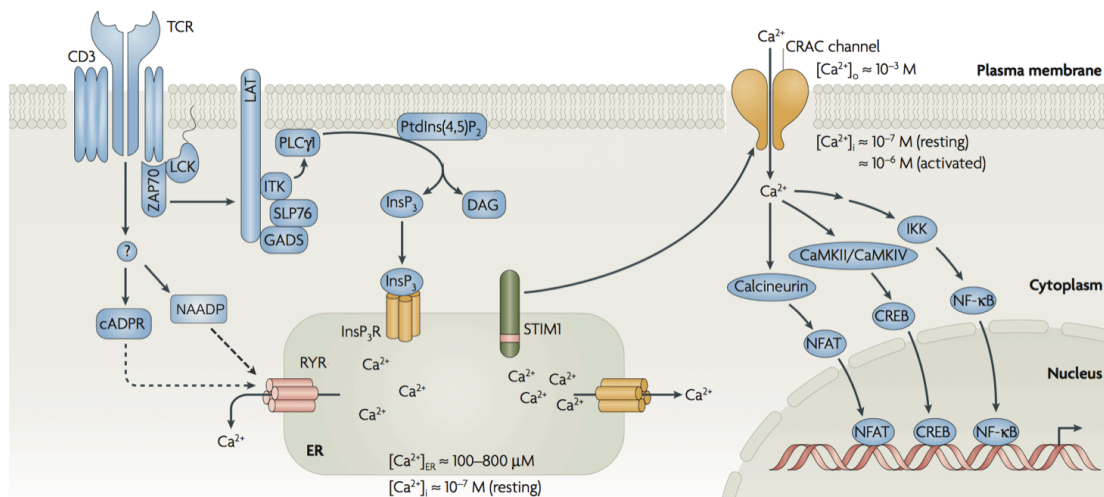


Fig. 1 Simplified model of the intracellular signaling pathways initiated after T lymphocyte activation through the TCR

After antigen recognition through the TCR complex protein tyrosine kinases, such as LCK and ZAP70 (ζ -chain-associated protein kinase of 70 kDa) are activated. This initiates the phosphorylation of adaptor proteins, like SLP76 (SRC-homology-2-domain-containing leukocyte protein of 76 kDa) and LAT (linker of activation of T cells). Next TEC kinase ITK (interleukin-2-inducible T-cell kinase) and phospholipase $\text{C}\gamma 1$ ($\text{PLC}\gamma 1$) are activated and recruited to the plasma membrane. The membrane phospholipid phosphatidylinositol-4,5-bisphosphate ($\text{PtdIns}(4,5)\text{P}_2$) is then selectively cleaved by $\text{PLC}\gamma 1$ resulting in two end products, inositol-1,4,5-trisphosphate (IP_3) and diacylglycerol (DAG). IP_3 as well as cyclic ADP-ribose (cADPR) and nicotinic acid adenine dinucleotide phosphate (NAADP) trigger the release of Ca^{2+} from intracellular stores resulting in an increased cytosolic Ca^{2+} concentration. Upon Ca^{2+} release from ER the stromal interaction molecule 1 (STIM1) is stimulated and translocates to the plasma membrane where in turn calcium-release-activated calcium (CRAC) channels are activated. Through the open CRAC channels Ca^{2+} can enter the cytosol, leading to a further and sustained elevation of the intracellular Ca^{2+} concentration and thus activating Ca^{2+} -dependent enzymes, like calcineurin. This in the end induces the translocation of transcription factors, like NFAT (nuclear factor of activated T cells), NF- κB (nuclear factor- κB) and CREB (cyclic-AMP- responsive-element-binding protein) to the nucleus. IP_3 receptors (IP_3Rs); CaMK (calmodulin-dependent kinase); GADS (growth-factor-receptor-bound-protein-2-related adaptor protein); IKK (inhibitor of NF- κB kinase); RyR (ryanodine receptor) (modified from Feske, 2007).

Signaling through the TCR complex alone is not sufficient to activate naïve T lymphocytes. APCs that can activate naïve T lymphocytes also express co-stimulatory molecules for example B7.1 (CD80) and B7.2 (CD86) on the cell surface. These co-stimulatory molecules bind to co-stimulatory receptors, in this case, CD28 on naïve T lymphocytes (reviewed in Acuto and Michel, 2003). To become fully activated T lymphocytes must bind to the antigen presented on MHC and the co-stimulatory molecule on the same APC, this contact has to last several hours to induce changes in gene expression, at least in CD4⁺ T lymphocytes (Feske, 2007). However, the lytic granule exocytosis from CTLs upon TCR stimulation and the first signs of cell death of the targeted cell occur within less than 5 mins after ligation (Lyubchenko et al., 2001). Instead of a cell-cell-interaction, the release of lytic granules was achieved by the addition of anti-CD3 antibodies (Lyubchenko et al., 2001). In Jurkat T lymphocytes Ca²⁺ signals upon activation with anti-CD3 antibodies (Okt3) were already observed within seconds (Guse et al., 1997a; da Silva et al., 1998).

1.2 Calcium - an universal messenger in signal transduction

Calcium ions (Ca²⁺) are a universal messenger in the human body and are used throughout the life history, beginning with fertilization and going on with proliferation, development, learning and memory (Berridge et al., 2000; Carafoli, 2003). Ca²⁺ plays a direct role in controlling transcriptional events and also apoptosis; thus, the Ca²⁺ concentrations inside the cell are tightly regulated. Through a complex system containing Ca²⁺-pumps and Ca²⁺-binding proteins (e.g. calmodulin) a high electrochemical gradient between cytosol, and the extracellular space and/or intracellular stores is established. In the cytosol the Ca²⁺ concentration at rest is approx. 30 to 100 nM compared to the extracellular space with a Ca²⁺ concentration around 1 mM (Berridge et al., 2000). Furthermore, intracellular Ca²⁺ stores like the endoplasmic reticulum (ER), lysosomes, or Golgi apparatus have luminal Ca²⁺ concentrations around 60-800 μM (Feske, 2007; Lloyd-Evans et al., 2008; Miyawaki et al., 1997; Pinton et al., 1998).

Once the cell is stimulated, the cytosolic Ca²⁺ concentration rises rapidly up to 1000 nM (Berridge et al., 2000). There are two possible ways Ca²⁺ can enter the cytosol, (1) from

the extracellular space through Ca^{2+} pores in the cell membrane, or (2) through Ca^{2+} release from intracellular Ca^{2+} stores (Berridge et al., 2000). The rise in $[\text{Ca}^{2+}]_i$ stimulates Ca^{2+} dependent signaling proteins. To return to the initial Ca^{2+} gradient the ER is replenished via sarco/endoplasmic reticulum Ca^{2+} -ATPases (SERCAs) on the intracellular membranes (Toyoshima and Nomura, 2002; Toyoshima et al., 2000) and Ca^{2+} ATPases in the plasma membrane (PMCA) pump Ca^{2+} into the extracellular space. Furthermore, various Ca^{2+} binding proteins buffer Ca^{2+} and thus control the Ca^{2+} concentration inside the cell (reviewed in Gilibert, 2012; Yáñez et al., 2012).

1.2.1 Release of Ca^{2+} from intracellular Ca^{2+} stores

The release of Ca^{2+} from intracellular Ca^{2+} stores is mediated by Ca^{2+} mobilizing second messengers. Up to now three different Ca^{2+} mobilizing second messengers have been described. These are *D-myo*-inositol 1,4,5-triphosphate (IP_3), cyclic ADP-ribose (cADPR) and nicotinic acid adenine dinucleotide phosphate (NAADP).

IP_3 is the best-characterized second messenger and its Ca^{2+} releasing activity was first described in the early nineteen eighties in pancreatic acinar cells (Streb et al., 1983). After T lymphocyte stimulation, membrane phospholipid phosphatidylinositol-4,5-bisphosphate ($\text{PtdIns}(4,5)\text{P}_2$) is enzymatically cleaved by $\text{PLC}\gamma_1$ resulting in two end products, IP_3 and diacylglycerol (DAG) (Feske, 2007). IP_3 binds to the IP_3 receptor (IP_3R), a ligand-activated Ca^{2+} channel, located on the ER which triggers Ca^{2+} release (reviewed in Foskett et al., 2007). There are three different subtypes of IP_3Rs ($\text{IP}_3\text{R}1$, -2, -3) (reviewed in Mikoshiba et al., 1994) which form homo- and heterotetrameric channels (Alzayady et al., 2013; Taylor et al., 1999; Wojcikiewicz and He, 1995). The activity of all IP_3R subtypes is mainly regulated by Ca^{2+} and IP_3 (Foskett et al., 2007). In general, low Ca^{2+} concentrations (100-300 nM) increase the open probability of IP_3R whereas higher Ca^{2+} concentrations (above 300 nM) inhibit the Ca^{2+} release from IP_3R (Berridge et al., 2000; Foskett et al., 2007). Interestingly, $\text{IP}_3\text{R}3$ has the highest affinity to Ca^{2+} followed by $\text{IP}_3\text{R}2$ and $\text{IP}_3\text{R}1$ shows the lowest affinity to Ca^{2+} (Tu et al., 2005). Just recently was discovered that each of the four IP_3R subunits must bind IP_3 before the receptor can open (Alzayady et al., 2016; Taylor and Konieczny, 2016).

Another Ca^{2+} mobilizing second messenger is cADPR whose function was first observed in sea urchin egg homogenates (Lee et al., 1989). By now cADPR has been shown to provoke Ca^{2+} signals in approx. 40 different cell types from protozoa to mammals (Galione and Churchill, 2002; Guse, 2004). Furthermore, cADPR is involved

in diverse cellular processes like fertilization, secretion, and contraction (Lee, 2001). cADPR is enzymatically synthesized from NAD by ADP-ribosylcyclases. In T lymphocytes stimulation via the TCR induces the production of cADPR (Guse et al., 1995a, 1997b, 1999). cADPR mobilizes Ca^{2+} release by targeting the Ryanodine receptor (RyR) on the ER (reviewed in Lee, 2001, 2011) and augments the Ca^{2+} induced Ca^{2+} release (Galione et al., 1991; Lee, 1993). Accordingly in RyR-knock down T lymphocytes a suppressed Ca^{2+} signal was observed (Schwarzmann et al., 2002).

The most potent Ca^{2+} releasing second messenger is NAADP (reviewed in Guse and Lee, 2008; Lee, 2000). In contrast to IP_3 and cADPR, NAADP releases Ca^{2+} from intracellular Ca^{2+} stores already at nanomolar concentrations. **Fig. 2** summarizes present data showing the concentrations of the second messengers upon T lymphocyte stimulation with their corresponding $[\text{Ca}^{2+}]_i$ increase. NAADP and its putative target receptors will be described in detail below, in chapter 1.3.

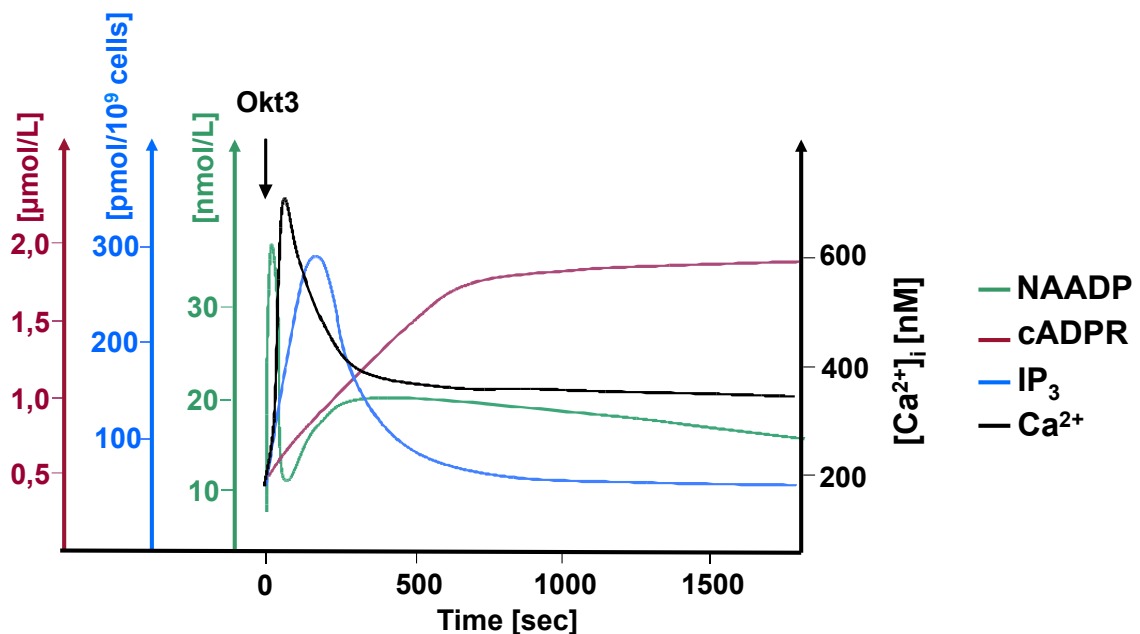


Fig. 2 Concentration of Ca^{2+} mobilizing second messengers after T lymphocyte stimulation with anti-CD3 antibodies (Okt3)

Shown are the concentrations of the Ca^{2+} mobilizing second messengers NAADP (Gasser et al., 2006), cADPR (Guse et al., 1999) and IP_3 (Guse et al., 1993) as well as the global $[\text{Ca}^{2+}]_i$ after stimulation of Jurkat T lymphocytes with anti-CD3 antibodies (Okt3). Arrow indicates addition of Okt3.

1.2.2 Ca²⁺ entry from extracellular space

Ca²⁺ signals arise from a combination of Ca²⁺ release from intracellular stores, predominantly from the ER, and Ca²⁺ entry across the plasma membrane. After the activation of T lymphocytes, Ca²⁺ release from intracellular Ca²⁺ stores leads to Ca²⁺ depletion in the lumen of the ER, which subsequently triggers Ca²⁺ entry from the extracellular space (Soboloff et al., 2012). In 2005 the stromal interaction molecules (STIM) (Liou et al., 2005; Roos et al., 2005) and a year later the calcium release-activated calcium modulator (Orai) were identified as key proteins in this process called SOCE (Feske et al., 2006; Vig et al., 2006; Zhang et al., 2006).

The STIM proteins (STIM1, STIM2) are highly conserved type 1a single-span membrane proteins (Manji et al., 2000) predominantly located in the ER (Hewavitharana et al., 2008; Williams et al., 2001). They are largely conserved across species and are broadly expressed in many tissues and organs (Oh-hora et al., 2008; Williams et al., 2001). Highest RNA expressions of STIM1 and STIM2 in human tissue samples were found in pancreas, skeletal muscle, placenta, brain and heart revealed by northern blot analysis (Williams et al., 2001). The luminal domain of the STIM proteins contains two EF-hand motifs, to sense small changes in the ER Ca²⁺ concentration and a sterile α -motif (SAM) domain (Stathopoulos et al., 2006, 2008). Furthermore, the cytosolic domain comprises an STIM-Orai activating region (SOAR), which mediates the coupling to Orai (Kawasaki et al., 2009; Yang et al., 2012; Yuan et al., 2009). Interestingly, STIM1 and STIM2 differ in their functional properties, e.g. the EF-hand domains of STIM1 and STIM2 have different affinities to Ca²⁺, respectively $\sim 250 \mu\text{M}$ and $\sim 500 \mu\text{M}$, (Stathopoulos et al., 2006, 2008; Zheng et al., 2008). Thus, STIM2 is already activated at smaller decreases in ER Ca²⁺ concentrations, near to the ER Ca²⁺ resting levels, compared to STIM1 (Brandman et al., 2007). Interestingly, upon activation STIM1 forms visual punctae with Orai1 at ER-plasma membrane junctions (Prakriya and Lewis, 2015). In contrast, STIM2 is not redistributing to visual punctae (Soboloff et al., 2006). In line with these results STIM2 is also a significantly weaker activator of Orai1 (Bird et al., 2009). This effect was recently pinpointed to the amino acid sequences of the SOARs (Wang et al., 2014b). The SOAR of STIM1, with a phenylalanine residue at position 394 is a full Orai1-agonist, whereas the SOAR of STIM2, with a leucine-replacement at position 394, is just a partial agonist (Wang et al., 2014b). Taken together, STIM1 seems to be the Ca²⁺ sensor for SOCE (Luik et al., 2008; Prakriya and

Lewis, 2015) while STIM2 regulates basal Ca^{2+} concentrations inside the cell (Bird et al., 2009).

The Orai proteins are composed of three subtypes (Orai1, Orai2 and Orai3) and form the calcium release activated channel (CRAC) pore (Prakriya et al., 2006; Yeromin et al., 2006; Zhou et al., 2010). In T lymphocytes, in particular Orai1, is responsible for SOCE (Shaw et al., 2013). When overexpressed in different cell types Orai2 and Orai3 form functional Ca^{2+} channels (DeHaven et al., 2007; Lis et al., 2007) but their physiological role in T lymphocytes are still undefined (McCarl et al., 2009). Orai3 is only expressed in mammals (Shuttleworth, 2012) and the Orai3-induced store-operated Ca^{2+} currents were significantly slower compared to Orai1 and Orai2 (Lis et al., 2007). In mast cells, Orai2 is localized on secretory granules, maybe hinting to a new, different function of Orai2 (Ikeya et al., 2014). Generally, the functional roles of Orai 2 and 3 are poorly understood (Ikeya et al., 2014; Shuttleworth, 2012). Orai1 contains four transmembrane domains with two extracellular and one intracellular loop (Feske et al., 2006; Vig et al., 2006; Zhang et al., 2006) and the assembly of a hexameric Orai forms a functional CRAC pore (Hou et al., 2012). In the C-terminal region of Orai1, a coiled-coil domain is present, which is required for the STIM1 binding and therefore the CRAC channel activation (Muik et al., 2008). Interestingly, in patch clamp experiments a fast (within tens of milliseconds) Ca^{2+} -dependent inactivation (CDI) of CRAC was observed, suggesting a local Ca^{2+} feedback (Shaw et al., 2013; Zweifach and Lewis, 1995).

Upon ER Ca^{2+} depletion, sensed by the dissociation of Ca^{2+} from luminal EF-hand domains, STIM proteins oligomerize (Covington et al., 2010) and undergo rapid, reversible translocation to the plasma membrane (**Fig. 3**; Deng et al., 2009; Prakriya and Lewis, 2015; Soboloff et al., 2012). For maximal CRAC channel activity, two STIM1 proteins need to bind one Orai1 (Hoover and Lewis, 2011) and dense ER-plasma membrane junctions are formed (Smyth et al., 2008). Once an activated STIM1-Orai1 complex is assembled Ca^{2+} enters the cytoplasm and a global and sustained Ca^{2+} influx is triggered, which in the end refills the luminal ER back to resting Ca^{2+} levels (reviewed in Prakriya and Lewis, 2015; Shaw and Feske, 2012; Shaw et al., 2013; Soboloff et al., 2012; Srikanth and Gwack, 2013). The luminal STIM1 EF-hand domains again sense this refilling through binding of Ca^{2+} , leading to retreat from ER-plasma membrane junctions and the deactivation of Orai1 (Smyth et al., 2008; Stathopoulos et al., 2008). The model for STIM1 activation and STIM1-Orai1 complex formation is shown in **Fig. 3**.

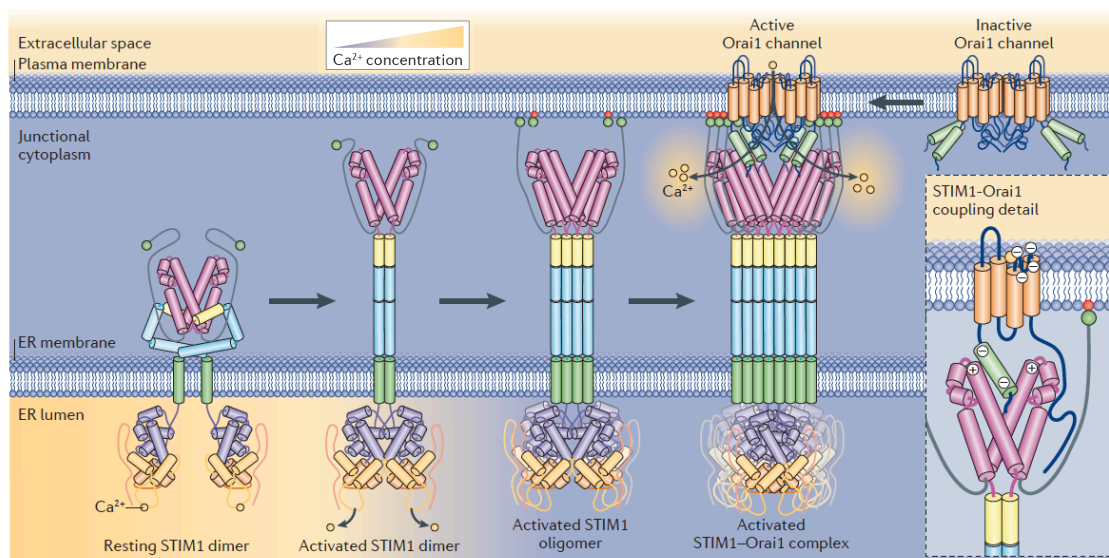


Fig. 3 Model of STIM1 activation and the Orai1 coupling process

In the resting state the EF-Hands of STIM1 dimers are bound to Ca²⁺. Upon Ca²⁺ release from the ER, Ca²⁺ dissociates from the luminal EF-Hands and STIM1 is activated. STIM1 then starts to oligomerize and translocate into ER-plasma membrane junctions. The STIM-Orai activating region (SOAR) domain binds to and activates Orai1 proteins and Ca²⁺ can enter the cytosol. Each SOAR dimer interacts with one Orai1 protein (inlet). Low Ca²⁺ concentrations are purple and high concentrations are orange as indicated (modified from Soboloff et al., 2012).

1.2.2.1 CRAC and SOCE in T lymphocyte activation

For an efficient development of an immune response, T lymphocytes require sustained calcium influx through CRAC (Kummerow et al., 2009; Shaw and Feske, 2012) and the formation of a mature immunological synapse (reviewed in Dustin, 2014). During T lymphocyte stimulation mRNA expression of Orai1 and STIM1 are up-regulated and they translocate into the immunological synapse (Lioudyno et al., 2008; Quintana et al., 2011). It is hypothesized that CRAC generate local Ca²⁺ influx microdomains for a sustained T lymphocyte and thus NFAT activation (Quintana et al., 2011; Srikanth and Gwack, 2013). Mitochondria are also found in close proximity to CRAC in a mature synapse and PMCA are re-distributed to decrease Ca²⁺ export (Quintana et al., 2011). Mitochondria are thought to act as Ca²⁺ buffers (Contreras et al., 2010; Pozzan et al., 2000) that prevent CDI of CRAC in the immune synapse (Quintana et al., 2011; Schwindling et al., 2010).

In patients with loss-of-function mutations in the *Orai1* or the *Stim1* genes, CRAC activation and consequently SOCE is abolished, resulting in severe immunodeficiency and autoimmunity with a clinical syndrome termed CRAC channelopathy (reviewed in Fes-

ke, 2010; Shaw and Feske, 2012). For example CD4⁺ T lymphocytes from those patients show strongly reduced NFAT translocation as well as declined production of cytokines like IL-2, IL-4, IFN γ and TNF α (Feske et al., 1996, 2001). In Orai1 knockout mice as well as non-functional Orai1 knock-in mice (Orai1^{KI/KI}) SOCE in naïve T lymphocytes is only partially reduced, hinting that unlike in humans, Orai2 and Orai3 may provide essential Ca²⁺ entry (McCarl et al., 2010; Vig et al., 2008). But after *in vitro* differentiation with plate-bound anti-CD3 and anti-CD28 for two days, Orai1^{KI/KI} T lymphocytes almost completely lack CRAC channel function (McCarl et al., 2010). These T lymphocytes failed to induce colitis and tolerated skin allografts longer than wildtype (WT) T lymphocytes (McCarl et al., 2010). Similar, deletion of either STIM1 or STIM2 in murine T lymphocytes resulted in a decreased cytokine and NFAT production (Oh-hora et al., 2008). A STIM1/STIM2 double knockout affected differentiation of T lymphocytes into T_{regs} and these mice establish signs of autoimmunity like blepharitis and dermatitis (Oh-hora et al., 2008).

1.3 Nicotinic acid adenine dinucleotide phosphate (NAADP)

NAADP (**Fig. 4**) is the most potent, endogenous Ca²⁺ mobilizing second messenger (Chini et al., 1995; Lee and Aarhus, 1995) and triggers the release of Ca²⁺ from intracellular Ca²⁺ stores already at low nanomolar concentrations (Berg et al., 2000; Clapper et al., 1987; Dammermann and Guse, 2005). In sea urchin egg homogenates this NAADP evoked Ca²⁺ release was first discovered, though it was thought at first that NADP was the effector (Clapper et al., 1987). It took eight years to reveal that NAADP, as an impurity of NADP, was the actual Ca²⁺ mobilizing second messenger (Chini et al., 1995; Lee and Aarhus, 1995).

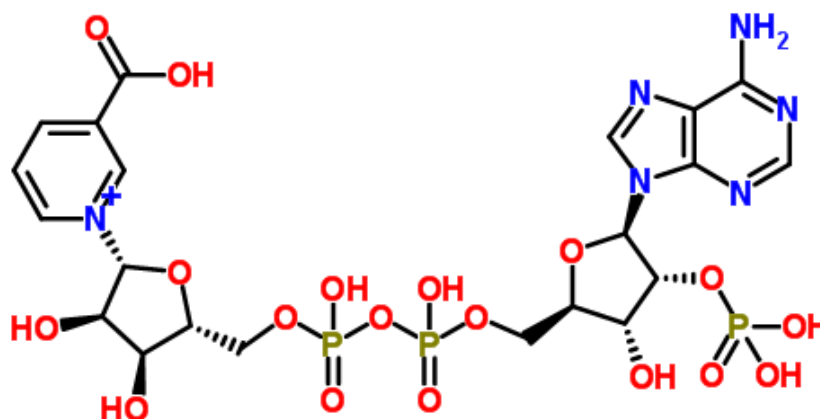


Fig. 4 Atomic Structure of Nicotinic acid adenine dinucleotide phosphate (NAADP)

(<http://www.chemspider.com/>)

Upon specific extracellular stimulation fast production of NAADP was observed in many different cell types from clonal pancreatic beta cells (Masgrau et al., 2003), mouse pancreatic acinar cells (Yamasaki et al., 2005), myometrial cells (Soares et al., 2007), adipocytes (Song et al., 2012), myocytes (Lewis et al., 2012) as well as lymphokine-activated killer cells (Rah et al., 2010) and human Jurkat T lymphoma cells (Gasser et al., 2006). The cytosolic concentration of NAADP in resting sea urchin eggs is approx. 290 nM (Churchill et al., 2003) opposed to mammalian cells types with cytosolic concentration around 10 nM (Churamani et al., 2004; Gasser et al., 2006; Schmid et al., 2012). Upon stimulation in Jurkat T lymphocytes the NAADP concentration increased up to approx. 35 nM, assuming an even distribution throughout the cell (Gasser et al., 2006). Hence, in microdomains the NAADP concentration might be a lot higher.

Already in 2000, NAADP was shown to be an essential regulator of T lymphocyte Ca^{2+} signaling and thus of the activation of the adaptive immune response (Berg et al., 2000). For example BZ194, a specific inhibitor of NAADP signaling (Dammermann et al., 2009), ameliorated the clinical symptoms of active experimental autoimmune encephalomyelitis (EAE; Cordiglieri et al., 2010), the T lymphocyte mediated animal model for multiple sclerosis (Wekerle et al., 1994). Moreover, the reactivation of effector T lymphocytes and also levels of pro-inflammatory cytokines like interferon-gamma ($\text{IFN}\gamma$) and interleukin-17 (IL-17) were significantly reduced (Cordiglieri et al., 2010). Thus, NAADP seems to be an essential regulator of T lymphocyte activation, whose primary function is to trigger initial Ca^{2+} release events, specifically blocking these initial Ca^{2+}

release leads to altered proliferation and cytokine secretion in T lymphocytes (Cordiglieri et al., 2010).

1.3.1 Metabolism of NAADP

In vivo, the formation pathway of NAADP is still unclear. CD38, a multifunctional ectoenzyme, *in vitro* catalyzes a base-exchange reaction using NADP as a substrate to generate NAADP. But this reaction only operates at non-physiological conditions at acidic pH (pH 5) and in the presence of excess of nicotinic acid (Guse et al., 2013). The topological paradox of an ectoenzyme forming intracellular active compounds was extensively discussed. In 1997 it was discovered that CD38 is also present on intracellular membranes (Yamada et al., 1997) and just recently CD38 was found in a minor amount also in type III orientation, where the carboxy-terminal catalytic domain is facing into the cytosol (Zhao et al., 2012). Also, CD38 mainly catalyzes the glycohydrolase reaction forming ADPR or 2'-phospho-ADPR (reviewed in Schuber and Lund, 2004). Surprisingly, in spleens and myometrial cells from CD38-KO mice, the NAADP concentration were increased (Schmid et al., 2011; Soares et al., 2007). Taken together, CD38 seems to be involved in the degradation on NAADP rather than in its formation. Thus, NAADP formation remains unclear. However NAADP is rapidly formed within 10 - 20 sec after the activation of Jurkat T lymphocytes (Gasser et al., 2006).

1.3.2 Proposed target receptors of NAADP

In 2009 it was shown that NAADP releases Ca^{2+} from acidic lysosomal stores via the activation of two-pore channels (TPCs) (Brailoiu et al., 2009; Calcraft et al., 2009; Ruas et al., 2010; Zong et al., 2009). However, the NAADP receptors and thus, the targeted organelles, are still controversially discussed (Guse et al., 2013). RyRs, TPCs, transient receptor potential channel, subtype mucolipin 1 (TRP-ML1) or subtype melastatin 2 (TRPM2) have been proposed as NAADP sensitive ion-channels (**Fig. 5**). So far, no binding site for NAADP on either one of the proposed ion-channels has been discovered. In 2012 with the help of 5-N₃-NAADP, a radioactively labeled NAADP, different proteins in mammalian cells have been discovered, which likely bind NAADP (Lin-Moshier et al., 2012). Hence, a unifying hypothesis for the NAADP signaling, probably

through a binding protein (bp), has been suggested (Fig. 5; Guse, 2012). The different putative target receptors of NAADP are presented in the next sections.

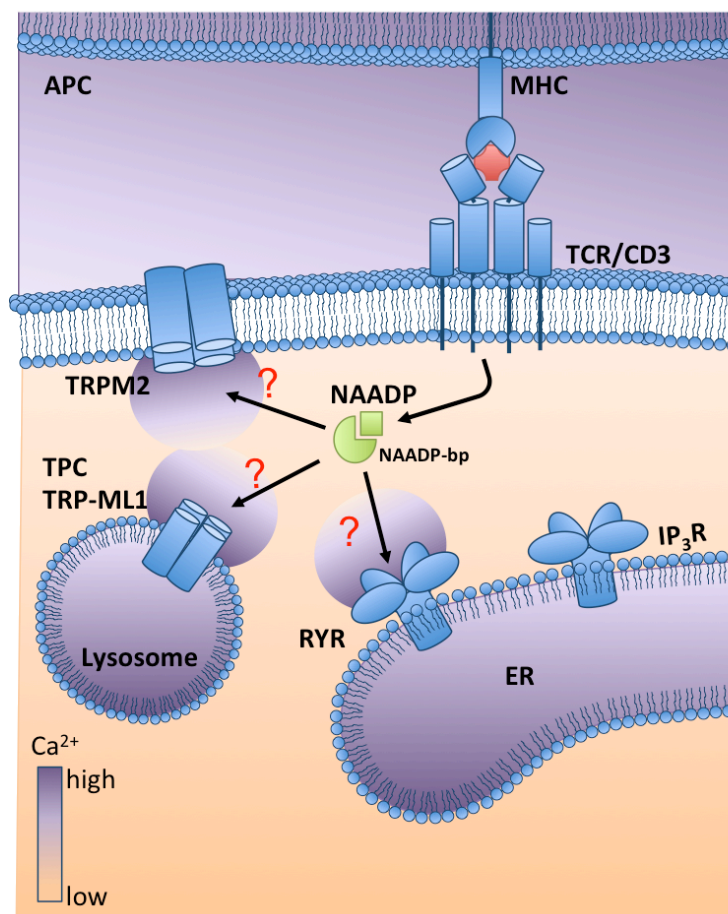


Fig. 5 Model of proposed NAADP receptors in T lymphocytes

After T lymphocyte activation, NAADP, probably through one or more binding proteins (NAADP-bp), triggers Ca^{2+} release/entry via different ion-channels. Proposed target receptors of NAADP are the RyR, the TPCs, TRPM2 as well as TRP-ML1 (modified from Ernst et al., 2013).

1.3.2.1 Ryanodine receptors (RyRs)

RyRs are Ca^{2+} release channels localized in the membrane of the sarcoplasmic reticulum and the ER. They form homotetramers and are the largest known ion channels (> 2 MDa; reviewed in Lanner et al., 2010; Zalk et al., 2007). Three different mammalian isoforms (RyR 1-3) with an amino acid identity of approx. 70% have been described (Rossi and Sorrentino, 2002). RyR1 is mainly expressed in skeletal muscle mediating excitation-contraction coupling, RyR2 is primarily found in cardiac muscles and RyR3 is mostly expressed in the brain (Ledbetter et al., 1994). In addition, the RyRs are also

expressed in various tissues and cells of the immune system like dendritic cells, B lymphocytes, and Jurkat T lymphocytes, mediating Ca^{2+} signaling and proliferation (Guse et al., 1999; Hosoi et al., 2001; O'Connell et al., 2002; Sei et al., 1999). The closed state structure of the whole RyR1 complex has just recently been published (Zalk et al., 2015), revealing a previously predicted EF-hand domain that modulates channel activity (Xiong et al., 2006).

The first evidence that NAADP targets the RyRs was observed already in 2001 (Mojzisoová et al., 2001). NAADP, in concentrations $\geq 1 \mu\text{M}$, increased the open probability of RyR2 from cardiac microsomes in lipid planar bilayers (Mojzisoová et al., 2001). Since the cytosolic NAADP concentration in mammalian cells is in the range of approx. 10 to 100 nM (Churamani et al., 2004; Gasser et al., 2006; Schmid et al., 2012), concentrations $\geq 1 \mu\text{M}$ are likely not physiological. In single channel recordings of purified RyR1 from skeletal muscle, NAADP increased the open probability in physiological concentrations of around 30 nM (Hohenegger et al., 2002). Furthermore ruthenium red and ryanodine blocked this effect and also NADP, a precursor of NAADP had no influence on the open probability (Hohenegger et al., 2002). Similar, microinjection of NAADP in Jurkat T lymphocytes resulted in global Ca^{2+} signals that were reduced via gene silencing of RyR as well as upon inhibition by ruthenium red (Langhorst et al., 2004). Interestingly, NAADP microinjection in Jurkat T lymphocytes (Dammermann and Guse, 2005) resulted in Ca^{2+} signals similar to those observed in the first seconds upon ligation of the TCR complex with anti-CD3 antibodies (Kunerth et al., 2003). These initial Ca^{2+} signals were found within ≤ 1.5 sec after microinjection close to the injection site (Dammermann and Guse, 2005) or, in the case of antibody stimulation, in close proximity to the plasma membrane (Kunerth et al., 2003). In addition, in a chicken B lymphocyte cell line (DT40; Kiselyov et al., 2001) and primary human T lymphocytes (Thakur et al., 2012) coupling between RyRs and CRAC channels were observed, suggesting a positive feedback relationship.

In contrast, in some publications, no effect of NAADP on RyRs from human β cells, skeletal muscle, and a mouse insulinoma β cell line (MIN6) was observed (Copello et al., 2001; Johnson and Mislser, 2002; Mitchell et al., 2003). Whether NAADP acts directly (or via a binding protein) on RyR or only through the RyR-dependent Ca^{2+} induced Ca^{2+} release (CICR) is still a matter of debate. In 2001 a two-pool model for NAADP signaling has been suggested where NAADP targets NAADP-sensitive stores and low amounts of Ca^{2+} are released (Churchill and Galione, 2001). This is taken up by

the ER resulting in overloading and hence, spontaneous Ca^{2+} release events from ER (Churchill and Galione, 2001). RyRs and IP_3Rs on the ER subsequently amplify these Ca^{2+} release events (Churchill and Galione, 2001). However, one of the major problems is the spatio-temporal resolution of the imaging systems to capture this low, initial Ca^{2+} signals.

Taken together, RyRs may be the target receptors of NAADP in some cell types like T lymphocytes, but the role of RyRs in NAADP signaling has yet to be further elucidated.

1.3.2.2 Two pore channels (TPCs)

TPCs are voltage-gated ion-channels that are localized on acidic Ca^{2+} stores within the endolysosomal system (reviewed in Patel, 2015). In humans and mice two isoforms (TPC1, TPC2) are described, whereas other primates, rodents, and sea urchins have three and plants only express one TPC (Brailoiu et al., 2010; Cai and Patel, 2010; Furuchi et al., 2001). The TPCs are predicted to function as homo- and heterodimers (Rietdorf et al., 2011) forming pseudo-tetrameric complexes (Zong et al., 2009). Each TPC subunit contains two hydrophobic domains, consisting of six transmembrane regions and a pore, and a connecting cytosolic loop (Churamani et al., 2012). *TPCN1* is usually higher expressed than *TPCN2*, but both are widely expressed in the body of mice (Zong et al., 2009).

Three independent groups published first evidence for NAADP sensitizing TPCs in 2009 (Brailoiu et al., 2009; Calcraft et al., 2009; Zong et al., 2009). For example, in human adenocarcinoma cell line SkBr₃, overexpressing TPCs, microinjection of 10 nM NAADP induced transient Ca^{2+} signals (Brailoiu et al., 2009). The TPCs were localized within the acidic organelles and Ca^{2+} signals were inhibited by vacuolar type H^+ -ATPase inhibitor bafilomycin A1 and also partially by ryanodine blocking the RyRs suggesting that NAADP triggers a Ca^{2+} release from TPC1, which is amplified by the RyRs (Brailoiu et al., 2009). Furthermore, in TPC gene knockout, small interfering RNA (siRNA) silencing and dominant-negative mutants, decreased NAADP-evoked Ca^{2+} signals have been observed (Brailoiu et al., 2009; Calcraft et al., 2009; Davis et al., 2012; Tugba Durlu-Kandilci et al., 2010). Very recently, a new TPC1/2 deficient (*Tpcn1/2^{-/-}*) mouse line was generated (Ruas et al., 2015). Embryonic fibroblasts from these mice showed significantly reduced NAADP-evoked Ca^{2+} signals and upon re-

expressing TPCs the NAADP-evoked Ca^{2+} signals were restored back to wild type levels (Ruas et al., 2015).

These findings suggest a role for TPCs in NAADP-evoked Ca^{2+} signals, however, many reports have observed contrary results (Cang et al., 2013, 2014a, 2014b; Wang et al., 2012). In all of these studies, TPCs were found to be primarily Na^+ selective ion-channels. Furthermore, no evidence for the regulation of TPCs by NAADP was observed, but instead, the membrane lipid $\text{PI}(3,5)\text{P}_2$ evoked Na^{2+} currents (Cang et al., 2013; Wang et al., 2012). $\text{PI}(3,5)\text{P}_2$ induced Na^+ currents were abrogated in TPC double-knockout mice (TPC1/2-KO) and no difference upon NAADP stimulation was found in WT, TPC1-KO or TPC2-KO (**Fig. 6B**; Wang et al., 2012). In a different study TPCs associated with mTOR (mammalian target of rapamycin) to form endolysosomal Na^+ channel complexes (lyso Na_{atp}) that detect nutrient status and are thus sensitive to ATP (Cang et al., 2013). Recently, Pitt and colleagues showed that TPC1 is permeable to Na^+ and Ca^{2+} but interestingly, also to protons (H^+) and potassium (K^+) with Ca^{2+} being least permeable (Pitt et al., 2014). Furthermore, they were able to trigger H^+ release by NAADP from TPC1 but $\text{PI}(3,5)\text{P}_2$ had no effect on the open probability (Pitt et al., 2014). In addition, data about TPCs targeted by NAADP in T lymphocytes is scarce. Only in cytotoxic T lymphocytes the Ca^{2+} -dependent exocytosis of cytolytic granules is mediated by NAADP via Ca^{2+} release through TPCs (Davis et al., 2012).

In summary, the involvement of TPCs in NAADP-evoked Ca^{2+} signaling, especially in T lymphocytes, remains inconclusive.

The latest model suggests that TPCs are likely co-regulated by NAADP and $\text{PI}(3,5)\text{P}_2$ and are permeable to H^+ , Na^+ and Ca^{2+} (maybe other cations) and are blocked by pharmaceuticals that bind to Na^+ and Ca^{2+} channels (**Fig. 6C**; Patel, 2015).

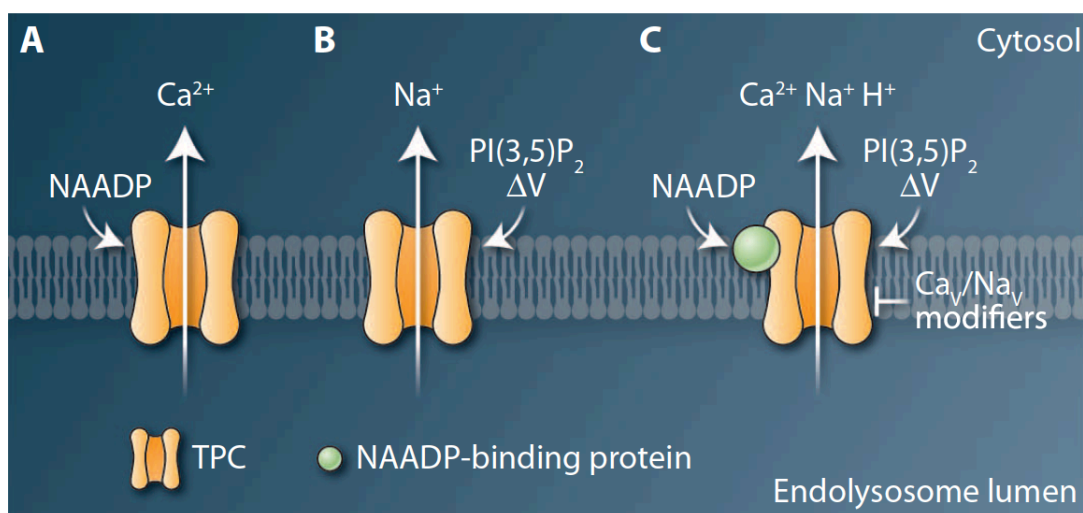


Fig. 6 Models of TPC activation

(A) First model based on findings from sea urchin egg homogenates. (B) Alternative model based on data that TPCs are mainly Na^+ channels activated by $\text{PI}(3,5)\text{P}_2$. (C) Latest model assuming that TPCs are co-regulated by NAADP, possibly via a binding protein, and $\text{PI}(3,5)\text{P}_2$ and that TPCs are permeable to H^+ , Na^+ and Ca^{2+} (Patel, 2015).

1.3.2.3 Transient receptor potential channel, subfamily melastatin, member 2 (TRPM2)

TRPM2 is a homotetrameric, Ca^{2+} -permeable nonselective cation channel and the second member of the transient receptor potential melastatin-related (TRPM) family (reviewed in Faouzi and Penner, 2014). TRPM2 was originally described as a plasma membrane channel, however; it has also been localized on lysosomal compartments in some cell types (Faouzi and Penner, 2014; Lange et al., 2009; Sumoza-Toledo et al., 2011). Especially high expressions of TRPM2 were found in the central nervous system (CNS) (Fonfria et al., 2006a, 2006b; Kraft et al., 2004; Lipski et al., 2006; Nagamine et al., 1998; Olah et al., 2009; Roedding et al., 2013) but TRPM2 amongst others was also detected in immune cells like neutrophils, monocytes, macrophages, B lymphoblast cells, mast cells and T lymphocytes (Faouzi and Penner, 2014; Heiner et al., 2003; Kashio et al., 2012; Knowles et al., 2012; Lange et al., 2008; Magnone et al., 2012; Oda et al., 2013; Roedding et al., 2012; Wenning et al., 2011; Yamamoto et al., 2008).

TRPM2 monomers consist of six putative transmembrane domains (S1-S6) with a pore-forming loop domain between the last two transmembrane domains (Fig. 7). The N terminus, the TRPM homology region, as well as the C terminus, are intracellular and the

C terminus contains an ADPR pyrophosphatase, homologous to the mitochondrial NUDT9 enzyme (Fig. 7; Perraud et al., 2001, 2003; Sano et al., 2001).

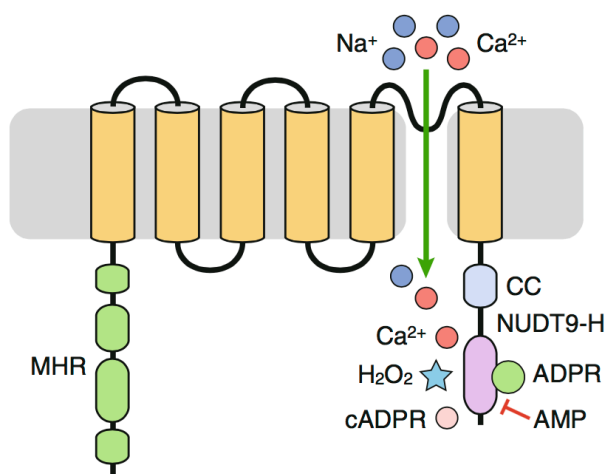


Fig. 7 Schematic membrane topology of TRPM2

TRPM2 consists six transmembrane domains and the N- and C- Termini are facing inside the cell. The C terminus contains a NUDT9 homology domain and TRPM2 is permeable to Na^+ and Ca^{2+} . Adenosine monophosphate (AMP) is a negative regulator of TRPM2 (from Faouzi and Penner, 2014).

In 2006, for the first time, it was shown that NAADP can activate TRPM2 directly (Beck et al., 2006). In patch-clamp experiments using Jurkat T lymphocytes, NAADP strongly activated TRPM2, although with a non-physiological EC_{50} of around $703 \mu\text{M}$, and this effect was completely suppressed by 8-Br-cADPR, a antagonist of TRPM2 (Beck et al., 2006). Furthermore, in primary human neutrophils a synergistic activation of TRPM2 by NAADP and ADPR was demonstrated (Lange et al., 2008). In subthreshold concentrations of ADPR (100 nM) TRPM2 was already partially activated by NAADP concentrations of approx. $1 \mu\text{M}$ (Lange et al., 2008). Opposing, Tóth and Csanády observed no synergistic effect NAADP and ADPR, further, they showed an agonistic effect of NAADP ($\text{EC}_{50} 104 \mu\text{M}$) alone, partially activating TRPM2 in *Xenopus* oocytes expressing human TRPM2 (Tóth and Csanády, 2010). Very recently, ADP ribose-2-phosphate (ADPRP) was further identified as a novel, true agonist TRPM2 (Toth et al., 2015). Moreover, impurities of ADPR and ADPRP in commercial preparations of NAADP, NAAD and NAD caused low activation of TRPM2 (Toth et al., 2015). After the purification with human mitochondrial NUDT9 hydrolase, neither NAADP nor NAAD nor NAD evoked gating of TRPM2. Thus, NAADP seems not to directly bind and activate TRPM2 (Toth et al., 2015).

In conclusion, activation of lysosomal TRPM2 by NAADP alone is rather unlikely. Considering the high ($\geq 100 \mu\text{M}$) EC_{50} values of NAADP for TRPM2 on one hand and the nanomolar endogenous concentration of NAADP inside for example Jurkat T lymphocytes on the other. A synergistic activation by NAADP together with ADPR is conceivable taken into account that in subcellular compartments concentrations of NAADP around $1 \mu\text{M}$ could be reached. However, it seems that NAADP effects on TRPM2 are rather due to impurities.

1.3.2.4 Transient receptor potential channel, subfamily mucolipin, member 1 (TRP-ML1)

Another proposed target channel for NAADP is TRP-ML1 (reviewed in Guse et al., 2013; Morgan et al., 2011). TRP-ML1 is a cation permeable channel localized on the membranes of late endosomes and lysosomes (Kiselyov et al., 2005; Venkatachalam et al., 2006; Zeevi et al., 2009) and is expressed in most tissues (Cheng et al., 2010) with the highest expression levels in the brain, kidney, spleen, liver and heart (Falardeau et al., 2002). Mutations of the TRP-ML1 gene (*MCOLN1*) in humans or in TRP-ML1-KO mice results in neurodegenerative disorder, with enlarged late endosomes and lysosomes as well as accumulation of lysosomal storage materials (Sun et al., 2000; Venugopal et al., 2007). Similar to TRPM2, and all other TRP channels, TRP-ML1 consists of six putative trans membrane domains with the N- and C-Termini facing inside the cytosol (Cheng et al., 2010; Slaugenhaupt, 2002). The pore-forming region is between the last two trans membrane domains (S5 and S6) (Cheng et al., 2010). TRP-ML1 is a nonselective cation channel, permeable to Ca^{2+} , iron ions (Fe^{2+}), zinc ions (Zn^{2+}), Na^{+} and K^{+} (Dong et al., 2009, 2008; Xu et al., 2007).

In 2007, for the first time direct evidence that NAADP activates TRP-ML1 in concentrations ranging from 1 nM to $1 \mu\text{M}$, was published (Zhang and Li, 2007). In rat liver lysosomes NAADP-sensitive Ca^{2+} release was observed that was markedly attenuated by anti-TRP-ML1 antibodies and also at higher NAADP concentrations ($10 - 100 \mu\text{M}$) (Zhang and Li, 2007). Interestingly, bafilomycin A1, as well as activators or blockers of ER, had no effect on the current (Zhang and Li, 2007). In addition, siRNA mediated knockdown of TRP-ML1 in coronary arterial myocytes significantly inhibited NAADP-sensitive Ca^{2+} release channel activity from lysosomes (Zhang et al., 2009). In human fibroblasts lacking TRP-ML1 expression, no NAADP-induced lysosomal Ca^{2+} release

was observed, but this effect could be restored by introducing TRP-ML1 transgene into the fibroblasts (Zhang et al., 2011). Contradictory to these findings, neither microinjection of NAADP nor stimulation with membrane-permeable NAADP-AM resulted in lysosomal Ca^{2+} release events in human SKBR cells, transfected with TRP-ML1 (Yamaguchi et al., 2011). Interestingly, overexpression of TPC1 and TPC2, in the same cells, evoked NAADP-induced Ca^{2+} releases (Yamaguchi et al., 2011). Furthermore, the knockout of TRP-ML1 in murine pancreatic acinar cells had no effect on NAADP responses (Yamaguchi et al., 2011). Hence, TRP-ML1 seems not to be essential for NAADP evoked Ca^{2+} signals (Yamaguchi et al., 2011).

Due to these controversial results, the involvement of TRP-ML1 in NAADP-mediated Ca^{2+} signaling has to be further elucidated.

1.4 Imaging subcellular Ca^{2+} signals

Basically, there are two ways Ca^{2+} signals can be monitored inside the cell, (1) using a genetically encoded Ca^{2+} indicator (e.g. GCaMP2 (Tallini et al., 2006)) or (2) loading cells with a chemical Ca^{2+} sensitive dye, that is membrane-permeable due to covalently bound acetoxymethyl ester (AM; e.g. Fura-2AM (Grynkiewicz et al., 1985)). The labile AM esters are cleaved by ubiquitously expressed esterases inside the cell generating a polycarboxylate form, which is membrane-impermeant, leading to accumulation of dye in the cytosol (**Fig. 8**; Hagen et al., 2012; Kao et al., 2010; Tsien, 1981). The chemical Ca^{2+} sensitive AM-dyes can be further separated into one-wavelength dyes (e.g. Fluo-4AM; Gee et al., 2000), dual-excitation (e.g. Fura-2AM) or dual-emission (e.g. Indo-1; Grynkiewicz et al., 1985) dyes. All Ca^{2+} indicators have in common that their fluorescence is sensitive to $[\text{Ca}^{2+}]$. Thus, upon Ca^{2+} binding the fluorescence intensity changes or the spectral shifts (Helmchen, 2011). High concentrations of Ca^{2+} dyes inside the cell may act as Ca^{2+} buffer and thus, may interfere with natural Ca^{2+} signals (Wang et al., 1997), therefore Ca^{2+} dye concentrations should be kept as low as possible.

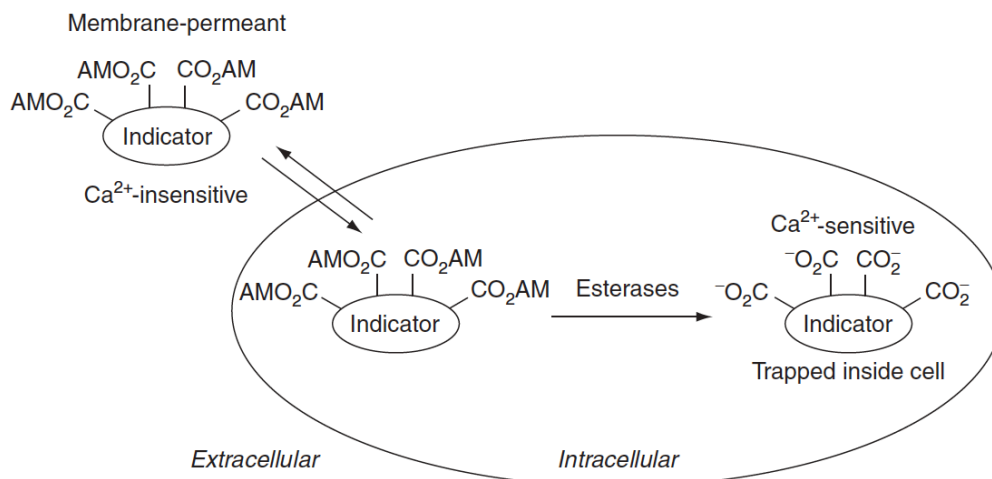


Fig. 8 Schematic loading of AM esterified Ca^{2+} indicators into cells

Hydrophobic AM ester diffuses into the cell through the plasma membrane. Ubiquitously expressed cellular esterases cleave the AM ester groups, generating a polycarboxylate the Ca^{2+} sensitive form of the dye. This polycarboxylated indicator is membrane-impermeant and thus trapped inside the cell (Kao et al., 2010).

One of the major problems to capture subcellular Ca^{2+} signals is the temporal resolution of the imaging systems. Subcellular Ca^{2+} release events arise in the ms range in myocytes (Shkryl and Blatter, 2013) and initial Ca^{2+} signal in T lymphocytes in ≤ 1.5 sec (Dammermann and Guse, 2005). To overcome this problem in myocytes, line scan techniques are used resulting in ultra-fast acquisition speeds up to 1000 frames/sec (Shkryl and Blatter, 2013). However, line scan data are one-dimensional while local Ca^{2+} signals proceed in three spatial dimensions. So far most of the subcellular Ca^{2+} imaging was performed in relatively large ($\sim 100 \mu\text{m}$; (Maier et al., 2002)) and excitable cardiac and skeletal myocytes (Brochet et al., 2005; Shkryl and Blatter, 2013; Weisleder et al., 2012; Zhang et al., 2013). Recent work in endothelial smooth muscle cells used frame scanning of Fluo4-loaded cells at 30 to 60 fps and under these conditions it was possible to optically record single channel openings (Sonkusare et al., 2012). In primary T lymphocytes Fura-2 (Liu et al., 2014; Schwarz et al., 2007), Indo-1 (Wei et al., 2007) as well as Fluo-4 (Lioudyno et al., 2008) were used to monitor subcellular Ca^{2+} signals but the temporal resolution was in the sec to 10sec range. Recently human T lymphocytes were loaded with a combination of two different Ca^{2+} dyes (Fluo-4 and Fura Red) to analyze calcium waves mediated via purinergic receptors (Wang et al., 2014a). However, the acquisition speed was still in the range of sec (Wang et al., 2014a).

1.4.1 Classification of different subcellular Ca²⁺ signals

Already in 1993, subcellular Ca²⁺ signals in quiescent rat cardiac cells were observed (Cheng et al., 1993). These spontaneous openings of Ca²⁺-release channels in the sarcoplasmic reticulum were termed Ca²⁺ sparks (Cheng et al., 1993). This was the beginning of the so-called “Sparkology” (reviewed in Cheng and Lederer, 2008). In summary, a specific duration, size and amplitude of Ca²⁺ signals were associated with specific ion-channels or clusters of ion-channels (Cheng and Lederer, 2008). Up to now there are many different classifications used for elemental signals and related structural components (overview Table 1 in Cheng and Lederer, 2008).

Well established are Ca²⁺ sparks which are defined as elementary Ca²⁺ release events in cardiac myocytes associated with the opening of RyR cluster and are characterized by an widely varying ratiometric amplitude of $\Delta F/F_0 \sim 0.2$ to ~ 4 , which resembles an amplitude of ~ 170 nM, a duration of signal of $\sim 10 - 100$ ms and a size of approx. $1 - 3 \mu\text{m}$ (Bootman et al., 2001; Cheng and Lederer, 2008; Niggli, 1999). Further, fundamental Ca²⁺ release events in cardiac myocytes were termed Ca²⁺ quarks (Lipp and Niggli, 1998; Niggli, 1999). Ca²⁺ quarks are associated with the Ca²⁺ release through single RyRs (Cheng and Lederer, 2008) and are characterized by an amplitude of ~ 37 nM and a spatial spread of $0.85 \mu\text{m}$ (Lipp and Niggli, 1998). Discrete local Ca²⁺ events mediated by IP₃Rs are called Ca²⁺ puffs. Typically these Ca²⁺ puffs result in amplitudes of $42 - 178$ nM, a diameter of $\sim 2.5 - 4.1 \mu\text{m}$ in none-excitabile cells (Bootman et al., 2001; Tovey et al., 2001). In addition Ca²⁺ blips correspond to the opening of only one or a few IP₃Rs (Cheng and Lederer, 2008).

Most of the classification of different Ca²⁺ signals was done in excitable myocytes, however, intracellular Ca²⁺ release events are universal to almost all cell types (Cheng and Lederer, 2008). Spark-like, subcellular Ca²⁺ release events have been observed also in nonexcitable cells like vascular endothelial cells (Hüser and Blatter, 1997), HeLa cells (Bootman et al., 1997) and T lymphocytes (Kunerth et al., 2003).

1.5 Study objective

The activation of T lymphocytes is tightly coordinated in a temporal and spatial fashion that in the end leads to an adaptive immune response (reviewed in Feske, 2007; Samelson, 2002). Ca^{2+} signaling is essential for T lymphocyte activation and is supposed to start by initial, localized Ca^{2+} microdomains. In contrast to excitable cells, in T lymphocytes, such initial Ca^{2+} microdomains have not yet been characterized.

Up to now three different Ca^{2+} mobilizing second messengers (IP_3 , cADPR, and NAADP) have been described. NAADP is the most potent Ca^{2+} mobilizing second messengers (Chini et al., 1995; Lee and Aarhus, 1995) and rapidly synthesized after T lymphocytes stimulation with anti-CD3 antibodies (Gasser et al., 2006). However, the NAADP target receptors are still controversially discussed (Guse et al., 2013). So far, RyRs, TPCs, TRP-ML1 or TRPM2 have been proposed as NAADP sensitive ion-channels.

The main objective of my doctoral thesis was to characterize the initial Ca^{2+} microdomains in T lymphocytes, presumably evoked by NAADP and hence, identify the NAADP target receptor. Therefore, a new Ca^{2+} live-cell-imaging method were initial microdomains after a directed T lymphocyte activation can be characterized, ought to be established. With the help of antibody-coated beads, the size of T lymphocytes, a directed stimulation similar to cell-cell interaction should be mimicked. Upon activation T lymphocytes re-organize their cellular structure during the formation of an immune synapse (Dustin, 2014; Kummerow et al., 2009), thus the new Ca^{2+} live-cell-imaging method had to be capable of fast acquisition rates despite cellular movement and changes in cell shape.

The Ca^{2+} live-cell-imaging method should be established in Jurkat T lymphocytes and later also adapted to primary murine T lymphocytes. In order to get more insights in the NAADP target channels, initial Ca^{2+} microdomains in WT and RyR knock down Jurkat T lymphocytes ought to be compared. Furthermore, primary T lymphocytes from RyR1-KO and TRPM2-KO mice should be investigated. Additionally, the post-processing workflow and deconvolution algorithms should be revised and possibly optimized.

2 Publications

2.1 Publication I

A Modular Framework for Post-Processing and Analysis of Fluorescence Microscopy Image Sequences of Subcellular Calcium Dynamics

Daniel Schetelig¹, Insa M.A. Wolf², Björn-P. Diercks²,
Ralf Fliegert², Andreas H. Guse², Alexander Schlaefer³, Rene Werner¹

¹Department of Computational Neuroscience

²Department of Biochemistry and Molecular Cell Biology,
University Medical Center Hamburg-Eppendorf

³Institute of Medical Technology, Hamburg University of Technology
r.werner@uke.de

Abstract. Calcium (Ca^{2+}) signaling is essential for activation of T-lymphocytes and can be understood as fundamental on-switch for the adaptive immune system. The activation is supposed to start by initial spatially and temporally localized Ca^{2+} signals. Imaging and analysis of these signals require high spatio-temporal resolution fluorescence microscopy – which, in turn, results in the need for an efficient and reliable post-processing and analysis workflow of the acquired image data. Started with a well established but time-consuming post-processing process, we report on our efforts to automatize and optimize it. The efforts led to a modular post-processing and analysis framework, which is presented. In addition, the influence of instances of the main blocks of the framework (e.g. bleaching correction, deconvolution) on Ca^{2+} dynamics analysis measures is evaluated.

1 Introduction

Calcium (Ca^{2+}) is a versatile intracellular second messenger associated with the activation of a wide range of cellular functions. The increase of the free cytosolic Ca^{2+} concentration ($[\text{Ca}^{2+}]_i$) mediates the activation of T-lymphocytes and is therefore essential for the specific immune response. The mechanisms underlying the initial formation of Ca^{2+} signals and the signal dispersion within the cells that precede the global $[\text{Ca}^{2+}]_i$ increase are, however and especially in T cells, still not entirely understood [1]. A more profound understanding could eventually lead to the development of advanced therapeutic treatment options for immunological diseases [2].

Initial Ca^{2+} signal formation and dispersion can be examined by single cell fluorescence microscopy. As signal formation and dispersion take place within fractions of a second, high spatial and temporal resolution imaging is required – which, in turn, results in the need for an efficient and reliable workflow for post-processing and analysis of the generated large image data volume. The current

2.1.1 Contribution to publication I

Daniel Schetelig, Insa M.A. Wolf, **Björn-P. Diercks**, Ralf Fliegert, Andreas H. Guse, Alexander Schlaefer, René Werner 2015 „A Modular Framework for Post-Processing and Analysis of Fluorescence Microscopy Image Sequences of Subcellular Calcium Dynamics“. DOI: 10.1007/978-3-662-46224-9_69 Conference: *Bildverarbeitung für die Medizin* 2015, At Lübeck, Volume: Informatik aktuell

In this publication, our well-established post processing workflow for subcellular Ca^{2+} dynamics was implemented in MATLAB (MathWorks; see 2.1 Fig 1). With this adapted modular post-processing pipeline, the single cell processing time decreased from 1 – 2 h to approx. 5 – 10 min. Furthermore, different deconvolution algorithms and bleach correction strategies were compared. I was involved in the data acquisition of subcellular Ca^{2+} signals in Jurkat T lymphocytes. In addition, I conducted the evaluation of deconvolution algorithms, bleach correction strategies, and assisted in writing the manuscript.

Place, date

Signature of the supervisor

2.2 Publication II

RESEARCH ARTICLE

CALCIUM SIGNALING

Frontrunners of T cell activation: Initial, localized Ca²⁺ signals mediated by NAADP and the type 1 ryanodine receptor

Insa M. A. Wolf,^{1*} Björn-Philipp Diercks,^{1*} Ellen Gattkowsky,¹ Frederik Czarniak,¹ Jan Kempski,¹ René Werner,² Daniel Schetelig,² Hans-Willi Mittrücker,³ Valéria Schumacher,³ Manuel von Osten,^{4,5} Dimitri Lodygin,^{4,5} Alexander Flügel,^{4,5} Ralf Fliegert,¹ Andreas H. Guse^{1†}

The activation of T cells is the fundamental on switch for the adaptive immune system. Ca²⁺ signaling is essential for T cell activation and starts as initial, short-lived, localized Ca²⁺ signals. The second messenger nicotinic acid adenine dinucleotide phosphate (NAADP) forms rapidly upon T cell activation and stimulates early Ca²⁺ signaling. We developed a high-resolution imaging technique using multiple fluorescent Ca²⁺ indicator dyes to characterize these early signaling events and investigate the channels involved in NAADP-dependent Ca²⁺ signals. In the first seconds of activation of either primary murine T cells or human Jurkat cells with beads coated with an antibody against CD3, we detected Ca²⁺ signals with diameters close to the limit of detection and that were close to the activation site at the plasma membrane. In Jurkat cells in which the ryanodine receptor (RyR) was knocked down or in primary T cells from RyR1^{-/-} mice, either these early Ca²⁺ signals were not detected or the number of signals was markedly reduced. Local Ca²⁺ signals observed within 20 ms upon microinjection of Jurkat cells with NAADP were also sensitive to RyR knockdown. In contrast, TRPM2 (transient receptor potential channel, subtype melastatin 2), a potential NAADP target channel, was not required for the formation of initial Ca²⁺ signals in primary T cells. Thus, through our high-resolution imaging method, we characterized early Ca²⁺ release events in T cells and obtained evidence for the involvement of RyR and NAADP in such signals.

INTRODUCTION

During intracellular Ca²⁺ signaling, early localized Ca²⁺ signals precede an increase in global free cytosolic Ca²⁺ concentration ([Ca²⁺]_i). These initial, short-lived Ca²⁺ signals are associated with the opening of either single intracellular Ca²⁺ release channels, termed fundamental Ca²⁺ release events, or clusters of these channels, termed elementary Ca²⁺ release events. The principal Ca²⁺ release channels mediating such events are the *D-myo*-inositol 1,4,5-trisphosphate receptor (IP₃R) and the ryanodine receptor (RyR) (1, 2). The latter are a family of three channels—RyR1, RyR2, and RyR3—which have homology to the IP₃R. The plant alkaloid ryanodine shows high affinity for the RyR, and it exerts an inhibitory effect at micromolar concentrations. Well-studied among initial, short-lived Ca²⁺ signals are Ca²⁺ sparks, elementary Ca²⁺ release events that are most frequently associated with the opening of clusters of RyRs in cardiac myocytes. Ca²⁺ sparks form by the opening of small clusters of RyRs, and they are characterized by an amplitude of ~170 nM, a duration of signal of ~10 to 100 ms, and a spatial spread of ~1 to 3 μm (3–6). The fundamental Ca²⁺ release events mediated by RyRs in cardiac myocytes, termed Ca²⁺ quarks, are believed to originate from the opening of single RyRs (6), and they have been previously characterized as

having an amplitude of 37 ± 6 nM and having diameters at half-maximal amplitude of 0.85 ± 0.2 μm or less (7). Elementary Ca²⁺ release events that are mediated by IP₃Rs, which are termed “Ca²⁺ puffs,” typically have amplitudes of 50 to 600 nM, a diameter of ~6 μm, and a total duration of about 1 s (5).

During the activation of T cells, Ca²⁺ signaling is initiated by the engagement of a T cell receptor (TCR) on the surface of a T cell with a peptide-bound major histocompatibility complex on the surface of an antigen-presenting cell (APC) at the contact point between the two cells, which is known as the immunological synapse. We previously demonstrated an important role for the second messenger nicotinic acid adenine dinucleotide phosphate (NAADP) in T cell activation. In Jurkat cells, NAADP is formed within ~10 s of their activation (8), and it evokes Ca²⁺ release at low nanomolar concentrations (9, 10). Furthermore, NAADP signaling is essential for the reactivation of effector T cells (11, 12). However, since the discovery of NAADP in 1987 (13), different candidate target channels, including RyRs, two-pore channels, transient receptor potential channel, subtype mucolipin 1 (TRPML1) or subtype melastatin 2 (TRPM2), have been proposed to lead to an NAADP-dependent increase in [Ca²⁺]_i (14). Nevertheless, the rapid formation of NAADP in different cell types (8, 15, 16) suggests that it plays a major role in early, local Ca²⁺ signals (17). Indeed, early local Ca²⁺ signals have been observed upon microinjection of NAADP into T cells (10, 18) and pulmonary arterial smooth muscle cells (19); however, in general, data showing elementary Ca²⁺ signaling events evoked by NAADP are scarce (18).

In contrast to Ca²⁺ imaging in large, adherent cells, such as cardiac myocytes, Ca²⁺ imaging in small cells, such as T cells, is challenging in different aspects. During immunological synapse formation, T cell morphology changes or T cells move. Furthermore, the spherical shape of T cells results in differential fluorescence intensities at central and peripheral parts of the cell. To obtain reliable images of local [Ca²⁺]_i, so-called ratiometric analysis

¹The Calcium Signalling Group, Department of Biochemistry and Molecular Cell Biology, University Medical Center Hamburg-Eppendorf, Martinistrasse 52, 20246 Hamburg, Germany. ²Department of Computational Neuroscience, University Medical Center Hamburg-Eppendorf, Martinistrasse 52, 20246 Hamburg, Germany. ³Department of Immunology, University Medical Center Hamburg-Eppendorf, Martinistrasse 52, 20246 Hamburg, Germany. ⁴Institute for Multiple Sclerosis Research, Department of Neuroimmunology, Gemeinnützige Hertie-Stiftung and University Medical Center Göttingen, Waldweg 33, 37073 Göttingen, Germany. ⁵Max-Planck-Institute for Experimental Medicine, Hermann-Rein-Strasse 3, 37075 Göttingen, Germany.
*These authors contributed equally to this work.
†Corresponding author. E-mail: guse@uke.de

2.2.1 Contribution to publication II

Insa M.A. Wolf*, **Björn-P. Diercks***, Ellen Gattkowsky, Frederik Czarniak, Jan Kemp-ski, René Werner, Daniel Schetelig, Hans-Willi Mittrücker, Valeá Schumacher, Manuel van Osten, Dimitri Lodygin, Alexander Flügel, Andreas Guse 2015 „Frontrunners of T cell activation: Initial, localized Ca^{2+} signals mediated by NAADP and the type 1 ryanodine receptor“. *Science Signaling* **8** (398), ra102. [doi: 10.1126/scisignal.aab0863].

* These authors contributed equally to this work.

In this publication, I contributed to the project planning. Furthermore, I performed most of the experiments and data analyses. The development of a high-resolution imaging technique to analyze initial, localized Ca^{2+} microdomains in T lymphocytes is described in this publication in detail. Therefore, I tested different Ca^{2+} indicators in Jurkat T lymphocytes. In order to obtain a directed activation of Jurkat as well as primary T lymphocytes, I added magnetic beads that were coated with anti-CD3 or a combination of anti-CD3 and anti CD-28 antibodies. With this newly established method, I investigated the involvement of RyR1 and TRPM2 on the formation of initial, localized Ca^{2+} microdomains. In addition, also a direct link between NAADP and RyRs, in microinjection experiments with RyR knockdown Jurkat cells, was verified. I was able to emphasize a role of RyR (RyR1 in primary) and NAADP in the early Ca^{2+} release events in T lymphocytes. Furthermore, I was decisively involved in Figure preparation and editing the manuscript.

Place, date

Signature of the supervisor

3 Discussion

The aim of this thesis was to understand the initial Ca^{2+} microdomain formation during T lymphocyte activation and to explore the second messengers and Ca^{2+} channels, which are involved. With a new Ca^{2+} live cell imaging method the initial, localized Ca^{2+} microdomains of T lymphocytes after a directed stimulation were analyzed for the first time. Furthermore, the post-processing workflow was optimized and different deconvolution algorithms and bleaching strategies were compared. The RyR1, as a proposed NAADP target receptor, seems to be essential for the development of Ca^{2+} microdomains in T lymphocytes after directed activation, while TRPM2, also a proposed NAADP target receptor, is apparently not involved in the formation of initial Ca^{2+} microdomains.

3.1 Establishing a method to detect subcellular, initial Ca^{2+} release events in T lymphocytes

Subcellular Ca^{2+} release events arise in the msec range in myocytes (Shkryl and Blatter, 2013) and initial Ca^{2+} signal in T lymphocytes in ≤ 1.5 sec (Dammermann and Guse, 2005). Until recently, most of the subcellular Ca^{2+} imaging was performed in relatively large (~ 100 μm ; Maier et al., 2002) and excitable cardiac and skeletal myocytes (Brochet et al., 2005; Shkryl and Blatter, 2013; Weisleder et al., 2012; Zhang et al., 2013). Furthermore, line scan techniques with a confocal laser scanning microscope were used resulting in ultra-fast acquisition speeds up to 1000 frames/sec in myocytes (Shkryl and Blatter, 2013). However, line scan data are one-dimensional while local Ca^{2+} signals proceed in three spatial dimensions. Another possible set-up would be a total internal reflection fluorescence (TIRF) microscope, however, the cells must adhere to a glass surface and only Ca^{2+} indicators that are very close to the cell surface (1 – 100 nm) are excited (Axelrod, 1981). The confocal spinning disk microscope enables for a fast acquisition of *in vivo* samples with confocal resolution (Gräf et al., 2005; In-

oué, 1990). However, in our experiments the high laser power necessary for imaging our samples in a confocal spinning disk microscope resulted in the activation of T lymphocytes (not published). Without any further stimulation, most T lymphocytes responded with an intracellular Ca^{2+} increase after 30 – 60 sec (not published). Thus, here a wide-field microscope in combination with deconvolution was used to obtain digital confocal images.

To analyze initial Ca^{2+} release events in Jurkat and primary mouse T lymphocytes a Ca^{2+} indicator with high fluorescence intensity was needed to obtain fast acquisition rates. Additionally, the Ca^{2+} dye should exhibit low photobleaching properties and a broad dynamic range. A genetically encoded Ca^{2+} biosensor was not applicable for the experiments because primary T lymphocytes are very difficult to transfect and the aim was to analyze initial, localized Ca^{2+} release events in primary mouse WT as well as KO T lymphocytes. Therefore, in this thesis, I focused on chemical Ca^{2+} sensitive dyes that are membrane-permeable due to a linked acetoxymethyl ester. So far Fura-2 (Liu et al., 2014; Schwarz et al., 2007), Indo-1 (Wei et al., 2007), as well as Fluo-4 (Lioudyno et al., 2008), were used to monitor subcellular Ca^{2+} signals in primary T lymphocytes, but the temporal resolution was in the second to 10 sec range. Recent work from Wang and co-workers showed a combination of two different Ca^{2+} dyes (Fluo-4 and Fura Red) to analyze Ca^{2+} waves mediated via purinergic receptors in human T lymphocytes (Wang et al., 2014a). However, the acquisition speed was still in the range of seconds (Wang et al., 2014a).

3.1.1 Single-wavelength Ca^{2+} indicators

In this thesis, three single-wavelength Ca^{2+} indicators, namely Fluo-3, Fluo-4 and Fluo-8 were tested in Jurkat T lymphocytes. Fluo-4 and Fluo-8 are analogues of the established cytoplasmic Ca^{2+} indicator Fluo-3 (Minta et al., 1989). *In vitro*, all three dyes have a similar ion dissociation constants ($K_d(\text{Ca}^{2+})$) of approx. 345 nM (Fluo-4) and 390 nM (Fluo-3 and Fluo-8; Gee et al., 2000; Hagen et al., 2012; Johnson, 2010). In their Ca^{2+} bound forms, they have excitation and emission maxima of 488 nm and 520 nm (Gee et al., 2000; Johnson, 2010). Interestingly the fluorescence quantum yields of Ca^{2+} -bound Fluo-3 and Fluo-4 are identical, but Fluo-4 absorbs 488 nm excitation

more efficiently generating a more intense fluorescence and consequently higher signal levels (Gee et al., 2000; Johnson, 2010).

Fluo-4 was also the most promising single wavelength Ca^{2+} indicator with a high dynamic range and low photobleaching properties (2.2 – Fig. S1 A, B, C). However, single-wavelengths Ca^{2+} indicators are most useful to measure relative, not absolute, changes in Ca^{2+} concentrations, considering that variations in fluorescence emission not necessarily mirror differences in Ca^{2+} concentrations (Bootman et al., 2013). An effective and commonly used way to address this uneven indicator concentration is to express the fluorescence signal relative to its starting signal (Bootman et al., 2013). Thereby all subsequent frames of the experiment (F) are divided by the first frame (F_0), resulting in an F/F_0 ratio (Bootman et al., 2013). For whole cell analysis this is a simple method, but since T lymphocytes are changing their morphological shape upon activation (Dammermann et al., 2009), an F/F_0 ratio results in systematic errors (2.2 – Fig. S2). These systematic errors especially occurred close to the plasma membrane and regions of interest (ROIs) could not be quantified correctly (2.2 – Fig. S2 B). Thus, Fluo-4 as a single-wavelength Ca^{2+} indicator was not applicable to measure initial, subcellular Ca^{2+} release events in T lymphocytes.

3.1.2 Dual wavelength dyes

To circumvent the systematic errors that occurred with the single-wavelength Ca^{2+} sensors, next dual-wavelength Ca^{2+} indicators were tested. The advantage of dual-wavelength dyes is that one can acquire ratiometric image pairs, thus cellular movements and morphological shape changes do not result in systemic errors. Moreover, dual-wavelength dyes can be used for the analysis of qualitative changes in Ca^{2+} concentrations (Bootman et al., 2013). However, one disadvantage of dual-wavelength indicators, compared to single-wavelength indicators, is that their dynamic range between Ca^{2+} -free and Ca^{2+} -bound state is often lower, hence, it may be difficult to detect small Ca^{2+} signals (Bootman et al., 2013). Furthermore, when using dual-excitation Ca^{2+} indicator the excitation wavelength has to switch.

Hence, Fura-2, a frequently used dual-excitation Ca^{2+} indicator in our laboratory was unsuitable for fast Ca^{2+} imaging, due to the switch of the excitation wavelength (340 nm and 380 nm), resulting in a delay of approx. 10 msec. Thus, two dual-emission Ca^{2+}

dyes, namely Indo-1 (Grynkiewicz et al., 1985) and Asante Calcium Red-1 (ACR-1; Hyrc et al., 2013; Jahn and Hille, 2014) were tested. Both are emission-shift dyes and with a single dichroic mirror the emission spectra can be split (Bootman et al., 2013; Hyrc et al., 2013). However, as previously reported (Scheenen et al., 1996) Indo-1 is prone to strong photobleaching (2.2 – Fig. S1 A, B). Moreover, after stimulation with an anti-CD3 mAb Okt3 no fluorescence dynamic was observed, probably due to the intense bleaching (2.2 – Fig. S1 B). ACR-1 exhibited the lowest intrinsic fluorescence at the start of acquisition; the intensities were barely above background levels (2.2 – Fig. S1 C). Taken together, both dual-emission Ca^{2+} indicators (Indo-1 and ACR-1) were not suitable for the measurement of fast initial Ca^{2+} signals in T lymphocytes.

3.1.3 Combining Fluo-4 and Fura Red for subcellular Ca^{2+} imaging

To maintain the advantage of an emission-shift ratiometric Ca^{2+} dye together with the photostability and dynamics of Fluo-4, a combination of two single-wavelength Ca^{2+} indicators, namely Fluo-4 and Fura Red was tested. The fluorescence of Fura Red excited at 488 nm decreases once the indicator binds Ca^{2+} (Johnson, 2010). Moreover, Fura Red has a very long wavelength emission maximum (~660 nm; Johnson, 2010) making Fura Red ideal for ratiometric Ca^{2+} imaging with Fluo-4. The combination of Fluo-3 with FuraRed for ratiometric Ca^{2+} imaging has been reported previously in cardiac myocytes and HeLa cells (Lipp and Niggli, 1993; Thomas et al., 2000) and very recently also the combination of Fluo-4 and Fura Red in human T lymphocytes (Wang et al., 2014a). Due to different intrinsic fluorescence intensities of the Fluo-dyes and Fura Red, cardiac myocytes and human T lymphocytes were loaded with a 1:2 mixture (Lipp and Niggli, 1993; Wang et al., 2014a) (2.2 – Fig. S2 A, C). In addition, the intracellular concentrations were kept as low as possible, respectively 10 μM and 20 μM , to circumvent the buffering of Ca^{2+} signals and thus the disruption of small Ca^{2+} events (Wang et al., 1997). In primary astrocytes loaded with 20 μM Fura-2 significantly reduced Ca^{2+} waves were observed compared to 2.5 μM Fura-2 loaded astrocytes (Wang et al., 1997). However, in isolated ventricular myocytes, a concentration of 33.33 μM Fluo-3 and 66.66 μM Fura Red (Lipp and Niggli, 1993) and in receptor neurons of *Xenopus laevis* even 50 μM Fluo-3 and 150 μM Fura Red were used to image Ca^{2+} signals (Schild et al., 1994).

One problem that may occur when two different Ca^{2+} indicators, with different K_d 's for Ca^{2+} , are loaded into one cell is that they could show different subcellular loading patterns and thus, no pixel-by-pixel ratioing should be applied (Floto et al., 1995). For example, Floto and co-workers identified problems with determining subcellular Ca^{2+} signals because of strong intercellular loading variations of Fluo-3 and Fura Red (Floto et al., 1995). Fortunately, Fluo-4 and Fura Red exhibited very similar intensity distributions inside the T lymphocytes that matched those of the two-emission wavelengths of Fura-2 (2.2 – Fig. S4, A and B). Ratioing resulted in very similar data sets, thus, intracellular variations were considerably low (2.2 – Fig. S4, A and B). Moreover, ratio images of Fluo-4 and Fura Red in Jurkat and primary T lymphocytes showed very similar distribution patterns compared to both dyes in a Ca^{2+} free-buffered solution (2.2 – Fig. S3). This implies that differences in the ratio values were caused by systemic noise of the CCD camera and not by differences in subcellular dye distributions.

Another problem that may occur when two different Ca^{2+} indicators are used is that these Ca^{2+} dyes are differently affected by photobleaching, which would lead to the domination of one Ca^{2+} dye in the ratio (Thomas et al., 2000). Unfortunately, Fura Red was affected stronger by photobleaching during fast acquisition than Fluo-4, but this could be corrected by a bi-exponential fitting curve (2.2 – Fig. S1 D). Photobleaching can generally be described by a negative exponential behavior that can be modeled with mono- or multi-exponential curves (L. L. Song, 1995; Vicente et al., 2007). Vicente and co-workers showed, that a bi-exponential fitting curve exhibited the most accurate way to correct for the photobleaching of fluorescein isothiocyanate (FITC; Vicente et al., 2007) and this was also true for the photobleaching alteration of Fura Red (2.2 – Fig. S1 D).

Through the combination of Fluo-4 and Fura Red, both dyes were utilized as a single-excitation dye with dual-emission, like Indo-1. Thus, one K_d for the Fluo-4/Fura Red dye combination was determined *in situ* (408 ± 12 nM; see Materials and Methods 2.2 – Fig. S9). Very recently, the first double- K_d model was published, where the classical Grynkiewicz equation, for the $[\text{Ca}^{2+}]_i$ calibration of ratiometric Ca^{2+} dyes with one K_d (Grynkiewicz et al., 1985) was extended for the use of two dyes with different K_d 's (Assinger et al., 2015). This double- K_d equation should result in a higher accuracy and a higher dynamic range (Assinger et al., 2015). Comparing the double- K_d model to the one- K_d model no huge difference were observed in the $[\text{Ca}^{2+}]_i$ calibration of primary and Jurkat T lymphocytes (Fig. 9). In primary T lymphocytes, the $[\text{Ca}^{2+}]_i$ calibration

with the one- K_d model led to an overestimation of up to 18% whereas the $[Ca^{2+}]_i$ calibration in Jurkat T lymphocytes with the one- K_d model led to slight underestimation of up to 10%. Still, here was one K_d used for the Fluo-4/Fura Red dye combination and the *in situ* K_d was similar to a previously published *in vitro* K_d for Fluo-3 and Fura Red, 381 nM respectively (Lipp and Niggli, 1993). Interestingly, the same group reported three years later a K_d for Fluo-3/Fura Red of approx. 1.69 μ M obtained *in vivo* in cardiac myocytes (Lipp et al., 1996). This emphasizes how the intracellular environment, e.g. Ca^{2+} binding proteins, enzymes, and ions affect the K_d of Ca^{2+} indicators (Lipp et al., 1996). Since the K_d for Fluo-4/Fura Red was obtained with Jurkat T lymphocytes that were lysed after loading, the whole intracellular environment was still present, possibly explaining the slightly higher K_d (408 ± 12 nM) compared to the *in vitro* value (381 nM; Lipp and Niggli, 1993).

Interestingly, the $[Ca^{2+}]_i$ calibration of Jurkat and primary T lymphocytes resulted in different calibration curves (**Fig. 9**). To determine a $[Ca^{2+}]_i$ calibration, the identical instrumental sensitivity, optical path length and effective total dye concentration is needed (Grynkiewicz et al., 1985). Since the same instrumental sensitivity and optical path length were used for primary and Jurkat T lymphocytes, it is likely that the total dye concentration inside the cells varied. In primary T lymphocytes the same Fluo-4/Fura Red ratio resulted in a higher Ca^{2+} concentration, compared to Jurkat T lymphocytes, thus, higher dye concentration could be assumed. Moreover, in Jurkat T lymphocytes, a cancer T lymphocyte cell line, a higher density of multidrug-resistant pumps could be likely, hence, Fluo-4 and Fura Red could be actively secreted, leading to a decreased dye concentration (Amaral et al., 2007).

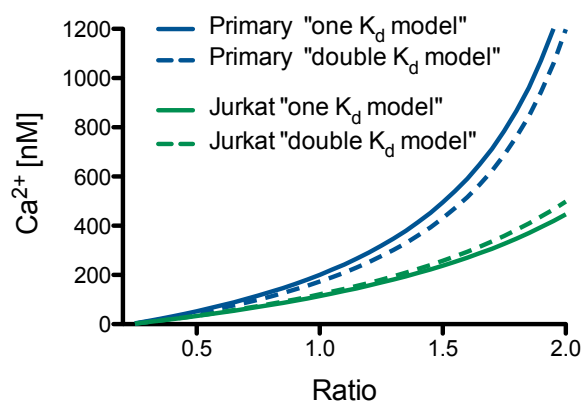


Fig. 9 Comparison of the $[Ca^{2+}]_i$ calibration from Jurkat and primary T lymphocytes using the one- and the double- K_d model

$[Ca^{2+}]_i$ calibration for the one- K_d model was performed as described by Grynkiewicz et al., 1985, with the *in situ* determined K_d of 408 ± 12 nM for Fluo-4/Fura Red dye combination. Jurkat and primary T lymphocytes were loaded with Fluo-4 AM and Fura Red AM. R_{max} was determined using ionomycin in saturated Ca^{2+} conditions and R_{min} was determined using the lowest ratio and fluorescence after chelation of Ca^{2+} with EGTA. The bleaching correction of Fura Red was not feasible in single-frame acquisition, thus it was assumed that the initial value of Fura Red was approx. as high as Fura Red after bleaching correction. For the double- K_d model the identical R_{max} and R_{min} values were used and the K_d for Fluo-4 (330 nM) and Fura Red (1069 nM) were taken from the Assinger et al., 2015 publication.

A general problem with the $[Ca^{2+}]_i$ calibration is that Ca^{2+} dyes inevitably alter the time course of $[Ca^{2+}]_i$ inside the cell through indicator buffering, even with an accurate calibration (Helmchen, 2011; Wang et al., 1997). Thus, the calibration of $[Ca^{2+}]_i$ is always only an approximate value and may not reflect the physiological levels that are reached in the absence of Ca^{2+} dyes (Helmchen, 2011).

Taken together, the combination of Fluo-4 and Fura Red allowed the calibration and for the first time also the measurement of subcellular Ca^{2+} microdomains in T lymphocytes with a temporal resolution of 40 frames/sec despite morphological cell shape changes (2.2 – Fig. S2 A lower panel, C).

3.1.4 Activation of T lymphocytes *in vitro*

There are many different methods to activate T lymphocytes *in vitro* under the microscope. The easiest way to stimulate T lymphocytes is obtained using soluble antibodies against the TCR complex, e.g. CD3, or co-stimulation with CD3 and CD28. One of the major disadvantages is that soluble antibodies bind their specific targets all over the T

lymphocyte plasma membrane, thus, the T lymphocytes are activated from all sides and no directed stimulation, as in an immune synapse, is possible.

In vivo T lymphocytes are activated via a directed stimulation by APCs, which present antigenic peptides bound to MHC together with co-stimulatory molecules (Kenneth Murphy, 2011; Kummerow et al., 2009). During this cell-cell-interaction T lymphocytes polarize and form a so-called immune synapse leading to morphological shape changes, with a central supramolecular activation cluster (cSMAC) consisting of TCR, a ring of adhesion molecules the peripheral SMAC (pSMAC) and a distal SMAC (dSMAC) with tyrosine phosphatase CD45 (Choudhuri et al., 2014; Dammermann et al., 2009; Freiberg et al., 2002; Kummerow et al., 2009; Monks et al., 1998).

One method to achieve a more directed activation of T lymphocytes is obtained by coating immobilized surfaces with anti-CD3 and anti-CD28 antibodies (Rossy et al., 2013). Rossy and co-workers could show a re-localization of lymphocyte-specific protein tyrosine kinase (Lck) starting 2 min after T lymphocyte activation via TCR triggering on coated glass cover slips (Rossy et al., 2013). Yet an immobilized surface, even when coated with antibodies cannot replace a cell-cell-interaction (Lillemeier et al., 2010). To address artifacts that can occur when using immobilized surfaces, activating fluid lipid bilayers containing potent peptide-MHC complexes (dimeric IE^k-MCC; Hamad et al., 1998) and intercellular adhesion molecule-1 (ICAM-1) could potentially stimulate T lymphocytes (Choudhuri et al., 2014; Lillemeier et al., 2010). In fluid lipid bilayers, peptides move freely, similar to peptides in the plasma membrane of cells, compared to solid surfaces. T lymphocytes activated via fluid lipid bilayers developed an immune synapse rapidly with a cSMAC after 5 min (Choudhuri et al., 2014). Already after 1 min a distribution of TCR and the linker of activated T cells (Lat) towards the center of the synapse was observed (Lillemeier et al., 2010).

A further improvement is the coating of antibodies on spheres, which mimic size and shape of T lymphocytes. Anti-CD3/CD28 coated beads are commonly used to activate and expand T lymphocytes *in vitro* (Guo et al., 2012; Hollyman et al., 2009; Li et al., 2007). Therefore, here magnetic beads coated with anti-CD3 antibodies (Jurkat T lymphocytes) or anti-CD3/ anti-CD28 antibodies (primary T lymphocytes) were used to activate the cells. The beads were similar in size and shape compared to the T lymphocytes and could activate them in a directed fashion, mimicking the T lymphocyte APC

interaction. Directly after contact with the coated beads Jurkat as well as primary T lymphocytes showed Ca^{2+} microdomains at the site of contact (2.2 – Fig. 1A, 3B).

Thus, compared to the *in vivo* activation a directed stimulation, with co-stimulation was feasible; still the activation with antibodies resembles not the *in vivo* activation with antigenic peptides bound to MHC. However, a cell-cell interaction could be mimicked with antibody-coated beads and initial subcellular Ca^{2+} microdomains in response to a directed, localized activation could be investigated for the first time.

3.1.5 Discrimination between signal and noise

One of the basic challenges with imaging data is the discrimination between noise and signals. Noise is defined, among other definitions, as “*unwanted disturbance superimposed upon a useful signal, which tends to obscure the signal’s information content*” (Dyer, 2004). Therefore, an optimal computational noise filter should remove these unwanted disturbance in the image while preserving the meaningful data, here the Ca^{2+} signals (Wang, 2003). Two different, commonly used, noise reduction approaches were applied, a temporal averaging and a low pass filter (Cardullo and Hinchcliffe, 2007; Wang, 2003). Temporal or frame averaging increases the signal-to-noise ratio and a major gain in noise reduction is already obtained with averaging just a few frames (Cardullo and Hinchcliffe, 2007). In contrast, a low pass filter eliminates high-frequency noise leading to a smoothing of the signal (Cardullo and Hinchcliffe, 2007).

First of all the noise of our system in ratio data of Fluo-4 and Fura Red was analyzed in a cell-free Ca^{2+} -EGTA buffer ($[\text{Ca}^{2+}] = 100 \text{ nM}$). In random regions of interest (ROIs), with a size of about $0.368 \mu\text{m}$ (the calculated spatial resolution for our system), the peak-to-peak amplitude was measured over time (2.2 – Fig. S2 D). The analysis of the raw data resulted in a mean amplitude of $21 \pm 4 \text{ nM } \text{Ca}^{2+}$ (Fluo-4/Fura Red ratio 0.15 ± 0.03). Applying a 2 Hz low pass filter resulted in a reduced peak-to-peak amplitude of $6 \pm 1 \text{ nM}$ (Fluo-4/Fura Red ratio 0.05 ± 0.01), while five-frame averaging, where five sequential images were merged to generate an average image, decreased the peak-to-peak amplitude to $9 \pm 2 \text{ nM}$ (Fluo-4/Fura Red ratio 0.06 ± 0.02 ; 2.2 – Fig. S2 D). To discriminate between noise and signal a commonly used factor is twice to three times the signal-to-noise ratio (SNR) for analytical method validation (Shrivastava and Gupta, 2011). Thus, here for the Ca^{2+} signals three times peak-to-peak amplitude was

used for the detection of initial subcellular Ca^{2+} release events. For 2 Hz low-pass filtered data, this was 18 nM in Jurkat T lymphocytes. Since the $[\text{Ca}^{2+}]_i$ calibration of primary T lymphocytes resulted in a steeper calibration curve (**Fig. 9**), three times peak-to-peak amplitude after 2 Hz low pass filtering was 32 nM. The five-frame averaging method was applied to ratio figures.

In conclusion, the newly established Ca^{2+} signaling method is technically limited by an amplitude differences as low as 18 nM (Jurkat T lymphocytes) or 32 nM (primary T lymphocytes) at a temporal resolution of ~ 40 frames/sec and a calculated spatial resolution of ~ 368 μm .

3.2 Automation of the post-processing workflow

The post-processing of single cell, subcellular Ca^{2+} imaging data is very time-consuming (**Fig. 10A**). After the acquisition with a Dual-View module in front of the EMCCD camera (electron-multiplying charge-coupled device camera; C9100, Hamamatsu) the emission signal of Fluo-4 and Fura Red was split in ImageJ (Schindelin et al., 2012). Moreover, both emission wavelengths were background-corrected and the bleaching of Fura Red was also corrected. In Openlab (Version 5.5.2, PerkinElmer Inc.) a no-neighbor deconvolution was applied to obtain digital confocal images. Before the ratioing, both emission wavelength images were registered manually in Openlab. The ratiometric images were median filtered (3x3 pixels) and exported as tiff or movie files. This whole post-processing took altogether approx. 1 - 2 hours to analyze one single cell (**Fig. 10A**). In cooperation with Dr. René Werner from the Department of Computational Neurosciences at the University Medical Center Hamburg-Eppendorf, we were able to automatize and optimize our established post-processing workflow (**Fig. 10B**).

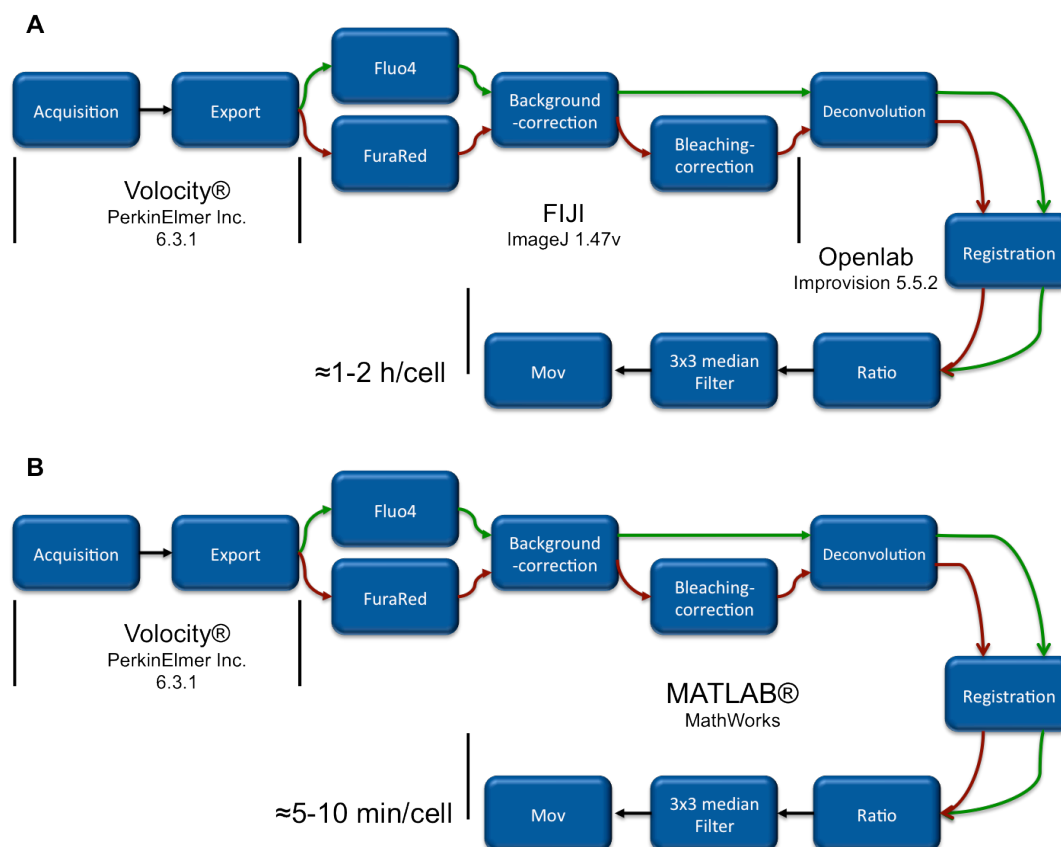


Fig. 10 Comparison of the post-processing workflows

Comparison of the established (A) and the automatized post-processing (B) workflow. (A) The acquisition and export of Ca^{2+} image data was done with Volocity (version 6.3.1; PerkinElmer Inc.). Afterwards in ImageJ 1.47v (Schindelin et al., 2012) the Fluo4 and Fura Red channels were split and both emission wavelengths were background corrected. Furthermore, the bleaching of Fura Red was corrected trough a bi-exponential decay function using a modified Bleach Corrector plug-in by K. Miura and J. Rietdorf (http://cmci.embl.de/downloads/bleach_corrector). Openlab software (Version 5.5.2, PerkinElmer Inc.) was used for image deconvolution, post-measurement registration, ratioing of the two emission wavelengths and applying a median filter (3x3 pixels). In the end movies or tiff files were saved. This workflow was very time-consuming and it took about 1-2 hours per cell to get a ratiometric movie. (B) The acquisition and export of Ca^{2+} image data was also done with Volocity (version 6.3.1; PerkinElmer Inc.); all other post-processing steps were automatized and implemented in MATLAB (MathWorks), leading to a 12 – 24 times faster post-processing workflow.

The automation of our established post-processing workflow decreased the single cell post-processing time to 5 – 10 min, leading to a 12 – 24 times faster post-processing time. Further, only one program was needed for the whole post-processing workflow and, for example, the manual registration was replaced by an automated rigid sum of squared intensity difference registration.

3.2.1 Comparison of different deconvolution algorithms

Deconvolution is an image-processing method that aims to computationally restore a distorted image and to reverse the effects of out-of-focus blurring in the microscope (Goodwin, 2014; Sibarita, 2005). Thus, the intention of deconvolution is to reassign optical out-of-focus blur to its original position and, hence, to reduce statistical noise (Sibarita, 2005). The blurring of a sample by an objective lens is represented by the point-spread function (PSF). The PSF can be either calculated computationally (Gibson and Lanni, 1991; Marian et al., 2007) or directly measured by imaging sub-resolution fluorescently-coated microspheres using the same optical set-up as for the samples (Wallace et al., 2001). Deconvolution can be generally divided in (A) deblurring and (B) image restoration algorithms (Goodwin, 2014).

In our established post-processing workflow, a classical deblurring algorithm (no-neighbor deconvolution algorithm) with an analytical PSF implemented in Openlab was used. Here, two different image restoration deconvolution algorithms were compared the Wiener deconvolution (WNR; Sibarita, 2005) and the Lucy-Richardson deconvolution (LR; Lucy, 1974; Richardson, 1972). Furthermore, analytically computed as well as experimentally acquired PSFs were tested. For the experimentally acquired PSF, fluorescently coated microspheres with a diameter of 0.1 μm were imaged in our set-up. Generally, better results are obtained using empirically acquired PSFs, especially with high-numerical aperture objective lenses (NA lenses; Hiraoka et al., 1987, 1990). To evaluate the quality of the different deconvolution algorithms and PSFs commonly used parameters were analyzed, like the SNR (Sibarita, 2005; Swedlow and Platani, 2002) and the full width at half maximum (FWHM) intensities (**Tab. 1**; Sedarat et al., 2004). The different deconvolution algorithms were applied to images of the same microspheres used for the empirically acquired PSF (**Tab. 1**). Moreover, the impact of the deconvolution approaches and the different PSFs was compared to the Ca^{2+} dynamics (number and diameter of local Ca^{2+} signals and maximum observed path lengths of Ca^{2+} signals over time) of the established post-processing workflow (2.1 – **Tab.1** upper part).

Tab. 1 Summary of the Full-Width-Half-Maximum and the Signal-to-Noise Ratio after different deconvolution algorithms of a 0.1 μm microsphere. RAW = unprocessed; LR = Lucy-Richardson deconvolution; WNR = Wiener deconvolution; Exp = experimentally acquired PSF; Analyt = analytically computed PSF.

| | Full-Width-Half-Maximum [μm] | Signal-to-Noise Ratio |
|-----------|--|-----------------------|
| RAW | 3.56 | 1631 \pm 0.07 |
| OpenLab | 1.55 | 190 \pm 0.27 |
| LRExp | 3.45 | 1816 \pm 0.03 |
| LRAlyt | 0.80 | 2333 \pm 0.02 |
| WNRExp | 8.94 | 59 \pm 0.001 |
| WNRAnalyt | 16.36 | --- |

The Wiener deconvolution algorithm failed to clearly separate signal and noise whatever PSF was applied (Tab. 1, 2.1 – Tab.1 upper part). In contrast, the LR deconvolution algorithm detected a similar number of Ca^{2+} signals, diameters and path length with both PSFs (2.1 – Tab.1 upper part). Interestingly the LR approach with the experimental PSF was closest to the reference of the established workflow, but the analytical PSF applied to the LR algorithm resulted in a superior SNR and was able to reduce the microsphere spreading by >40% (Tab. 1). McNally and co-workers also observed good similarity between analytically computed and experimentally acquired PSFs using low-NA objective lenses (McNally et al., 1994).

Additionally, Jurkat T lymphocytes were loaded with LysoTracker[®] (Molecular Probes, Life Technologies) to compare the LR deconvolution with unprocessed images and the OpenLab deconvolution in a whole cell (Fig. 11). Lysosomes are spherical compartments inside the cell with a diameter of approx. 0.55 μm in mammalian cells (Glunde et al., 2003). Since Ca^{2+} signals can be very small and spherical, here the loaded lysosomes were used for comparison.

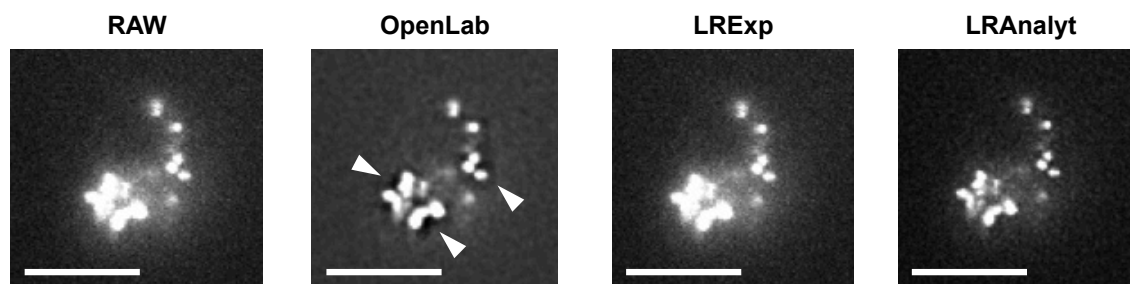


Fig. 11 Impact of different deconvolution algorithms on image quality

Jurkat T lymphocytes were loaded with 75 nM LysoTracker[®] (Molecular Probes, LifeTechnologies) for 1h at 37°C. Imaging was performed using a Leica IRBE2 microscope with 100x magnification, a Sutter DG-4 as lights source and an electron-multiplying charge-coupled device camera (C9100, Hamamatsu). Arrowheads indicate dark artifacts. Scale Bar represents 10 μm . RAW = unprocessed; LR = Lucy-Richardson deconvolution; Exp = experimentally acquired PSF; Analyt = analytically computed PSF.

The LR deconvolution approach with the experimentally obtained PSF (LRExp) is almost identical to the unprocessed image (RAW; **Fig. 11**). The Openlab deconvolution resulted in a higher background and moreover, some dark artifacts appeared around the lysosomes (indicated with arrow-heads). In conclusion, the LR deconvolution algorithm with the analytically derived PSF resulted in the best restoration of the lysosomes and Ca^{2+} signals in T lymphocytes (**Fig. 11**), although in our microscope set-up high-NA objective lenses are used.

3.2.2 Evaluation of bleaching correction strategies

Bleaching or photobleaching is a process where fluorophores are irreversibly damaged by the radiation within the excitation spectrum, hence, the overall intensity decreases (Vicente et al., 2007). Fluorophores in their excited state can react with oxygen and thereby generate non-fluorescent molecules (Bootman et al., 2013).

Fura Red is strongly affected by photobleaching during fast acquisition but in the established post-processing workflow, the bleaching was corrected by a bi-exponential fitting curve with a multiplicative correction (2.2 – Fig. S1 D). This means that the bleaching correction was performed by multiplying all fluorescence values with one correction factor according to the bi-exponential fitting curve (**Fig. 12**). For the parameters of the bi-exponential fitting curve, data from four different cells was obtained. Using these parameters, the correction factor for each frame was calculated (**Fig. 12**).

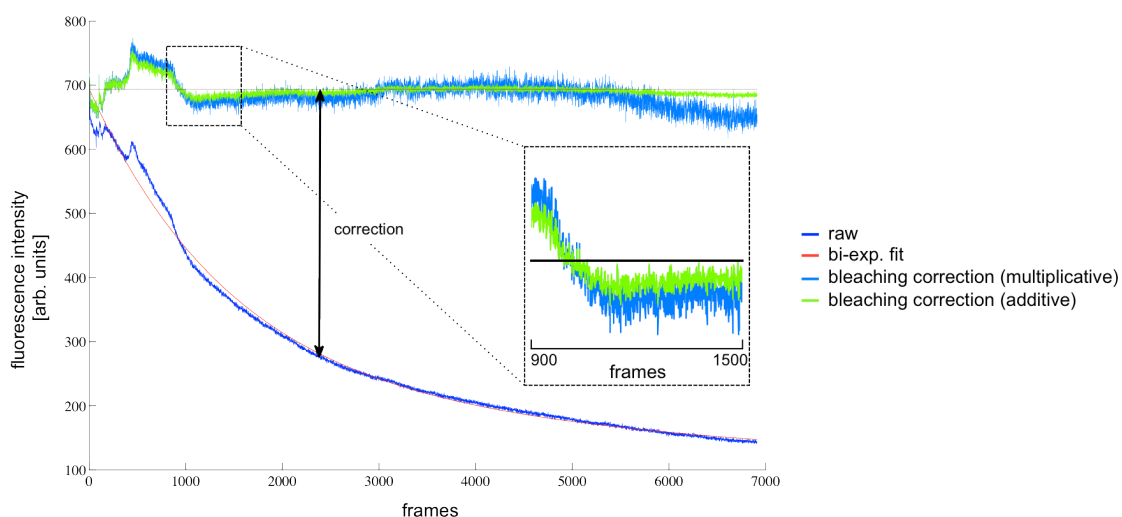


Fig. 12 Comparison of the multiplicative and additive bi-exponential bleaching correction of Fura Red in WT T lymphocytes

The dark blue line shows the unprocessed (RAW) characteristics of Fura Red in a WT T lymphocyte after stimulation with antibody-coated bead. The bi-exponential fitting curve is depicted in red (bi-exp. fit) and the different bleaching correction strategies are displayed in light blue (multiplicative) and green (additive). Inlet magnifies the different bleaching correction strategies in the first 600 frames (approx. 40 frames/sec thus 15sec) after bead contact.

However, a multiplicative correction led to higher standard deviation and thus an amplification of the signal noise over time compared to an additive correction (**Fig. 12**). Therefore, the conservative additive correction strategy, where the difference in intensity due to bleaching, was summated rather than multiplied, was tested (**Fig. 12**). Even more, instead of the bi-exponential fitting curve, the bleaching of Fura Red was antagonized via specific elevation of single pixels to the overall mean intensity values at the start of the measurement (**Fig. 13**). This was done for each frame, hereafter named frame-by-frame approach. Hence, the mean value of Fura Red at the beginning of the acquisition remained the same during the measurement through additive as well as a multiplicative correction (**Fig. 13A**).

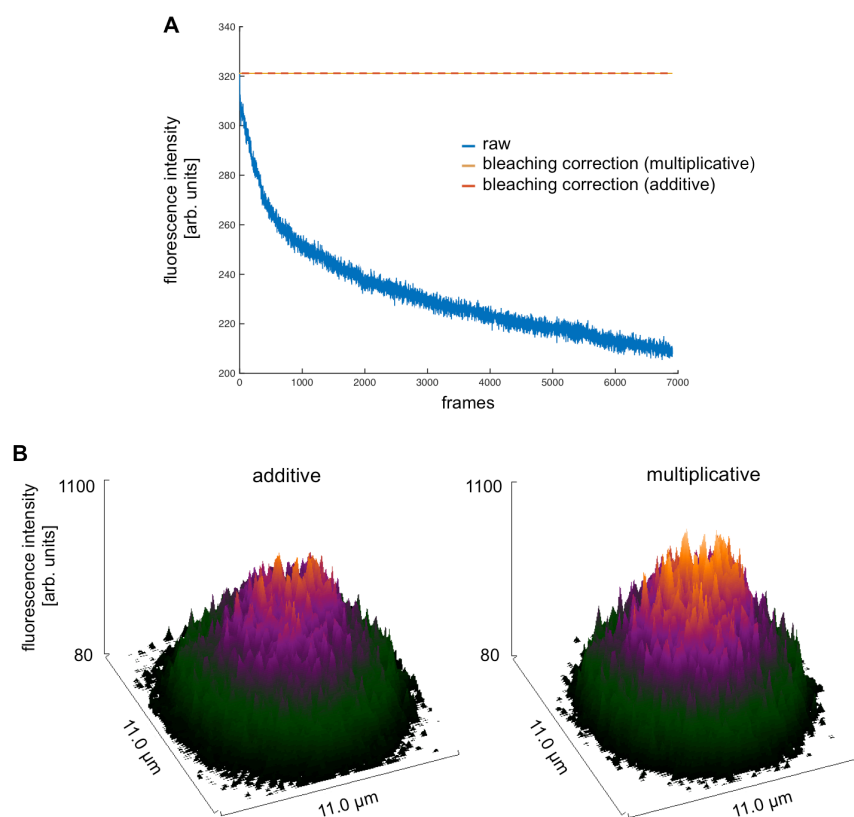


Fig. 13 Comparison of the frame-by-frame elevation using additive and multiplicative approaches

(A) The blue line shows the unprocessed (RAW) characteristics of Fura Red in a $CD3^+$ WT T lymphocyte after stimulation with antibody-coated bead and the different bleaching correction strategies are displayed in dashed lines in orange (multiplicative) and red (additive). (B) Comparison of the Fura Red fluorescence after different bleaching correction strategies (as indicated) at the end of the measurement.

While the additive, as well as multiplicative bleaching corrections, resulted in the same mean intensity (**Fig. 13A**), the intensity values inside the cells varied dramatically, with a higher signal noise using the multiplicative approach (**Fig. 13B**). Furthermore, with the frame-by-frame bleaching correction Fura Red is not anymore participating to the dynamics of the Ca^{2+} induced fluorescent signal, but it is exclusively dominated by Fluo-4 resulting in a pseudo-ratiometric measurement (Morgan et al., 2015). Hence, for the $[Ca^{2+}]_i$ calibration the *in situ* obtained K_d for Fluo-4 only is needed in further experiments as shown for pseudo-ratiometric imaging in lysosomes (Lloyd-Evans et al., 2008; Morgan et al., 2015; Sherwood et al., 2007). In lysosomes, a combination of Fluo-3 and Texas Red, a Ca^{2+} insensitive dye, was used (Morgan et al., 2015). Though the dynamic range of the ratio was reduced, only the K_d of Fluo-3 was needed for the calibration (Morgan et al., 2015).

To further evaluate the different bleaching correction approaches, the same Ca^{2+} dynamic parameters as for the comparison of the different deconvolution algorithms were used (2.1 – Tab.1 lower part). Comparing the bi-exponential fitting curve with the frame-by-frame elevation using the multiplicative correction resulted in a similar amplitude of Ca^{2+} signals, signal diameter and maximum observed path lengths of Ca^{2+} signals over time (2.1 – Tab.1 lower part). For the additive correction less, Ca^{2+} signals were found and the observed path lengths were shorter, as expected due to the potentially noise amplifying potential of the multiplicative approach (2.1 – Tab.1 lower part). Comparing the bi-exponential fitting curve with the frame-by-frame elevation approach using the additive correction rather small differences were obtained, but suboptimal bi-exponential fitting of Fura Red resulted in artificial Ca^{2+} signals (**Fig. 12**). Thus, although the amount of available fluorophores was reduced due to photobleaching and thus potential useful information was eliminated (Vicente et al., 2007), the frame-by-frame elevation approach using the additive correction provided the most robust bleaching correction strategy for Fura Red in T lymphocytes and with this approach only one K_d for the $[\text{Ca}^{2+}]_i$ calibration is needed.

3.3 Analyzing the fundamental Ca^{2+} network during T lymphocyte activation

Already in 2000, it was shown that NAADP is an essential regulator of T lymphocyte Ca^{2+} signaling and activation of the adaptive immune response (Berg et al., 2000). Thus, the initial Ca^{2+} signals triggered by NAADP seem to regulate the fate of the T lymphocytes. Upon specific extracellular stimulation, fast production of NAADP after 10 sec has been observed in human Jurkat T lymphocytes (Gasser et al., 2006). Still the proposed target receptors of NAADP, RyRs, the TPCs, TRPM2, and TRP-ML1, are controversially discussed (Guse et al., 2013).

3.3.1 Initial Ca^{2+} microdomains in T lymphocytes

The major problem to capture initial Ca^{2+} signals was the spatio-temporal resolution of imaging systems. With the new Ca^{2+} live cell-imaging method developed in this thesis

this problem could be solved and for the first time initial, local Ca^{2+} microdomains after directed stimulation could be analyzed.

Directly after contact with an antibody-coated bead, Ca^{2+} microdomains were observed at the site of stimulation in Jurkat and primary WT T lymphocytes (2.2 – Fig. 1A, 3B, 6A). To exclude unspecific activation of the T lymphocytes, beads were coated with an unspecific anti-IgG antibody. In ~20% of the primary WT T lymphocytes stimulated with these beads Ca^{2+} signals were observed, but the number of signals per cells and the amplitude was dramatically reduced. Hence, beads coated with anti-CD3 or anti-CD3/anti-CD28 specifically activated the T lymphocytes (2.2 – Fig. 3A).

Interestingly, the initial Ca^{2+} signals showed a bi-phasic pattern. For example in Jurkat T lymphocytes the first signals were observed directly at the plasma membrane after 0.13 sec for approx. 1 sec. Then the initial signals nearly completely diminished but after approx. 8 sec new Ca^{2+} signal arose still close to the site of stimulation, but not directly at the plasma membrane (2.2 – Fig. 1A). Similar responses were also observed in primary WT T lymphocytes but on a slightly different time-scale (2.2 – Fig. 3B, 6A). In primary WT T lymphocytes, the initial Ca^{2+} microdomains were also observed directly after bead contact at the site of stimulation and diminished again after approx. 1 sec. However, the second Ca^{2+} response was observed in a range between 9 - 50 sec after the initial activation (2.2 – Fig. 3B, 6A). TCR-mediated signaling of primary T lymphocytes is likely modulated by differentiation conditions (Farber et al., 1997; Hussain et al., 2002). The freshly isolated primary T lymphocytes were a mixture of naïve, effector and memory T lymphocytes with characteristic differentiation conditions, and this could explain the huge variation and the slower second Ca^{2+} response in comparison to Jurkat cells. Naïve T lymphocytes are mature but resting T lymphocytes that have never encountered an antigen in the periphery and thus have not been activated (Berard and Tough, 2002; Broere et al., 2011; Hussain et al., 2002). In contrast effector or memory T lymphocytes have been activated in the periphery (Berard and Tough, 2002). Generally, effector T lymphocytes are hyper-responsive to TCR stimulation with anti-CD3 (Ahmadzadeh et al., 2001), although the CD3 expression is down-modulated (Liu et al., 2000). In contrast, memory T lymphocytes are hypo-responsive and naïve T lymphocytes exhibit an activation kinetic midway of those two in proliferation assays (Ahmadzadeh et al., 2001). Moreover, these T lymphocytes subsets differ in their expression of lymphocyte cytosolic protein 2 (LCP2 or SLP-76; Hussain et al., 2002). SLP-76 is an adapter protein that is phosphorylated via ZAP-70 upon TCR-mediated

stimulation of the T lymphocytes. Relative to naïve T lymphocytes, memory T lymphocytes express fewer amounts while effector T lymphocytes express similar to elevated levels of SLP-76 (Hussain et al., 2002), corresponding to the proliferation kinetic after TCR stimulation with anti-CD3 (Ahmadzadeh et al., 2001). Furthermore, the RyR1 expression is significantly increased *in vitro* in effector T lymphocytes (von Osten, 2015). This could lead to a faster release of Ca^{2+} from the ER, hence a faster second Ca^{2+} response and also a higher proliferation rate.

Taken together, these differences in functional and differentiation conditions could explain the variable and mostly slower Ca^{2+} response in primary T lymphocytes. Therefore it would be interesting to analyze particularly primary effector T lymphocytes; possibly their bi-phasic response would be closer to the Jurkat T lymphocytes, although Jurkat T lymphocytes, especially the JMP clone used in our laboratory, has a high CD3 expression.

3.3.1.1 Initial bi-phasic Ca^{2+} response in T lymphocytes

How could such an initial bi-phasic Ca^{2+} response in T lymphocytes be explained? One possibility may be that these first, initial signals are artifacts, which result from the low intrinsic fluorescence of the magnetic beads added to stimulate the T lymphocytes. However, using IgG-coated beads no such initial signals directly at the site of stimulation could be observed (**Fig. 14**). Thus, it seems very unlikely that the initial Ca^{2+} signals are artifacts caused by the magnetic beads.

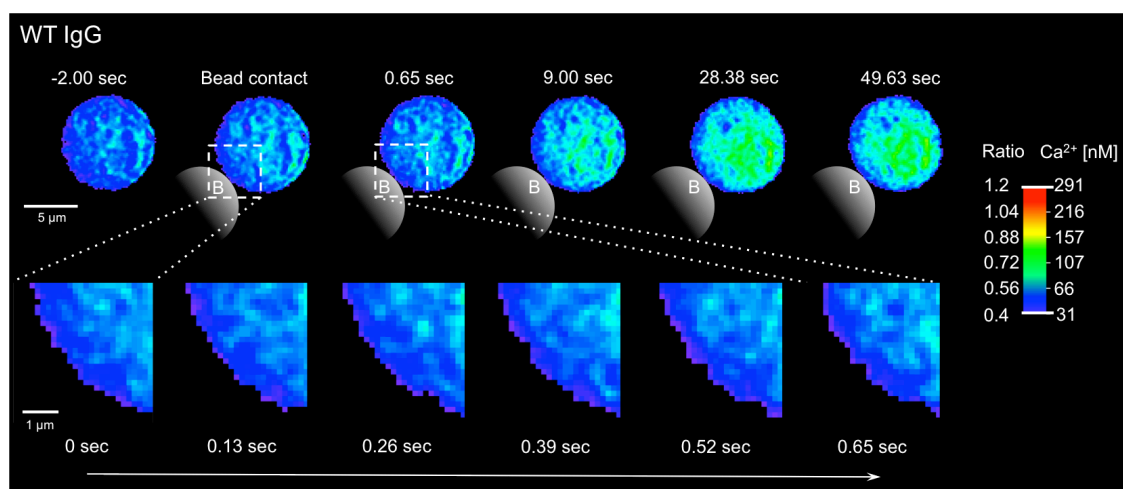


Fig. 14 Ca^{2+} microdomains in primary T lymphocytes after stimulation with IgG-coated beads

Shown is one representative cell from the 9 WT neg. cells (2.2 – Fig. 3A). Primary CD3^+ WT T lymphocytes were freshly isolated from spleens by negative selection. The cells were loaded with Fluo-4 AM and Fura Red AM and Ca^{2+} imaging was performed as described Materials and Methods section 2.2. IgG-coated beads were used to stimulate the cells and bead contact sites are indicated schematically. Top: Frame scan of initial localized Ca^{2+} release events in a primary WT T lymphocyte upon bead contact. Bottom: Frame scan of a magnified region ($4 \times 4 \mu\text{m}$) of the same cell near the bead is presented from the time of bead contact until 0.65 sec after contact. Five sequential images were merged to generate an average image to decrease noise.

Another explanation would be that two different compartments or Ca^{2+} releasing second messengers are involved; especially since the Ca^{2+} signals do not occur at the same positions (2.2 – Fig. 1A).

NAADP is the most potent, endogenous Ca^{2+} mobilizing second messenger (Chini et al., 1995; Lee and Aarhus, 1995) that is synthesized rapidly after T lymphocytes stimulation with anti-CD3 antibodies (Gasser et al., 2006). Thus, NAADP is the best candidate to be responsible for the formation of initial Ca^{2+} microdomains; the first Ca^{2+} responses. However, a significant increase of NAADP after Okt3 stimulation in Jurkat T lymphocytes was observed first after 10 sec (Gasser et al., 2006). However, for these experiments, an enzymatic cycling assay was used to quantify the endogenous NAADP concentration of whole cell lysates after stimulation and no shorter time points were analyzed (Gasser et al., 2006). Hence, it is possible that the NAADP concentration already rises in T lymphocytes directly after stimulation and NAADP triggers the development of initial Ca^{2+} microdomains.

In 2001 a two-pool model for NAADP signaling has been suggested which was redefined in 2012 by a unifying hypothesis (Churchill and Galione, 2001; Guse, 2012). This

unifying hypothesis divided actions of NAADP in different steps. First, NAADP is formed, followed by the interaction with a putative binding protein (bp). The NAADP-bp has not yet been identified. However, with the help of 5-N₃-NAADP, a radioactively labeled NAADP photo affinity analog, small cytosolic proteins (22/23 kDa) have been discovered in mammalian cells that showed the highest affinity to NAADP (Lin-Moshier et al., 2012). If NAADP mediates the initial Ca²⁺ events coupled to a bp already in msec (2.2 – Fig. 1A, 3B, 6A) the NAADP-bp has to be constantly available inside the cell. Presumably, the bp may get directly activated upon NAADP binding or could be activated by phosphorylation or de-phosphorylation. Reversible phosphorylation is the most widespread protein modification (Cieřla et al., 2011) and an essential step in the activation of T lymphocytes (Lillemeier et al., 2010; Rossy et al., 2013).

After the NAADP-bp complex is formed, low amounts of Ca²⁺ are released in a trigger zone probably through lysosomal receptors (TPCs and TRP-ML1). RyRs and IP₃Rs on the ER subsequently amplify these initial Ca²⁺ signals through CICR. Thus, the first Ca²⁺ signals could be triggered by TPC and/or TRP-ML1, amplified by RyRs and IP₃Rs on the ER. Interestingly, the inhibition of IP₃R neither reduced the number of Ca²⁺ signals nor the number of responding Jurkat T lymphocytes after bead stimulation (2.2 – Table 1). Thus, IP₃ does not seem to be involved in the early CICR. Moreover, the formation of IP₃ in Jurkat T lymphocytes after stimulation with anti-CD3 (Okt3) antibodies was observed after 3 – 5 min rather than in secs (Guse et al., 1995b), thus IP₃ seems not to trigger the initial Ca²⁺ microdomains.

A recent publication showed that in pancreatic acinar cells both the RyRs and TPCs are required for NAADP-induced intracellular Ca²⁺ release events (Gerasimenko et al., 2015). Inhibition of RyR1 with antibodies in these cells resulted in a similar decreased NAADP-induced Ca²⁺ release as TPC2-KOs where TPC1 was additionally blocked with antibodies (Gerasimenko et al., 2015). Still in both experiments, few NAADP-induced Ca²⁺ signals were observed, which were explained by the cooperation of RyR1 and TPC1/2 (Gerasimenko et al., 2015). Controversially, in many reports TPCs were found to be Na⁺ selective ion-channels, and not primarily Ca²⁺ selective ion-channels (Cang et al., 2013, 2014a, 2014b; Wang et al., 2012). Furthermore, no evidence for the regulation of TPCs by NAADP was found, but instead, the membrane lipid PI(3,5)P₂ evoked Na²⁺ currents (Cang et al., 2013; Wang et al., 2012). In T lymphocytes, there is good evidence that the RyRs might be involved in the formation of initial Ca²⁺ microdomains targeted by NAADP (Dammermann and Guse, 2005; Dammermann et al., 2009;

Langhorst et al., 2004). In other cell types, like the pancreatic acinar cells, also the TPCs might participate (Gerasimenko et al., 2015). Furthermore, the NAADP-bp could be the missing link for understanding the different NAADP sensitive channels in different cell types (Guse, 2012).

Since the first signals were observed directly at the plasma membrane TRPM2 or the CRAC channels could be involved in the formation of trigger Ca^{2+} . However, CRAC channel formation in Jurkat T lymphocytes was first observed 8 min after Raji cell contact (Quintana et al., 2011). Further, STIM1 redistributed to punctae near the plasma membrane after 10 min (Smyth et al., 2008).

Taken together, for the first time, a bi-phasic Ca^{2+} pattern in T lymphocytes was observed in the first seconds after a directed activation. However, many different Ca^{2+} channels could be involved in the formation of this initial bi-phasic Ca^{2+} pattern in T lymphocytes.

3.3.1.2 Comparison of initial Ca^{2+} microdomains in T lymphocytes to previously described Ca^{2+} sparks and quarks

The Ca^{2+} signals observed in Jurkat T lymphocytes in the first 15 secs after bead stimulation were characterized by an amplitude of ~ 79 nM (Fluo-4/Fura Red ratio 0.79 ± 0.01) and a diameter of ~ 0.43 μm . A summary of previously described Ca^{2+} sparks and quarks in comparison to the initial Ca^{2+} microdomains observed in Jurkat and primary T lymphocytes is shown in **Tab. 2**.

Tab. 2 Comparison of initial Ca^{2+} signals to previously described Ca^{2+} sparks and quarks.

Jurkat = Jurkat T lymphocytes; primary = primary T lymphocytes.

| | Ca^{2+} amplitude [nM] | ratiometric amplitude | diameter [μm] |
|--|------------------------------------|--------------------------|-------------------------------|
| Jurkat | 79 ± 4 | 0.79 ± 0.01 | 0.43 |
| primary | 180 ± 5 | 0.90 ± 0.02 | 0.37 |
| Ca^{2+} sparks (Bootman et al., 2001; Cheng and Lederer, 2008; Niggli, 1999) | ~ 170 | $\Delta 0.2 - 4.0$ | 2.0 |

| | | | |
|--|--------|-----|------------|
| Ca ²⁺ quarks (Cheng and Lederer, 2008; Lipp and Niggli, 1998) | 37 ± 6 | --- | 0.4 – 0.85 |
|--|--------|-----|------------|

Ca²⁺ sparks have been proposed to result from clusters of RyRs and to underlie the CICR (Lipp and Niggli, 1998). The ratiometric amplitude of Ca²⁺ sparks varies widely, from $\Delta F/F_0 \sim 0.2$ to ~ 4 in ventricular myocytes which resemble a calibrated amplitude of ~ 170 nM (Bootman et al., 2001; Cheng and Lederer, 2008; Niggli, 1999). Furthermore the FWHM of Ca²⁺ sparks in cardiac muscle cells were $2.0 \mu\text{m}$ during the peak signal (Cheng and Lederer, 2008). Hence, the observed Ca²⁺ signals were approx. five times smaller in size and nearly half the calibrated amplitude of Ca²⁺ sparks, suggesting that these initial Ca²⁺ signals were more closely related to Ca²⁺ quarks. Ca²⁺ quarks are associated with the Ca²⁺ release through single RyRs (Cheng and Lederer, 2008) and are characterized by an amplitude of $\sim 37 \pm 6$ nM and a spatial spread of $0.85 \pm 0.2 \mu\text{m}$, although the size of the smallest Ca²⁺ signaling events were $\sim 0.4 \mu\text{m}$ (Lipp and Niggli, 1998).

Interestingly, a marked difference in the amplitude between Jurkat and primary T lymphocytes was observed. In primary WT T lymphocytes the initial Ca²⁺ release events were even smaller in size but the amplitude (~ 180 nM; Fluo-4/Fura Red ratio 0.90 ± 0.02) was nearly twice as high, compared to Jurkat T lymphocytes. Maybe larger clusters of RyRs are activated, more NAADP is synthesized or less Ca²⁺ binding proteins are expressed in primary T lymphocytes that buffer the Ca²⁺ signal. Additionally, when comparing Ca²⁺ signals with published Ca²⁺ sparks and quarks one has to take into account that different cell types (e.g. cell size, expression levels of Ca²⁺-bp, -channels, -pumps) and also different Ca²⁺ indicators and microscopes (e.g. cameras, light-sources, filters) are used for the analysis Ca²⁺ sparks and quarks, thus a direct comparison is challenging.

3.3.2 Using knockouts to decode the fundamental Ca²⁺ network T lymphocytes

Among others, RyRs and TRPM2, are considered as the target receptors of NAADP (Beck et al., 2006; Dammermann and Guse, 2005; Hohenegger et al., 2002; Lange et al.,

2008; Langhorst et al., 2004). Here RyR knockdown Jurkat T lymphocytes, RyR1-KO and TRPM2-KO primary T lymphocytes were analyzed to understand the formation of the initial, bi-phasic Ca^{2+} response.

3.3.2.1 Involvement of RyRs in the formation of initial Ca^{2+} signals in T lymphocytes

RyR knockdown in Jurkat cells, as well as the RyR1-KO in primary T lymphocytes, had similar effects on initial Ca^{2+} signals (2.2 – Fig. 3A). The number of responding cells was reduced about ~45% of the cells, no bi-phasic Ca^{2+} pattern and no initial Ca^{2+} microdomains at the site of stimulation could be observed (2.2 – Fig. 2A, 3C). Additionally, the numbers of signals per cell were approx. twofold reduced in comparison to the control and WT T lymphocytes. If the initial Ca^{2+} signals would be exclusively mediated by RyRs one would expect a lower spatial spread of these signals but interestingly the size of the initial Ca^{2+} signals was not altered in RyR knockdown Jurkat cells and RyR1-KO in primary T lymphocytes compared to the controls, hence additional Ca^{2+} channels have to be involved. Still the $[\text{Ca}^{2+}]_i$ amplitude was significantly lower in RyR knockdown Jurkat cells and RyR1-KO in primary T lymphocytes compared to the controls (2.2 – Fig. 3A). Thus, the RyRs, at least partly, are involved in shaping the bi-phasic Ca^{2+} pattern and formation of the initial Ca^{2+} microdomains. Although RyR3 is expressed in effector T lymphocytes (von Osten, 2015), RyR3 does not seem to be the additional Ca^{2+} channel involved in the formation of initial Ca^{2+} microdomains (**Fig. 15**). There is no significant difference in the number of responding cells, the number of signals per cell and $[\text{Ca}^{2+}]_i$ amplitude in the first 15 sec after T lymphocyte stimulation with anti-CD3/anti-CD28 coated beads. However, there is a slight reduction in $[\text{Ca}^{2+}]_i$ amplitude in RyR3-KO T lymphocytes, implying that RyR3 has minor effects on the Ca^{2+} release from the ER but the RyR3-KO is probably compensated by RyR1.

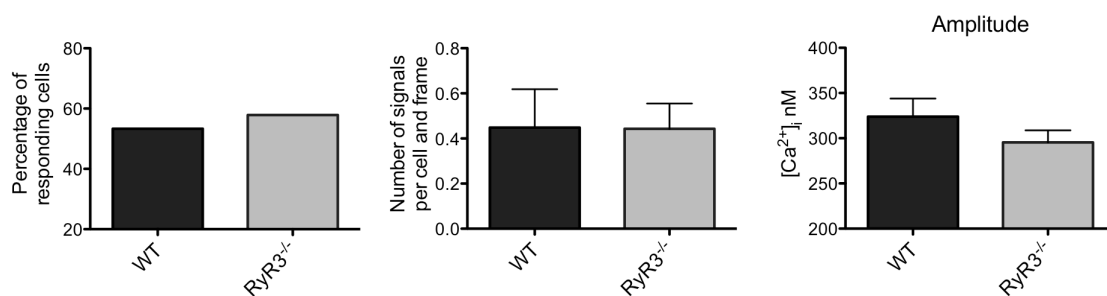


Fig. 15 Initial Ca²⁺ microdomains in primary WT and RyR3-KO T lymphocytes

Primary CD3⁺ WT and RyR3-KO T lymphocytes were freshly isolated from spleens by negative selection. The cells were loaded with Fluo-4 AM and Fura Red AM and Ca²⁺ imaging was performed as described Materials and Methods section 2.2. Anti-CD3/ anti-CD28-coated beads were used to stimulate the cells and the characteristics of initial Ca²⁺ microdomains were analyzed using MATLAB. In every frame of the first 15 sec Ca²⁺ signals with an amplitude $\geq 112,5$ nM and size ≥ 368 nm were detected. Data are means \pm SEM of 30 to 38 cells. * $P < 0.05$, ** $P < 0.01$, *** $P < 0.001$ by the Mann-Whitney U test.

To easily compare the initial, localized Ca²⁺ signals of different cell types and treatments a combined parameter was formed. This so-called “mean responsiveness” is the product of the number of signals per cell and the amplitude. In the mean responsiveness, a statistically significant decrease between control cells and RyR knockdown and primary RyR1-KO T lymphocyte was found (2.2 – Fig. 4). Furthermore, pharmacological inhibition of RyRs in control Jurkat T lymphocytes with 50 μ M ryanodine reduced the number of responding cells and the amplitude while the number of signals per cell was not affected (2.2 – Table 1). Interestingly, also significant differences in global Ca²⁺ signals were observed comparing Jurkat WT and RyR knockdown T lymphocytes (2.2 – Fig. S5) indicating that these initial Ca²⁺ release events are essential for the global Ca²⁺ T cell activation and that RyRs are essential for the CICR in T lymphocytes.

In conclusion, these results suggest that the RyRs (RyR1 in primary T lymphocytes) are involved in the formation of initial Ca²⁺ signals and CICR in T lymphocytes. RyR3, at least in primary T lymphocytes, seems to have no association in Ca²⁺ microdomain development. Still the initiation of these initial Ca²⁺ signals did not strictly depend on RyRs, thus, additional Ca²⁺ channels seemed to be involved.

3.3.2.2 TRPM2 is not linked to the formation of initial Ca^{2+} signals in primary T lymphocytes

Since TRPM2 has been proposed as one of the target receptors of NAADP (Beck et al., 2006; Lange et al., 2008) and has been described as a plasma membrane and lysosomal channel (Faouzi and Penner, 2014), TRPM2 may be the missing link for the bi-phasic Ca^{2+} response of T lymphocytes. However, TRPM2 in primary T lymphocytes is not involved in the formation of initial Ca^{2+} signals (2.2 – Fig. 6). Neither the number of signals per cell, the amplitude nor the mean responsiveness was reduced in primary TRPM2-KO T lymphocytes; even more, all these parameters were slightly but not significantly increased in TRPM2-KO cells (2.2 – Fig. 6C). Only the number of responding cells was slightly decreased in TRPM2-KO T lymphocytes. Furthermore, the initial Ca^{2+} microdomains in TRPM2-KO T lymphocytes were located directly at the bead contact site, similar to WT T lymphocytes and these also showed a distinct bi-phasic Ca^{2+} pattern (2.2 – Fig. 6A, B). Considering the high ($\geq 100 \mu\text{M}$) EC_{50} values of NAADP for TRPM2 (Tóth and Csanády, 2010) and the low endogenous NAADP concentration inside T lymphocytes after stimulation ($\sim 35 \text{ nM}$; Gasser et al., 2006) the involvement of TRPM2 in the formation of initial Ca^{2+} microdomains seemed rather unlikely and this assumption was experimentally confirmed here. Furthermore, it was very recently shown that impurities of ADPR and ADPRP in commercial preparations of NAADP, NAAD and NAD caused low activation of TRPM2 (Toth et al., 2015). Thus, it seems that the NAADP effects on TRPM2 were rather due to impurities. However, TRPM2 seems to be important in later stages in the Ca^{2+} signaling cascade because primary TRPM2-KO T lymphocytes exhibit a reduced cytokine production after stimulation with anti-CD3/anti-CD28 beads *in vitro* and an ameliorated EAE phenotype was observed in TRPM2-KO mice (Melzer et al., 2012). Taken together, ADPR and ADPRP seem to be the only true agonists for TRPM2 (Toth et al., 2015).

3.3.3 NAADP and initial, localized Ca^{2+} signals

NAADP is the most potent Ca^{2+} releasing second messenger (Chini et al., 1995; Lee and Aarhus, 1995) and is rapidly formed after T lymphocyte stimulation with anti-CD3 antibodies (Gasser et al., 2006). Further, NAADP is an essential regulator of T lymphocyte Ca^{2+} signaling and thus the activation of the adaptive immune response (Berg et al., 2000). To validate the influence of NAADP on the initial localized Ca^{2+} signals,

NAADP was directly microinjected in Jurkat control (E2) and RyR-knockdown (#10; Langhorst et al., 2004) T lymphocytes (2.2 – Fig. 5B). Since the NAADP concentration upon stimulation in Jurkat T lymphocytes increased up to approx. 35 nM, assuming an even distribution throughout the cell (Gasser et al., 2006), the NAADP concentration in the microinjection pipette was adjusted to 60 nM. Still matter of debate was whether NAADP acts directly (or via a binding protein) on RyR or only through the RyR-dependent CICR (Guse, 2012). In Jurkat, control cells (E2) initial Ca^{2+} signals after microinjection of NAADP were already observed after 20 msec following a global activation of the cell (2.2 – Fig. 5A). Thus, if NAADP acts via a bp, the protein seems to be directly activated by NAADP-binding within 20 msec, as discussed earlier. The initial Ca^{2+} signals after microinjection of NAADP were $\sim 1.07 \mu\text{m}$ in diameter with $[\text{Ca}^{2+}]_i$ amplitude of approx. 374 nM (Fluo-4/Fura Red ratio ~ 1.6 ; 2.2 – Fig. S8 B). The size and ratiometric amplitude of these initial Ca^{2+} signals corresponded to Ca^{2+} sparks in cardiac and ventricular myocytes (**Tab. 2**; Cheng and Lederer, 2008; Niggli, 1999). However the calibrated amplitude of approx. 374 nM seemed to be too high for Ca^{2+} sparks (Niggli, 1999).

In RyR-knockdown Jurkat T lymphocytes (#10) neither initial Ca^{2+} signals nor a global activation was observed (2.2 – Fig. 5B). Thus, already the initial, very fast Ca^{2+} signals were dependent on functional RyRs, suggesting that the RyRs are directly targeted by NAADP. The RyR-knockdown Jurkat cells still responded to IP_3 (2.2 – Fig. 3C) and even showed significantly higher Ca^{2+} amplitudes compared to WT Jurkat T lymphocytes (2.2 – Fig. S8). Hence, the release of Ca^{2+} from the ER was not altered in these cells and maybe knockdown of RyRs was compensated by a higher expression of IP_3 Rs. Moreover, the IP_3 -induced Ca^{2+} release events were slightly broader in diameter ($\sim 1.15 \mu\text{m}$) compared to NAADP-induced Ca^{2+} signals, while the amplitude was more than twofold reduced ($\sim 151 \text{ nM}$; 2.2 – Fig. S8 B). This confirms again, that NAADP is a potent Ca^{2+} releasing second messenger and moreover, this may imply a higher density of RyRs in the ER membrane compared to IP_3 Rs in Jurkat T lymphocytes (2.2 – Fig. S8).

IP_3 -induced Ca^{2+} signals are differentiated into Ca^{2+} puffs, discrete local Ca^{2+} events mediated by several IP_3 Rs, and Ca^{2+} blips that correspond to the opening of only one or a few IP_3 Rs (Bootman et al., 2001; Cheng and Lederer, 2008; Parker and Yao, 1996; Parker et al., 1996; Smith and Parker, 2009). A summary of the previously described

Ca²⁺ puffs and blips in comparison to IP₃-induced Ca²⁺ signals observed in Jurkat T lymphocytes is shown in **Tab. 3**.

Tab. 3 Comparison of IP₃-induced Ca²⁺ signals to previously described Ca²⁺ blips and puffs. Jurkat = Jurkat T lymphocytes.

| | Ca ²⁺ amplitude [nM] | ratiometric amplitude | diameter [μm] |
|--|------------------------------------|--------------------------|------------------|
| Jurkat | 151 ± 23 | 1.17 ± 0.1 | 1.15 ± 0.13 |
| Ca ²⁺ puffs (Tovey et al., 2001) | 42 – 178 | --- | 2.5 – 4.1 |
| Ca ²⁺ blips (Parker and Yao, 1996) | ~ 1/5 < Ca ²⁺ puffs | Δ 0.11 ± 0.01 | --- |

Typically Ca²⁺ puffs in non-excitable cells result in amplitudes of 42 – 178 nM, a diameter of ~2.5 – 4.1 μm (Tovey et al., 2001). Thus, the amplitude of IP₃-induced Ca²⁺ signals corresponded to Ca²⁺ puffs but the diameter seemed to be a bit too small for Ca²⁺ puffs. However, the previously described Ca²⁺ puffs were obtained in different cell types with a different microscopic set-up and Fluo-3 compared to dye combination of Fluo-4/Fura Red, thus, this could lead to a smaller Ca²⁺ puff diameter in Jurkat T lymphocytes. On the other hand, maybe the density of IP₃Rs in the ER membrane is decreased in Jurkat T lymphocytes compared to the non-excitable cells analyzed by Tovey and co-workers (Tovey et al., 2001), this could also result in a decreased Ca²⁺ puff diameter.

Taken together, the strong dependence of RyRs in NAADP-induced Ca²⁺ signals in T lymphocytes, suggest that initial, localized Ca²⁺ signals are formed through NAADP targeting the RyRs and probably not through RyR-dependent CICR. However, to test this assumption NAADP has to be measured directly combined with fluorescently labeled RyRs. If NAADP directly targets the RyRs then the NAADP signal should exactly overlap with the fluorescently labeled RyRs.

3.3.4 Strengths and limitations of the presented method

With the here presented Ca^{2+} imaging method for the first time, subcellular Ca^{2+} microdomains in Jurkat and primary T lymphocytes could be characterized. Using antibody-coated beads having the size of T lymphocytes, a cell-cell interaction was mimicked and thus a directed activation of T lymphocytes was obtained.

However, the activation with antibodies resembles not the *in vivo* activation. Thus, a more physiological approach would be if antigenic peptides bound to MHC could be used for the activation of T lymphocytes. Since normally every T lymphocyte expresses a unique TCR which recognizes only the specific antigenic peptide (Kenneth Murphy, 2011), T lymphocyte from so-called OT1 or OT2 transgenic T lymphocytes could be used. All CD4^+ (OT2; Barnden et al., 1998) or CD8^+ (OT1; Clarke et al., 2000) T lymphocyte from these mice express a specific TCR for the recognition of ovalbumin (OVA) peptides. For example, bone-marrow-derived-dendritic cells (BMDCs) may be loaded with OVA-peptides *in vitro*, if the transgenic T lymphocytes encounter an OVA-peptide presented on BMDCs via MHC, these T lymphocytes should be activated in a more physiological manner and respond with Ca^{2+} signals. First experiments were already performed and it was possible to image and analyze global Ca^{2+} signals in this set-up, however, further development needs to be done for the measurement of subcellular Ca^{2+} microdomains using Ova-peptides presented on BMDCs.

With the presented method, so far only Ca^{2+} signals and not Ca^{2+} releasing second messengers and/or Ca^{2+} channels could be imaged. To verify the involvement of NAADP during the bi-phasic Ca^{2+} response of the very first Ca^{2+} microdomains, NAADP has to be measured directly. One possibility would be a fluorescence resonance energy transfer-based (FRET) biosensor (Gorshkov and Zhang, 2014). Epac1-camp, for example, is a FRET-based biosensor that binds the second messenger 3',5'-cyclic adenosine monophosphate (cAMP) using a specific binding domain of the exchange protein activated by cAMP 1 (Epac1) flanked by cyan fluorescent protein (CFP) and YFP (Nikolaev et al., 2004). Upon binding, the FRET-based biosensor changes the conformation, leading to a fluorescent readout (Gorshkov and Zhang, 2014; Nikolaev et al., 2004). To develop such an FRET-based biosensor for NAADP a specific binding domain is needed, which changes its conformation upon binding. However, a suitable NAADP binding domain, e.g. from the NAADP-bp is not yet available and since NAADP functions in low nM concentrations the buffering of the biosensor might be a problem.

To image the Ca^{2+} channels directly, it would be possible to tag a fluorescent fusion protein, like CFP or YFP, for example to the RyRs (Smyth and Shaw, 2008). However, the RyRs form the largest known ion channels each protein is approx. 500 kDa (Lanner et al., 2010; Zalk et al., 2007), thus the cloning and the transfection of such a large protein could be complicated, especially since Jurkat and primary T lymphocytes are difficult to transfect. Furthermore, to resolve single ion-channels under the microscope an advanced confocal or TIRF microscope is needed.

Another limitation of the presented method is the deconvolution. Generally, it is always better to record the best possible data than to apply correction algorithms afterwards. Still, deconvolution algorithms are routinely used in biomedical research (Wallace et al., 2001). Here classical no neighbor and LR deconvolution algorithms were applied, but recently published new deconvolution algorithms should significantly improve the resolution (Arigovindan et al., 2013; Nieuwenhuizen et al., 2013). Thus, it would be interesting to see how these new algorithms perform compared to the classical ones used here and if these algorithms optimize our Ca^{2+} microdomain detection.

Furthermore, with the here presented Ca^{2+} imaging method, Ca^{2+} signals are detected in one layer of the T lymphocytes in two spatial dimensions, but local Ca^{2+} signals proceed in three spatial dimensions. A possible approach to analyzing spreading of Ca^{2+} microdomains in three dimensions would be to analyze, for example, three layers with different z-axis orientation. Therefore, one layer above and one layer below the layer of interest has to be recorded. This could be achieved using a piezoelectric motor, to step through the T lymphocyte in the z-direction. With this additional information, a three-dimensional spreading of Ca^{2+} microdomains could be reconstructed. However, since the three different layers are not recorded at the same time, this might lead to systematic errors and due to the stepping in the z-direction, with only three layers the acquisition rate would be more than three times slower.

3.3.5 Working model and open questions

After T lymphocyte stimulation, via the TCR complex, here mediated by antibodies, NAADP is rapidly formed and the first Ca^{2+} microdomains are directly observed at the site of activation. Probably via a binding-protein (Guse, 2012; Lin-Moshier et al., 2012) located in the cytosol of T lymphocytes, NAADP targets directly RyR1 leading to bi-

phasic Ca^{2+} response and an initial release of Ca^{2+} from the ER in the first secs. These initial Ca^{2+} release events boost a CICR by IP_3 R and further RyRs. The depletion of Ca^{2+} from the ER is sensed by STIM1/2, which thereupon change their conformation and activate Orai1. Then, Ca^{2+} from the extracellular space can enter the cytosol (Prakriya and Lewis, 2015; Shaw and Feske, 2012; Shaw et al., 2013; Soboloff et al., 2012; Srikanth and Gwack, 2013). Since knockout of TRPM2 had no effect on localized initial Ca^{2+} signals in primary T lymphocytes, TRPM2 could be excluded as a possible target of NAADP, at least in mouse T lymphocytes. The results and open questions are summarized in Fig. 16.

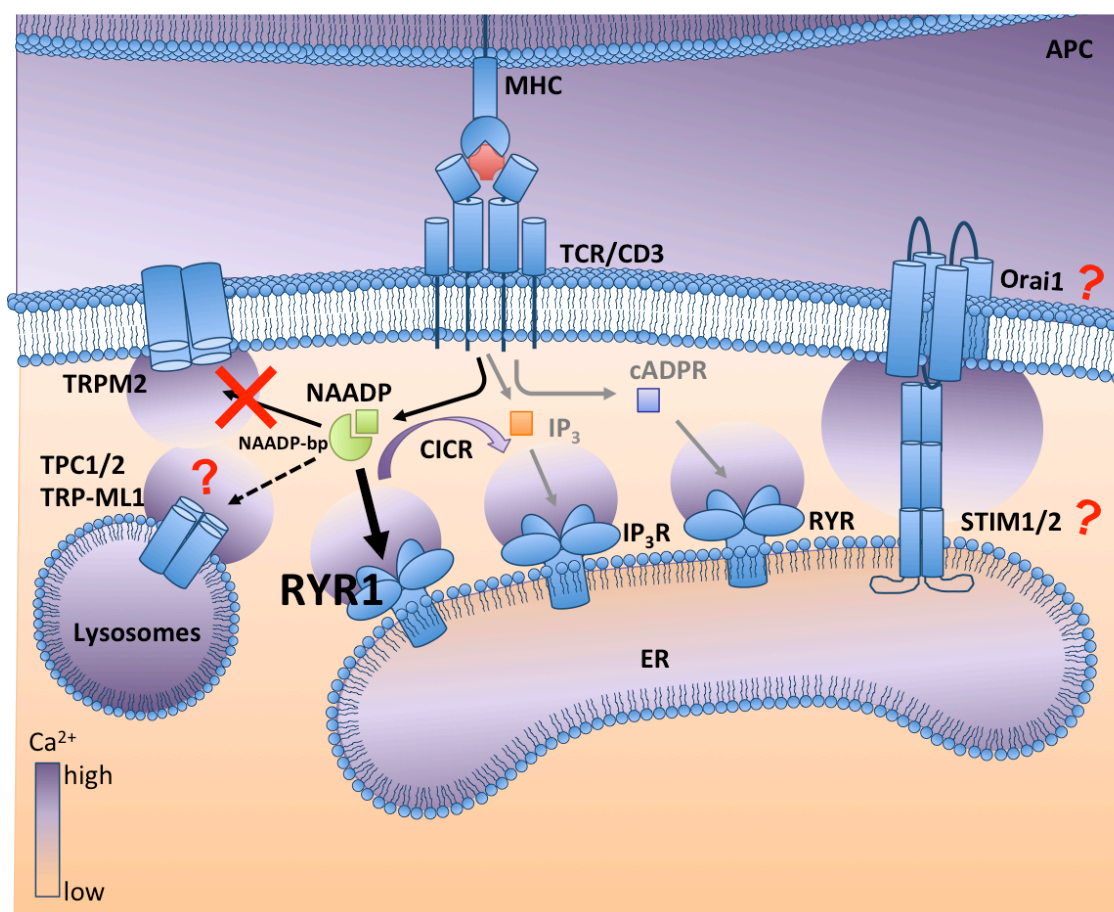


Fig. 16 Summary of the obtained results and open questions

Upon activation of T lymphocytes Ca^{2+} releasing second messenger are formed. NAADP (Nicotinic acid adenine dinucleotide phosphate), probably via a binding protein (NAADP-bp), mediates the initial Ca^{2+} release through RyRs (RyR1 in primary T lymphocytes). TRPM2 (transient receptor potential channel, subfamily melastatin, member 2) is not involved in the formation of initial Ca^{2+} signals. The role of TPC1/2 (two-pore channel 1,2) and TRP-ML1 (Transient receptor potential channel, subfamily mucolipin, member 1) as possible target receptors of NAADP needs to be investigated (indicated by a red question mark). The initial Ca^{2+} signals trigger further Ca^{2+} release events via Ca^{2+} -induced Ca^{2+} -release (CICR) and subsequently STIM1/2 (stromal interaction molecules 1,2) translocates to the plasma membrane and activates Orai1

(Calcium release-activated calcium channel protein 1). The CRAC-channel formation leads to a global activation by Ca^{2+} entry from the extracellular space. The involvement of STIM1/2 and Orai1 during the formation of initial Ca^{2+} signaling events needs to be investigated (indicated by a red question mark). APC (antigen-presenting cell); MHC (growth-factor-receptor-bound-protein-2-related adaptor protein); TCR (T cell receptor); IP_3 receptors (IP_3Rs); D-*myo*-inositol-1,4,5-trisphosphate (IP_3); cyclic adenosine diphosphate ribose (cADPR) (adapted from Ernst et al., 2013; Soboloff et al., 2012).

However, the initial Ca^{2+} microdomains are not exclusively mediated by RyRs (RyR1 in primary T lymphocytes) as discussed earlier. Interestingly, some RyR1-KO T lymphocytes showed initial Ca^{2+} microdomains at the site of stimulation, similar to the appearance of initial Ca^{2+} microdomains in WT T lymphocytes, but without a global activation after 50 sec (2.2 – Fig. S7). Furthermore, stimulation of WT and RyR knockdown Jurkat cells in Ca^{2+} free buffer resulted in a significant decrease in the mean responsiveness (2.2 – Fig. 4A). These results indicate that the Ca^{2+} entry channels are involved in forming the initial Ca^{2+} microdomains. Interestingly, in primary human T lymphocytes coupling between RyRs and the CRAC channels was observed, suggesting a positive feedback relationship (Thakur et al., 2012). The inhibition of RyRs by ryanodine reduced the SOCE in activated primary T lymphocytes while the store refilling under physiological conditions was enhanced (Thakur et al., 2012). Hence, the RyRs seemed to be coupled to the CRAC channel machinery. However, a co-localization of RyRs with STIM1 was first observed after 10 min following store depletion of HEK293 cells (Thakur et al., 2012). Thus, the involvement of the CRAC channels during initial Ca^{2+} signaling events in primary T lymphocytes needs to be further investigated, especially during the first phase of the bi-phasic response.

As discussed earlier, there is also evidence from other cell types that the RyRs and TPCs are required for NAADP-induced intracellular Ca^{2+} release events (Gerasimenko et al., 2015). Inhibition of RyR1 with antibodies in permeabilized pancreatic acinar cells resulted in a similar decreased NAADP-induced Ca^{2+} release as TPC2-KOs where TPC1 was additionally blocked with antibodies (Gerasimenko et al., 2015). Similarly, here in RyR1-KO as well as RyR knockdown T lymphocytes still Ca^{2+} signals were observed, indicating that the initial Ca^{2+} signals are not strictly depended on RyRs. Nevertheless, the publications regarding TPC1 and TPC2 are very divergent. Hence, also a role of TPC1 and TPC2 in initial Ca^{2+} signaling events should be analyzed in primary T lymphocytes.

Further, TRP-ML1 was shown to be activated by NAADP in concentrations ranging from 1 nM to 1 μ M (Zhang and Li, 2007). Despite, no evidence for a link between RyRs and TRP-ML1 the involvement of TRP-ML1 should also be analyzed in primary knockout T lymphocytes, too.

In conclusion, RyRs seemed to be targeted directly by NAADP (or NAADP-bp) during the initial Ca^{2+} microdomains, however to completely understand the fundamental Ca^{2+} network during T lymphocyte activation the involvement of TPCs, TRP-ML1 and the CRAC system (Orai1 and STIM1, 2) during the first phase of activation needs to be further investigated.

References

- Acuto, O., and Michel, F. (2003). CD28-mediated co-stimulation: a quantitative support for TCR signalling. *Nat. Rev. Immunol.* *3*, 939–951.
- Ahmadzadeh, M., Hussain, S.F., and Farber, D.L. (2001). Heterogeneity of the Memory CD4 T Cell Response: Persisting Effectors and Resting Memory T Cells. *J. Immunol.* *166*, 926–935.
- Alzayady, K.J., Wagner, L.E., Chandrasekhar, R., Monteagudo, A., Godiska, R., Tall, G.G., Joseph, S.K., and Yule, D.I. (2013). Functional Inositol 1,4,5-Trisphosphate Receptors Assembled from Concatenated Homo- and Heteromeric Subunits. *J. Biol. Chem.* *288*, 29772–29784.
- Alzayady, K.J., Wang, L., Chandrasekhar, R., Wagner, L.E., Van Petegem, F., and Yule, D.I. (2016). Defining the stoichiometry of inositol 1,4,5-trisphosphate binding required to initiate Ca²⁺ release. *Sci. Signal.* *9*, ra35.
- Amaral, L., Engi, H., Viveiros, M., and Molnar, J. (2007). Comparison of Multidrug Resistant Efflux Pumps of Cancer and Bacterial Cells with Respect to the Same Inhibitory Agents. *In Vivo* *21*, 237–244.
- Arigovindan, M., Fung, J.C., Elnatan, D., Mennella, V., Chan, Y.-H.M., Pollard, M., Branlund, E., Sedat, J.W., and Agard, D.A. (2013). High-resolution restoration of 3D structures from widefield images with extreme low signal-to-noise-ratio. *Proc. Natl. Acad. Sci.* *110*, 17344–17349.
- Assinger, A., Volf, I., and Schmid, D. (2015). A Novel, Rapid Method to Quantify Intraplatelet Calcium Dynamics by Ratiometric Flow Cytometry. *PLoS ONE* *10*.
- Axelrod, D. (1981). Cell-substrate contacts illuminated by total internal reflection fluorescence. *J. Cell Biol.* *89*, 141–145.
- Barnden, M.J., Allison, J., Heath, W.R., and Carbone, F.R. (1998). Defective TCR expression in transgenic mice constructed using cDNA-based α - and β -chain genes under the control of heterologous regulatory elements. *Immunol. Cell Biol.* *76*, 34–40.
- Beck, A., Kolisek, M., Bagley, L.A., Fleig, A., and Penner, R. (2006). Nicotinic acid adenine dinucleotide phosphate and cyclic ADP-ribose regulate TRPM2 channels in T lymphocytes. *FASEB J* *20*, 962–964.
- Berard, M., and Tough, D.F. (2002). Qualitative differences between naïve and memory T cells. *Immunology* *106*, 127–138.
- Berg, I., Potter, B.V.L., Mayr, G.W., and Guse, A.H. (2000). Nicotinic Acid Adenine

- Dinucleotide Phosphate (Naadp⁺) Is an Essential Regulator of T-Lymphocyte Ca²⁺-Signaling. *J. Cell Biol.* *150*, 581–588.
- Berridge, M.J., Lipp, P., and Bootman, M.D. (2000). The versatility and universality of calcium signalling. *Nat. Rev. Mol. Cell Biol.* *1*, 11–21.
- Bird, G.S., Hwang, S.-Y., Smyth, J.T., Fukushima, M., Boyles, R.R., and Putney Jr., J.W. (2009). STIM1 Is a Calcium Sensor Specialized for Digital Signaling. *Curr. Biol.* *19*, 1724–1729.
- Bootman, M., Niggli, E., Berridge, M., and Lipp, P. (1997). Imaging the hierarchical Ca²⁺ signalling system in HeLa cells. *J. Physiol.* *499 (Pt 2)*, 307–314.
- Bootman, M.D., Lipp, P., and Berridge, M.J. (2001). The organisation and functions of local Ca(2+) signals. *J. Cell Sci.* *114*, 2213–2222.
- Bootman, M.D., Rietdorf, K., Collins, T., Walker, S., and Sanderson, M. (2013). Ca²⁺-Sensitive Fluorescent Dyes and Intracellular Ca²⁺ Imaging. *Cold Spring Harb. Protoc.* *2013*, pdb.top066050 – pdb.top066050.
- Brailoiu, E., Churamani, D., Cai, X., Schrlau, M.G., Brailoiu, G.C., Gao, X., Hooper, R., Boulware, M.J., Dun, N.J., Marchant, J.S., et al. (2009). Essential requirement for two-pore channel 1 in NAADP-mediated calcium signaling. *J. Cell Biol.* *186*, 201–209.
- Brailoiu, E., Hooper, R., Cai, X., Brailoiu, G.C., Keebler, M.V., Dun, N.J., Marchant, J.S., and Patel, S. (2010). An Ancestral Deuterostome Family of Two-pore Channels Mediates Nicotinic Acid Adenine Dinucleotide Phosphate-dependent Calcium Release from Acidic Organelles. *J. Biol. Chem.* *285*, 2897–2901.
- Brandman, O., Liou, J., Park, W.S., and Meyer, T. (2007). STIM2 Is a Feedback Regulator that Stabilizes Basal Cytosolic and Endoplasmic Reticulum Ca²⁺ Levels. *Cell* *131*, 1327–1339.
- Brochet, D.X.P., Yang, D., Maio, A.D., Lederer, W.J., Franzini-Armstrong, C., and Cheng, H. (2005). Ca²⁺ blinks: Rapid nanoscopic store calcium signaling. *Proc. Natl. Acad. Sci.* *102*, 3099–3104.
- Broere, F., Apasov, S.G., Sitkovsky, M.V., and Eden, W. van (2011). A2 T cell subsets and T cell-mediated immunity. In *Principles of Immunopharmacology*, F.P. Nijkamp, and M.J. Parnham, eds. (Birkhäuser Basel), pp. 15–27.
- Cai, X., and Patel, S. (2010). Degeneration of an Intracellular Ion Channel in the Primate Lineage by Relaxation of Selective Constraints. *Mol. Biol. Evol.* *27*, 2352–2359.
- Calcraft, P.J., Ruas, M., Pan, Z., Cheng, X., Arredouani, A., Hao, X., Tang, J., Rietdorf, K., Teboul, L., Chuang, K.-T., et al. (2009). NAADP mobilizes calcium from acidic organelles through two-pore channels. *Nature* *459*, 596–600.

- Call, M.E., Pyrdol, J., Wiedmann, M., and Wucherpfennig, K.W. (2002). The Organizing Principle in the Formation of the T Cell Receptor-CD3 Complex. *Cell* *111*, 967–979.
- Cang, C., Zhou, Y., Navarro, B., Seo, Y.-J., Aranda, K., Shi, L., Battaglia-Hsu, S., Nissim, I., Clapham, D.E., and Ren, D. (2013). mTOR regulates lysosomal ATP-sensitive two-pore Na⁽⁺⁾ channels to adapt to metabolic state. *Cell* *152*, 778–790.
- Cang, C., Aranda, K., and Ren, D. (2014a). A non-inactivating high-voltage-activated two-pore Na⁽⁺⁾ channel that supports ultra-long action potentials and membrane bistability. *Nat. Commun.* *5*, 5015.
- Cang, C., Bekele, B., and Ren, D. (2014b). The voltage-gated sodium channel TPC1 confers endolysosomal excitability. *Nat. Chem. Biol.* *10*, 463–469.
- Carafoli, E. (2003). The calcium-signalling saga: tap water and protein crystals. *Nat. Rev. Mol. Cell Biol.* *4*, 326–332.
- Cardullo, R.A., and Hinchcliffe, E.H. (2007). Digital Manipulation of Brightfield and Fluorescence Images: Noise Reduction, Contrast Enhancement, and Feature Extraction. B.-M. in *C. Biology*, ed. (Academic Press), pp. 285–314.
- Cheng, H., and Lederer, W.J. (2008). Calcium Sparks. *Physiol. Rev.* *88*, 1491–1545.
- Cheng, H., Lederer, W.J., and Cannell, M.B. (1993). Calcium sparks: elementary events underlying excitation-contraction coupling in heart muscle. *Science* *262*, 740–744.
- Cheng, X., Shen, D., Samie, M., and Xu, H. (2010). Mucolipins: Intracellular TRPML1-3 Channels. *FEBS Lett.* *584*, 2013–2021.
- Chini, E.N., Beers, K.W., and Dousa, T.P. (1995). Nicotinate adenine dinucleotide phosphate (NAADP) triggers a specific calcium release system in sea urchin eggs. *J. Biol. Chem.* *270*, 3216–3223.
- Choudhuri, K., Llodrá, J., Roth, E.W., Tsai, J., Gordo, S., Wucherpfennig, K.W., Kam, L.C., Stokes, D.L., and Dustin, M.L. (2014). Polarized release of T-cell-receptor-enriched microvesicles at the immunological synapse. *Nature* *507*, 118–123.
- Churamani, D., Carrey, E.A., Dickinson, G.D., and Patel, S. (2004). Determination of cellular nicotinic acid-adenine dinucleotide phosphate (NAADP) levels. *Biochem. J.* *380*, 449–454.
- Churamani, D., Hooper, R., Brailoiu, E., and Patel, S. (2012). Domain assembly of NAADP-gated two-pore channels. *Biochem. J.* *441*, 317–323.
- Churchill, G.C., and Galione, A. (2001). NAADP induces Ca²⁺ oscillations via a two-pool mechanism by priming IP₃- and cADPR-sensitive Ca²⁺ stores. *EMBO J.* *20*, 2666–2671.

- Churchill, G.C., O'Neill, J.S., Masgrau, R., Patel, S., Thomas, J.M., Genazzani, A.A., and Galione, A. (2003). Sperm Deliver a New Second Messenger. *Curr. Biol.* *13*, 125–128.
- Cieśla, J., Frączyk, T., and Rode, W. (2011). Phosphorylation of basic amino acid residues in proteins: important but easily missed. *Acta Biochim. Pol.* *58*, 137–148.
- Clapper, D.L., Walseth, T.F., Dargie, P.J., and Lee, H.C. (1987). Pyridine nucleotide metabolites stimulate calcium release from sea urchin egg microsomes desensitized to inositol trisphosphate. *J. Biol. Chem.* *262*, 9561–9568.
- Clarke, S.Rm., Barnden, M., Kurts, C., Carbone, F.R., Miller, J.F., and Heath, W.R. (2000). Characterization of the ovalbumin-specific TCR transgenic line OT-I: MHC elements for positive and negative selection. *Immunol. Cell Biol.* *78*, 110–117.
- Contreras, L., Drago, I., Zampese, E., and Pozzan, T. (2010). Mitochondria: The calcium connection. *Biochim. Biophys. Acta BBA - Bioenerg.* *1797*, 607–618.
- Copello, J.A., Qi, Y., Jeyakumar, L.H., Ogunbunmi, E., and Fleischer, S. (2001). Lack of effect of cADP-ribose and NAADP on the activity of skeletal muscle and heart ryanodine receptors. *Cell Calcium* *30*, 269–284.
- Cordiglieri, C., Odoardi, F., Zhang, B., Nebel, M., Kawakami, N., Klinkert, W.E.F., Lodygin, D., Lühder, F., Breunig, E., Schild, D., et al. (2010). Nicotinic acid adenine dinucleotide phosphate-mediated calcium signalling in effector T cells regulates autoimmunity of the central nervous system. *Brain J. Neurol.* *133*, 1930–1943.
- Covington, E.D., Wu, M.M., and Lewis, R.S. (2010). Essential Role for the CRAC Activation Domain in Store-dependent Oligomerization of STIM1. *Mol. Biol. Cell* *21*, 1897–1907.
- Dammermann, W., and Guse, A.H. (2005). Functional ryanodine receptor expression is required for NAADP-mediated local Ca^{2+} signaling in T-lymphocytes. *J. Biol. Chem.* *280*, 21394–21399.
- Dammermann, W., Zhang, B., Nebel, M., Cordiglieri, C., Odoardi, F., Kirchberger, T., Kawakami, N., Dowden, J., Schmid, F., Dornmair, K., et al. (2009). NAADP-mediated Ca^{2+} signaling via type 1 ryanodine receptor in T cells revealed by a synthetic NAADP antagonist. *Proc. Natl. Acad. Sci. U. S. A.* *106*, 10678–10683.
- Davis, L.C., Morgan, A.J., Chen, J.-L., Snead, C.M., Bloor-Young, D., Shenderov, E., Stanton-Humphreys, M.N., Conway, S.J., Churchill, G.C., Parrington, J., et al. (2012). NAADP activates two-pore channels on T cell cytolytic granules to stimulate exocytosis and killing. *Curr. Biol. CB* *22*, 2331–2337.
- DeHaven, W.I., Smyth, J.T., Boyles, R.R., and Putney, J.W. (2007). Calcium Inhibition and Calcium Potentiation of Orai1, Orai2, and Orai3 Calcium Release-activated Calci-

- um Channels. *J. Biol. Chem.* 282, 17548–17556.
- Deng, X., Wang, Y., Zhou, Y., Soboloff, J., and Gill, D.L. (2009). STIM and Orai: Dynamic Intermembrane Coupling to Control Cellular Calcium Signals. *J. Biol. Chem.* 284, 22501–22505.
- Dong, X., Wang, X., Shen, D., Chen, S., Liu, M., Wang, Y., Mills, E., Cheng, X., Delling, M., and Xu, H. (2009). Activating mutations of the TRPML1 channel revealed by proline-scanning mutagenesis. *J. Biol. Chem.* 284, 32040–32052.
- Dong, X.-P., Cheng, X., Mills, E., Delling, M., Wang, F., Kurz, T., and Xu, H. (2008). The type IV mucopolidosis-associated protein TRPML1 is an endolysosomal iron release channel. *Nature* 455, 992–996.
- Dustin, M.L. (2014). The Immunological Synapse. *Cancer Immunol. Res.* 2, 1023–1033.
- Dyer, S.A. (2004). *Wiley Survey of Instrumentation and Measurement* (John Wiley & Sons).
- Endo, M. (2009). Calcium-Induced Calcium Release in Skeletal Muscle. *Physiol. Rev.* 89, 1153–1176.
- Ernst, I.M.A., Fliegert, R., and Guse, A.H. (2013). Adenine Dinucleotide Second Messengers and T-lymphocyte Calcium Signaling. *Front. Immunol.* 4.
- Exley, M., Terhorst, C., and Wileman, T. (1991). Structure, assembly and intracellular transport of the T cell receptor for antigen. *Semin. Immunol.* 3, 283–297.
- Falardeau, J.L., Kennedy, J.C., Acierno, J.S., Sun, M., Stahl, S., Goldin, E., and Slaughaupt, S.A. (2002). Cloning and characterization of the mouse *Mcoln1* gene reveals an alternatively spliced transcript not seen in humans. *BMC Genomics* 3, 3.
- Faouzi, M., and Penner, R. (2014). TRPM2. In *Mammalian Transient Receptor Potential (TRP) Cation Channels*, B. Nilius, and V. Flockerzi, eds. (Springer Berlin Heidelberg), pp. 403–426.
- Farber, D.L., Acuto, O., and Bottomly, K. (1997). Differential T cell receptor-mediated signaling in naive and memory CD4 T cells. *Eur. J. Immunol.* 27, 2094–2101.
- Feske, S. (2007). Calcium signalling in lymphocyte activation and disease. *Nat. Rev. Immunol.* 7, 690–702.
- Feske, S. (2010). CRAC channelopathies. *Pflugers Arch.* 460, 417–435.
- Feske, S., Müller, J.M., Graf, D., Kroczeck, R.A., Dräger, R., Niemeyer, C., Baeuerle, P.A., Peter, H.-H., and Schlesier, M. (1996). Severe combined immunodeficiency due to defective binding of the nuclear factor of activated T cells in T lymphocytes of two male siblings. *Eur. J. Immunol.* 26, 2119–2126.

- Feske, S., Giltnane, J., Dolmetsch, R., Staudt, L.M., and Rao, A. (2001). Gene regulation mediated by calcium signals in T lymphocytes. *Nat. Immunol.* 2, 316–324.
- Feske, S., Gwack, Y., Prakriya, M., Srikanth, S., Puppel, S.-H., Tanasa, B., Hogan, P.G., Lewis, R.S., Daly, M., and Rao, A. (2006). A mutation in *Orai1* causes immune deficiency by abrogating CRAC channel function. *Nature* 441, 179–185.
- Floto, R.A., Mahaut-Smith, M.P., Somasundaram, B., and Allen, J.M. (1995). IgG-induced Ca^{2+} oscillations in differentiated U937 cells; a study using laser scanning confocal microscopy and co-loaded fluo-3 and fura-red fluorescent probes. *Cell Calcium* 18, 377–389.
- Fonfria, E., Murdock, P.R., Cusdin, F.S., Benham, C.D., Kellsell, R.E., and McNulty, S. (2006a). Tissue distribution profiles of the human TRPM cation channel family. *J Recept Signal Transduct Res* 26, 159–178.
- Fonfria, E., Mattei, C., Hill, K., Brown, J.T., Randall, A., Benham, C.D., Skaper, S.D., Campbell, C.A., Crook, B., Murdock, P.R., et al. (2006b). TRPM2 is elevated in the tMCAO stroke model, transcriptionally regulated, and functionally expressed in C13 microglia. *J Recept Signal Transduct Res* 26, 179–198.
- Foskett, J.K., White, C., Cheung, K.-H., and Mak, D.-O.D. (2007). Inositol Trisphosphate Receptor Ca^{2+} Release Channels. *Physiol. Rev.* 87, 593–658.
- Freiberg, B.A., Kupfer, H., Maslanik, W., Delli, J., Kappler, J., Zaller, D.M., and Kupfer, A. (2002). Staging and resetting T cell activation in SMACs. *Nat. Immunol.* 3, 911–917.
- Furuichi, T., Cunningham, K.W., and Muto, S. (2001). A Putative Two Pore Channel AtTPC1 Mediates Ca^{2+} Flux in Arabidopsis Leaf Cells. *Plant Cell Physiol.* 42, 900–905.
- Galione, A., and Churchill, G.C. (2002). Interactions between calcium release pathways: multiple messengers and multiple stores. *Cell Calcium* 32, 343–354.
- Galione, A., Lee, H.C., and Busa, W.B. (1991). Ca^{2+} -induced Ca^{2+} release in sea urchin egg homogenates: modulation by cyclic ADP-ribose. *Science* 253, 1143–1146.
- Gasser, A., Bruhn, S., and Guse, A.H. (2006). Second messenger function of nicotinic acid adenine dinucleotide phosphate revealed by an improved enzymatic cycling assay. *J. Biol. Chem.* 281, 16906–16913.
- Gee, K.R., Brown, K.A., Chen, W.-N.U., Bishop-Stewart, J., Gray, D., and Johnson, I. (2000). Chemical and physiological characterization of fluo-4 Ca^{2+} -indicator dyes. *Cell Calcium* 27, 97–106.
- Gerasimenko, J.V., Charlesworth, R.M., Sherwood, M.W., Ferdek, P.E., Mikoshiba, K., Parrington, J., Petersen, O.H., and Gerasimenko, O.V. (2015). Both RyRs and TPCs are

required for NAADP-induced intracellular Ca^{2+} release. *Cell Calcium*.

Gibson, S.F., and Lanni, F. (1991). Experimental test of an analytical model of aberration in an oil-immersion objective lens used in three-dimensional light microscopy. *J. Opt. Soc. Am. A* 8, 1601.

Gilabert, J.A. (2012). Cytoplasmic calcium buffering. *Adv. Exp. Med. Biol.* 740, 483–498.

Glunde, K., Guggino, S.E., Solaiyappan, M., Pathak, A.P., Ichikawa, Y., and Bhujwala, Z.M. (2003). Extracellular Acidification Alters Lysosomal Trafficking in Human Breast Cancer Cells. *Neoplasia N. Y. N* 5, 533–545.

Goodwin, P.C. (2014). Quantitative deconvolution microscopy. *Methods Cell Biol.* 123, 177–192.

Gorshkov, K., and Zhang, J. (2014). Visualization of cyclic nucleotide dynamics in neurons. *Front. Cell. Neurosci.* 8, 395.

Gräf, R., Rietdorf, J., and Zimmermann, T. (2005). Live Cell Spinning Disk Microscopy. In *Microscopy Techniques*, J. Rietdorf, ed. (Springer Berlin Heidelberg), pp. 57–75.

Grynkiewicz, G., Poenie, M., and Tsien, R.Y. (1985). A new generation of Ca^{2+} indicators with greatly improved fluorescence properties. *J. Biol. Chem.* 260, 3440–3450.

Guo, X., Jie, Y., Ren, D., Zeng, H., Zhang, Y., He, Y., and Pan, Z. (2012). In vitro-expanded $\text{CD4}^+\text{CD25}^{\text{high}}\text{Foxp3}^+$ regulatory T cells controls corneal allograft rejection. *Hum. Immunol.* 73, 1061–1067.

Guse, A. (2004). Biochemistry, Biology, and Pharmacology of Cyclic Adenosine Diphosphoribose (cADPR). *Curr. Med. Chem.* 11, 847–855.

Guse, A.H. (2012). Linking NAADP to ion channel activity: a unifying hypothesis. *Sci. Signal.* 5, pe18.

Guse, A.H., and Lee, H.C. (2008). NAADP: a universal Ca^{2+} trigger. *Sci. Signal.* 1, re10.

Guse, A.H., Roth, E., and Emmrich, F. (1993). Intracellular Ca^{2+} pools in Jurkat T-lymphocytes. *Biochem. J.* 291, 447–451.

Guse, A.H., da Silva, C.P., Emmrich, F., Ashamu, G.A., Potter, B.V., and Mayr, G.W. (1995a). Characterization of cyclic adenosine diphosphate-ribose-induced Ca^{2+} release in T lymphocyte cell lines. *J. Immunol. Baltim. Md 1950* 155, 3353–3359.

Guse, A.H., Goldwich, A., Weber, K., and Mayr, G.W. (1995b). Non-radioactive, isomer-specific inositol phosphate mass determinations: high-performance liquid chromatography-micro-metal-dye detection strongly improves speed and sensitivity of analyses from cells and micro-enzyme assays. *J. Chromatogr. B Biomed. Appl.* 672, 189–198.

- Guse, A.H., De Wit, C., Klokow, T., Schweitzer, K., and Mayr, G.W. (1997a). Unique properties of the capacitative Ca^{2+} -entry antagonist LU 52396: its inhibitory activity depends on the activation state of the cells. *Cell Calcium* 22, 91–97.
- Guse, A.H., Berg, I., da Silva, C.P., Potter, B.V., and Mayr, G.W. (1997b). Ca^{2+} entry induced by cyclic ADP-ribose in intact T-lymphocytes. *J. Biol. Chem.* 272, 8546–8550.
- Guse, A.H., da Silva, C.P., Berg, I., Skapenko, A.L., Weber, K., Heyer, P., Hohenegger, M., Ashamu, G.A., Schulze-Koops, H., Potter, B.V., et al. (1999). Regulation of calcium signalling in T lymphocytes by the second messenger cyclic ADP-ribose. *Nature* 398, 70–73.
- Guse, A.H., Ernst, I.M.A., and Fliegert, R. (2013). NAADP signaling revisited. *Curr. Top. Med. Chem.* 13, 2978–2990.
- Hagen, B.M., Boyman, L., Kao, J.P.Y., and Lederer, W.J. (2012). A comparative assessment of fluo Ca^{2+} indicators in rat ventricular myocytes. *Cell Calcium* 52, 170–181.
- Hamad, A.R.A., O'Herrin, S.M., Lebowitz, M.S., Srikrishnan, A., Bieler, J., Schneck, J., and Pardoll, D. (1998). Potent T Cell Activation with Dimeric Peptide–Major Histocompatibility Complex Class II Ligand: The Role of CD4 Coreceptor. *J. Exp. Med.* 188, 1633–1640.
- Heiner, I., Eisfeld, J., Halaszovich, C.R., Wehage, E., Jüngling, E., Zitt, C., and Lückhoff, A. (2003). Expression profile of the transient receptor potential (TRP) family in neutrophil granulocytes: evidence for currents through long TRP channel 2 induced by ADP-ribose and NAD. *Biochem. J.* 371, 1045–1053.
- Helmchen, F. (2011). Calibration of Fluorescent Calcium Indicators. *Cold Spring Harb. Protoc.* 2011, pdb.top120.
- Hewavitharana, T., Deng, X., Wang, Y., Ritchie, M.F., Girish, G.V., Soboloff, J., and Gill, D.L. (2008). Location and Function of STIM1 in the Activation of Ca^{2+} Entry Signals. *J. Biol. Chem.* 283, 26252–26262.
- Hiraoka, Y., Sedat, J.W., and Agard, D.A. (1987). The use of a charge-coupled device for quantitative optical microscopy of biological structures. *Science* 238, 36–41.
- Hiraoka, Y., Sedat, J.W., and Agard, D.A. (1990). Determination of three-dimensional imaging properties of a light microscope system. Partial confocal behavior in epifluorescence microscopy. *Biophys. J.* 57, 325–333.
- Hohenegger, M., Suko, J., Gscheidlinger, R., Drobny, H., and Zidar, A. (2002). Nicotinic acid-adenine dinucleotide phosphate activates the skeletal muscle ryanodine receptor. *Biochem. J.* 367, 423–431.
- Hollyman, D., Stefanski, J., Przybylowski, M., Bartido, S., Borquez-Ojeda, O., Taylor,

- C., Yeh, R., Capacio, V., Olszewska, M., Hosey, J., et al. (2009). Manufacturing validation of biologically functional T cells targeted to CD19 antigen for autologous adoptive cell therapy. *J. Immunother. Hagerstown Md* 1997 32, 169–180.
- Hoover, P.J., and Lewis, R.S. (2011). Stoichiometric requirements for trapping and gating of Ca^{2+} release-activated Ca^{2+} (CRAC) channels by stromal interaction molecule 1 (STIM1). *Proc. Natl. Acad. Sci. U. S. A.* 108, 13299–13304.
- Hosoi, E., Nishizaki, C., Gallagher, K.L., Wyre, H.W., Matsuo, Y., and Sei, Y. (2001). Expression of the Ryanodine Receptor Isoforms in Immune Cells. *J. Immunol.* 167, 4887–4894.
- Hou, X., Pedi, L., Diver, M.M., and Long, S.B. (2012). Crystal structure of the calcium release-activated calcium channel Orai. *Science* 338, 1308–1313.
- Hüser, J., and Blatter, L.A. (1997). Elementary events of agonist-induced Ca^{2+} release in vascular endothelial cells. *Am. J. Physiol. - Cell Physiol.* 273, C1775–C1782.
- Hussain, S.F., Anderson, C.F., and Farber, D.L. (2002). Differential SLP-76 Expression and TCR-Mediated Signaling in Effector and Memory CD4 T Cells. *J. Immunol.* 168, 1557–1565.
- Hyrz, K.L., Minta, A., Escamilla, P.R., Chan, P.P.L., Meshik, X.A., and Goldberg, M.P. (2013). Synthesis and Properties of Asante Calcium Red –a Novel Family of Long Excitation Wavelength Calcium Indicators. *Cell Calcium* 54.
- Ikeya, M., Yamanoue, K., Mochizuki, Y., Konishi, H., Tadokoro, S., Tanaka, M., Suzuki, R., and Hirashima, N. (2014). Orai-2 is localized on secretory granules and regulates antigen-evoked Ca^{2+} mobilization and exocytosis in mast cells. *Biochem. Biophys. Res. Commun.* 451, 62–67.
- Inoué, S. (1990). Foundations of Confocal Scanned Imaging in Light Microscopy. In *Handbook of Biological Confocal Microscopy*, J.B. Pawley, ed. (Springer US), pp. 1–14.
- Jahn, K., and Hille, C. (2014). Asante Calcium Green and Asante Calcium Red—Novel Calcium Indicators for Two-Photon Fluorescence Lifetime Imaging. *PLoS ONE* 9, e105334.
- Johnson, I. (2010). *The Molecular Probes Handbook: A Guide to Fluorescent Probes and Labeling Technologies*, 11th Edition (Life Technologies Corporation).
- Johnson, J.D., and Mislser, S. (2002). Nicotinic acid-adenine dinucleotide phosphate-sensitive calcium stores initiate insulin signaling in human beta cells. *Proc. Natl. Acad. Sci. U. S. A.* 99, 14566–14571.

- Kao, J.P.Y., Li, G., and Auston, D.A. (2010). Chapter 5 - Practical Aspects of Measuring Intracellular Calcium Signals with Fluorescent Indicators. In *Methods in Cell Biology*, M. Whitaker, ed. (Academic Press), pp. 113–152.
- Kashio, M., Sokabe, T., Shintaku, K., Uematsu, T., Fukuta, N., Kobayashi, N., Mori, Y., and Tominaga, M. (2012). Redox signal-mediated sensitization of transient receptor potential melastatin 2 (TRPM2) to temperature affects macrophage functions. *Proc. Natl. Acad. Sci. U. S. A.* *109*, 6745–6750.
- Kawasaki, T., Lange, I., and Feske, S. (2009). A minimal regulatory domain in the C terminus of STIM1 binds to and activates ORAI1 CRAC channels. *Biochem. Biophys. Res. Commun.* *385*, 49–54.
- Kenneth Murphy (2011). *Janeway's Immunobiology* (Garland Science).
- Kiselyov, K., Shin, D.M., Shcheynikov, N., Kurosaki, T., and Muallem, S. (2001). Regulation of Ca²⁺-release-activated Ca²⁺ current (I_{crac}) by ryanodine receptors in inositol 1,4,5-trisphosphate-receptor-deficient DT40 cells. *Biochem. J.* *360*, 17–22.
- Kiselyov, K., Chen, J., Rbaibi, Y., Oberdick, D., Tjon-Kon-Sang, S., Shcheynikov, N., Muallem, S., and Soyombo, A. (2005). TRP-ML1 is a lysosomal monovalent cation channel that undergoes proteolytic cleavage. *J. Biol. Chem.* *280*, 43218–43223.
- Knowles, H., Li, Y., and Perraud, A.-L. (2012). The TRPM2 ion channel, an oxidative stress and metabolic sensor regulating innate immunity and inflammation. *Immunol. Res.* *55*, 241–248.
- Kraft, R., Grimm, C., Grosse, K., Hoffmann, A., Sauerbruch, S., Kettenmann, H., Schultz, G., and Harteneck, C. (2004). Hydrogen peroxide and ADP-ribose induce TRPM2-mediated calcium influx and cation currents in microglia. *Am J Physiol Cell Physiol* *286*, C129–C137.
- Kummerow, C., Junker, C., Kruse, K., Rieger, H., Quintana, A., and Hoth, M. (2009). The immunological synapse controls local and global calcium signals in T lymphocytes. *Immunol. Rev.* *231*, 132–147.
- Kunerth, S., Mayr, G.W., Koch-Nolte, F., and Guse, A.H. (2003). Analysis of subcellular calcium signals in T-lymphocytes. *Cell. Signal.* *15*, 783–792.
- Lange, I., Penner, R., Fleig, A., and Beck, A. (2008). Synergistic regulation of endogenous TRPM2 channels by adenine dinucleotides in primary human neutrophils. *Cell Calcium* *44*, 604–615.
- Lange, I., Yamamoto, S., Partida-Sanchez, S., Mori, Y., Fleig, A., and Penner, R. (2009). TRPM2 Functions as a Lysosomal Ca²⁺-Release Channel in β Cells. *Sci. Signal.* *2*, ra23.

- Langhorst, M.F., Schwarzmann, N., and Guse, A.H. (2004). Ca^{2+} release via ryanodine receptors and Ca^{2+} entry: major mechanisms in NAADP-mediated Ca^{2+} signaling in T-lymphocytes. *Cell. Signal.* *16*, 1283–1289.
- Lanner, J.T., Georgiou, D.K., Joshi, A.D., and Hamilton, S.L. (2010). Ryanodine Receptors: Structure, Expression, Molecular Details, and Function in Calcium Release. *Cold Spring Harb. Perspect. Biol.* *2*.
- Ledbetter, M.W., Preiner, J.K., Louis, C.F., and Mickelson, J.R. (1994). Tissue distribution of ryanodine receptor isoforms and alleles determined by reverse transcription polymerase chain reaction. *J. Biol. Chem.* *269*, 31544–31551.
- Lee, H.C. (1993). Potentiation of calcium- and caffeine-induced calcium release by cyclic ADP-ribose. *J. Biol. Chem.* *268*, 293–299.
- Lee, H.C. (2000). NAADP: An emerging calcium signaling molecule. *J. Membr. Biol.* *173*, 1–8.
- Lee, H.C. (2001). Physiological Functions of Cyclic Adp-Ribose and Naadp as Calcium Messengers. *Annu. Rev. Pharmacol. Toxicol.* *41*, 317–345.
- Lee, H.C. (2011). Cyclic ADP-ribose and NAADP: fraternal twin messengers for calcium signaling. *Sci. China Life Sci.* *54*, 699–711.
- Lee, H.C., and Aarhus, R. (1995). A derivative of NADP mobilizes calcium stores insensitive to inositol trisphosphate and cyclic ADP-ribose. *J. Biol. Chem.* *270*, 2152–2157.
- Lee, H.C., Walseth, T.F., Bratt, G.T., Hayes, R.N., and Clapper, D.L. (1989). Structural determination of a cyclic metabolite of NAD^+ with intracellular Ca^{2+} -mobilizing activity. *J. Biol. Chem.* *264*, 1608–1615.
- Lewis, A.M., Aley, P.K., Roomi, A., Thomas, J.M., Masgrau, R., Garnham, C., Shipman, K., Paramore, C., Bloor-Young, D., Sanders, L.E.L., et al. (2012). β -Adrenergic receptor signaling increases NAADP and cADPR levels in the heart. *Biochem. Biophys. Res. Commun.* *427*, 326–329.
- Li, J., Theofanous, L., Stickel, S., Bouton-Verville, H., Burgin, K.E., Jakubchak, S., Wagner, T.E., and Wei, Y. (2007). Transfer of in vitro expanded T lymphocytes after activation with dendritomas prolonged survival of mice challenged with EL4 tumor cells. *Int. J. Oncol.* *31*, 193–197.
- Lillemeier, B.F., Mörtelmaier, M.A., Forstner, M.B., Huppa, J.B., Groves, J.T., and Davis, M.M. (2010). TCR and Lat are expressed on separate protein islands on T cell membranes and concatenate during activation. *Nat. Immunol.* *11*, 90–96.
- Lin-Moshier, Y., Walseth, T.F., Churamani, D., Davidson, S.M., Slama, J.T., Hooper,

- R., Brailoiu, E., Patel, S., and Marchant, J.S. (2012). Photoaffinity labeling of nicotinic acid adenine dinucleotide phosphate (NAADP) targets in mammalian cells. *J. Biol. Chem.* *287*, 2296–2307.
- Liou, J., Kim, M.L., Do Heo, W., Jones, J.T., Myers, J.W., Ferrell Jr., J.E., and Meyer, T. (2005). STIM Is a Ca^{2+} Sensor Essential for Ca^{2+} -Store-Depletion-Triggered Ca^{2+} Influx. *Curr. Biol.* *15*, 1235–1241.
- Lioudyno, M.I., Kozak, J.A., Penna, A., Safrina, O., Zhang, S.L., Sen, D., Roos, J., Stauderman, K.A., and Cahalan, M.D. (2008). Orai1 and STIM1 move to the immunological synapse and are up-regulated during T cell activation. *Proc. Natl. Acad. Sci.* *105*, 2011–2016.
- Lipp, P., and Niggli, E. (1993). Ratiometric confocal Ca^{2+} -measurements with visible wavelength indicators in isolated cardiac myocytes. *Cell Calcium* *14*, 359–372.
- Lipp, P., and Niggli, E. (1998). Fundamental calcium release events revealed by two-photon excitation photolysis of caged calcium in Guinea-pig cardiac myocytes. *J. Physiol.* *508 (Pt 3)*, 801–809.
- Lipp, P., Lüscher, C., and Niggli, E. (1996). Photolysis of caged compounds characterized by ratiometric confocal microscopy: a new approach to homogeneously control and measure the calcium concentration in cardiac myocytes. *Cell Calcium* *19*, 255–266.
- Lipski, J., Park, T.I.H., Li, D., Lee, S.C.W., Trevarton, A.J., Chung, K.K.H., Freestone, P.S., and Bai, J.-Z. (2006). Involvement of TRP-like channels in the acute ischemic response of hippocampal CA1 neurons in brain slices. *Brain Res.* *1077*, 187–199.
- Lis, A., Peinelt, C., Beck, A., Parvez, S., Monteilh-Zoller, M., Fleig, A., and Penner, R. (2007). CRACM1, CRACM2, and CRACM3 Are Store-Operated Ca^{2+} Channels with Distinct Functional Properties. *Curr. Biol.* *17*, 794–800.
- Liu, B., Chen, W., Evavold, B.D., and Zhu, C. (2014). Accumulation of Dynamic Catch Bonds between TCR and Agonist Peptide-MHC Triggers T Cell Signaling. *Cell* *157*, 357–368.
- Liu, H., Rhodes, M., Wiest, D.L., and Vignali, D.A.A. (2000). On the Dynamics of TCR:CD3 Complex Cell Surface Expression and Downmodulation. *Immunity* *13*, 665–675.
- Lloyd-Evans, E., Morgan, A.J., He, X., Smith, D.A., Elliot-Smith, E., Sillence, D.J., Churchill, G.C., Schuchman, E.H., Galione, A., and Platt, F.M. (2008). Niemann-Pick disease type C1 is a sphingosine storage disease that causes deregulation of lysosomal calcium. *Nat. Med.* *14*, 1247–1255.
- L. L. Song, E.J.H. (1995). Photobleaching Kinetics of Fluorescein in Quantitative Fluorescence Microscopy. *Biophys. J.* *68*, 2588–2600.

- Lucy, L.B. (1974). An iterative technique for the rectification of observed distributions. *Astron. J. Vol. 79*, p. 745–754.
- Luik, R.M., Wang, B., Prakriya, M., Wu, M.M., and Lewis, R.S. (2008). Oligomerization of STIM1 couples ER calcium depletion to CRAC channel activation. *Nature 454*, 538–542.
- Lyubchenko, T.A., Wurth, G.A., and Zweifach, A. (2001). Role of Calcium Influx in Cytotoxic T Lymphocyte Lytic Granule Exocytosis during Target Cell Killing. *Immunity 15*, 847–859.
- Magnone, M., Bauer, I., Poggi, A., Mannino, E., Sturla, L., Brini, M., Zocchi, E., De Flora, A., Nencioni, A., and Bruzzone, S. (2012). NAD^+ Levels Control Ca^{2+} Store Replenishment and Mitogen-induced Increase of Cytosolic Ca^{2+} by Cyclic ADP-ribose-dependent TRPM2 Channel Gating in Human T Lymphocytes. *J. Biol. Chem. 287*, 21067–21081.
- Maier, S.K.G., Westenbroek, R.E., Schenkman, K.A., Feigl, E.O., Scheuer, T., and Catterall, W.A. (2002). An unexpected role for brain-type sodium channels in coupling of cell surface depolarization to contraction in the heart. *Proc. Natl. Acad. Sci. 99*, 4073–4078.
- Manji, S.S.M., Parker, N.J., Williams, R.T., van Stekelenburg, L., Pearson, R.B., Dziadek, M., and Smith, P.J. (2000). STIM1: a novel phosphoprotein located at the cell surface. *Biochim. Biophys. Acta BBA - Protein Struct. Mol. Enzymol. 1481*, 147–155.
- Marian, A., Charrière, F., Colomb, T., Montfort, F., Kühn, J., Marquet, P., and Depeursinge, C. (2007). On the complex three-dimensional amplitude point spread function of lenses and microscope objectives: theoretical aspects, simulations and measurements by digital holography. *J. Microsc. 225*, 156–169.
- Masgrau, R., Churchill, G.C., Morgan, A.J., Ashcroft, S.J.H., and Galione, A. (2003). NAADP: a new second messenger for glucose-induced Ca^{2+} responses in clonal pancreatic beta cells. *Curr. Biol. CB 13*, 247–251.
- McCarl, C.-A., Picard, C., Khalil, S., Kawasaki, T., Röther, J., Papolos, A., Kutok, J., Hivroz, C., LeDeist, F., Plogmann, K., et al. (2009). ORAI1 deficiency and lack of store-operated Ca^{2+} entry cause immunodeficiency, myopathy and ectodermal dysplasia. *J. Allergy Clin. Immunol. 124*, 1311–1318.e7.
- McCarl, C.-A., Khalil, S., Ma, J., Oh-hora, M., Yamashita, M., Roether, J., Kawasaki, T., Jairaman, A., Sasaki, Y., Prakriya, M., et al. (2010). Store-Operated Ca^{2+} Entry through ORAI1 Is Critical for T Cell-Mediated Autoimmunity and Allograft Rejection. *J. Immunol. 185*, 5845–5858.
- McNally, J.G., Preza, C., Conchello, J.A., and Thomas, L.J. (1994). Artifacts in compu-

- tational optical-sectioning microscopy. *J. Opt. Soc. Am. A Opt. Image Sci. Vis.* *11*, 1056–1067.
- Melzer, N., Hicking, G., Göbel, K., and Wiendl, H. (2012). TRPM2 cation channels modulate T cell effector functions and contribute to autoimmune CNS inflammation. *PLoS One* *7*, e47617.
- Mignen, O., Thompson, J.L., and Shuttleworth, T.J. (2008). Orail subunit stoichiometry of the mammalian CRAC channel pore. *J. Physiol.* *586*, 419–425.
- Mikoshiya, K., Furuichi, T., and Miyawaki, A. (1994). Structure and function of IP₃ receptors. *Semin. Cell Biol.* *5*, 273–281.
- Minta, A., Kao, J.P., and Tsien, R.Y. (1989). Fluorescent indicators for cytosolic calcium based on rhodamine and fluorescein chromophores. *J. Biol. Chem.* *264*, 8171–8178.
- Mitchell, K.J., Lai, F.A., and Rutter, G.A. (2003). Ryanodine Receptor Type I and Nicotinic Acid Adenine Dinucleotide Phosphate Receptors Mediate Ca²⁺ Release from Insulin-containing Vesicles in Living Pancreatic β-Cells (MIN6). *J. Biol. Chem.* *278*, 11057–11064.
- Miyawaki, A., Llopis, J., Heim, R., McCaffery, J.M., Adams, J.A., Ikura, M., and Tsien, R.Y. (1997). Fluorescent indicators for Ca²⁺ based on green fluorescent proteins and calmodulin. *Nature* *388*, 882–887.
- Mojzisoová, A., Krizanová, O., Záciková, L., Komínková, V., and Ondrias, K. (2001). Effect of nicotinic acid adenine dinucleotide phosphate on ryanodine calcium release channel in heart. *Pflüg. Arch. Eur. J. Physiol.* *441*, 674–677.
- Monks, C.R.F., Freiberg, B.A., Kupfer, H., Sciaky, N., and Kupfer, A. (1998). Three-dimensional segregation of supramolecular activation clusters in T cells. *Nature* *395*, 82–86.
- Morgan, A.J., Platt, F.M., Lloyd-Evans, E., and Galione, A. (2011). Molecular mechanisms of endolysosomal Ca²⁺ signalling in health and disease. *Biochem. J.* *439*, 349–374.
- Morgan, A.J., Davis, L.C., and Galione, A. (2015). Chapter 9 - Imaging approaches to measuring lysosomal calcium. In *Methods in Cell Biology*, F.P. and N. Platt, ed. (Academic Press), pp. 159–195.
- Muik, M., Frischauf, I., Derler, I., Fahrner, M., Bergsmann, J., Eder, P., Schindl, R., Hesch, C., Polzinger, B., Fritsch, R., et al. (2008). Dynamic Coupling of the Putative Coiled-coil Domain of ORAI1 with STIM1 Mediates ORAI1 Channel Activation. *J. Biol. Chem.* *283*, 8014–8022.
- Nagamine, K., Kudoh, J., Minoshima, S., Kawasaki, K., Asakawa, S., Ito, F., and

- Shimizu, N. (1998). Molecular cloning of a novel putative Ca^{2+} channel protein (TRPC7) highly expressed in brain. *Genomics* *54*, 124–131.
- Nieuwenhuizen, R.P.J., Lidke, K.A., Bates, M., Puig, D.L., Grünwald, D., Stallinga, S., and Rieger, B. (2013). Measuring image resolution in optical nanoscopy. *Nat. Methods* *10*, 557–562.
- Niggli, E. (1999). Localized intracellular Calcium signaling in muscle: Calcium Sparks and Calcium Quarks. *Annu. Rev. Physiol.* *61*, 311–335.
- Nikolaev, V.O., Bünemann, M., Hein, L., Hannawacker, A., and Lohse, M.J. (2004). Novel Single Chain cAMP Sensors for Receptor-induced Signal Propagation. *J. Biol. Chem.* *279*, 37215–37218.
- O’Connell, P.J., Klyachko, V.A., and Ahern, G.P. (2002). Identification of functional type 1 ryanodine receptors in mouse dendritic cells. *FEBS Lett.* *512*, 67–70.
- Oda, S., Uchida, K., Wang, X., Lee, J., Shimada, Y., Tominaga, M., and Kadowaki, M. (2013). TRPM2 contributes to antigen-stimulated Ca^{2+} influx in mucosal mast cells. *Pflüg. Arch. Eur. J. Physiol.* *465*, 1023–1030.
- Oh-hora, M., Yamashita, M., Hogan, P.G., Sharma, S., Lamperti, E., Chung, W., Prakriya, M., Feske, S., and Rao, A. (2008). Dual functions for the endoplasmic reticulum calcium sensors STIM1 and STIM2 in T cell activation and tolerance. *Nat. Immunol.* *9*, 432–443.
- Olah, M.E., Jackson, M.F., Li, H., Perez, Y., Sun, H.-S., Kiyonaka, S., Mori, Y., Tymianski, M., and MacDonald, J.F. (2009). Ca^{2+} -dependent induction of TRPM2 currents in hippocampal neurons. *J. Physiol.* *587*, 965–979.
- von Osten, M. (2015). Ryanodine receptors in experimental autoimmune encephalomyelitis, an animal model of multiple sclerosis.
- Parker, I., and Yao, Y. (1996). Ca^{2+} transients associated with openings of inositol trisphosphate-gated channels in *Xenopus* oocytes. *J. Physiol.* *491*, 663–668.
- Parker, I., Choi, J., and Yao, Y. (1996). Elementary events of InsP_3 -induced Ca^{2+} liberation in *Xenopus* oocytes: hot spots, puffs and blips. *Cell Calcium* *20*, 105–121.
- Patel, S. (2015). Function and dysfunction of two-pore channels. *Sci. Signal.* *8*, re7.
- Penna, A., Demuro, A., Yeromin, A.V., Zhang, S.L., Safrina, O., Parker, I., and Cahalan, M.D. (2008). The CRAC channel consists of a tetramer formed by Stim-induced dimerization of Orai dimers. *Nature* *456*, 116–120.
- Perraud, A.L., Fleig, A., Dunn, C.A., Bagley, L.A., Launay, P., Schmitz, C., Stokes, A.J., Zhu, Q., Bessman, M.J., Penner, R., et al. (2001). ADP-ribose gating of the calcium-permeable LTRPC2 channel revealed by Nudix motif homology. *Nature* *411*, 595–

599.

Perraud, A.-L., Shen, B., Dunn, C.A., Rippe, K., Smith, M.K., Bessman, M.J., Stoddard, B.L., and Scharenberg, A.M. (2003). NUDT9, a member of the Nudix hydrolase family, is an evolutionarily conserved mitochondrial ADP-ribose pyrophosphatase. *J Biol Chem* 278, 1794–1801.

Pinton, P., Pozzan, T., and Rizzuto, R. (1998). The Golgi apparatus is an inositol 1,4,5-trisphosphate-sensitive Ca^{2+} store, with functional properties distinct from those of the endoplasmic reticulum. *EMBO J.* 17, 5298–5308.

Pitt, S.J., Lam, A.K.M., Rietdorf, K., Galione, A., and Sitsapesan, R. (2014). Reconstituted Human TPC1 Is a Proton-Permeable Ion Channel and Is Activated by NAADP or Ca^{2+} . *Sci. Signal.* 7, ra46–ra46.

Pozzan, T., Magalhães, P., and Rizzuto, R. (2000). The comeback of mitochondria to calcium signalling. *Cell Calcium* 28, 279–283.

Prakriya, M., and Lewis, R.S. (2015). Store-Operated Calcium Channels. *Physiol. Rev.* 95, 1383–1436.

Prakriya, M., Feske, S., Gwack, Y., Srikanth, S., Rao, A., and Hogan, P.G. (2006). Orai1 is an essential pore subunit of the CRAC channel. *Nature* 443, 230–233.

Quintana, A., Pasche, M., Junker, C., Al-Ansary, D., Rieger, H., Kummerow, C., Nuñez, L., Villalobos, C., Meraner, P., Becherer, U., et al. (2011). Calcium microdomains at the immunological synapse: how ORAI channels, mitochondria and calcium pumps generate local calcium signals for efficient T-cell activation: Calcium microdomains at the immunological synapse. *EMBO J.* 30, 3895–3912.

Rah, S.-Y., Mushtaq, M., Nam, T.-S., Kim, S.H., and Kim, U.-H. (2010). Generation of cyclic ADP-ribose and nicotinic acid adenine dinucleotide phosphate by CD38 for Ca^{2+} signaling in interleukin-8-treated lymphokine-activated killer cells. *J. Biol. Chem.* 285, 21877–21887.

Richardson, W.H. (1972). Bayesian-Based Iterative Method of Image Restoration*. *J. Opt. Soc. Am.* 62, 55.

Rietdorf, K., Funnell, T.M., Ruas, M., Heinemann, J., Parrington, J., and Galione, A. (2011). Two-pore Channels Form Homo- and Heterodimers♦. *J. Biol. Chem.* 286, 37058–37062.

Roedding, A.S., Gao, A.F., Au-Yeung, W., Scarcelli, T., Li, P.P., and Warsh, J.J. (2012). Effect of oxidative stress on TRPM2 and TRPC3 channels in B lymphoblast cells in bipolar disorder. *Bipolar Disord.* 14, 151–161.

Roedding, A.S., Tong, S.Y., Au-Yeung, W., Li, P.P., and Warsh, J.J. (2013). Chronic

oxidative stress modulates TRPC3 and TRPM2 channel expression and function in rat primary cortical neurons: relevance to the pathophysiology of bipolar disorder. *Brain Res.* 1517, 16–27.

Roos, J., DiGregorio, P.J., Yeromin, A.V., Ohlsen, K., Lioudyno, M., Zhang, S., Safirina, O., Kozak, J.A., Wagner, S.L., Cahalan, M.D., et al. (2005). STIM1, an essential and conserved component of store-operated Ca^{2+} channel function. *J. Cell Biol.* 169, 435–445.

Rossi, D., and Sorrentino, V. (2002). Molecular genetics of ryanodine receptors Ca^{2+} -release channels. *Cell Calcium* 32, 307–319.

Rossy, J., Owen, D.M., Williamson, D.J., Yang, Z., and Gaus, K. (2013). Conformational states of the kinase Lck regulate clustering in early T cell signaling. *Nat. Immunol.* 14, 82–89.

Ruas, M., Rietdorf, K., Arredouani, A., Davis, L.C., Lloyd-Evans, E., Koegel, H., Funnell, T.M., Morgan, A.J., Ward, J.A., Watanabe, K., et al. (2010). Purified TPC isoforms form NAADP receptors with distinct roles for Ca^{2+} signaling and endolysosomal trafficking. *Curr. Biol.* CB 20, 703–709.

Ruas, M., Davis, L.C., Chen, C.-C., Morgan, A.J., Chuang, K.-T., Walseth, T.F., Grimm, C., Garnham, C., Powell, T., Platt, N., et al. (2015). Expression of Ca^{2+} -permeable two-pore channels rescues NAADP signalling in TPC-deficient cells. *EMBO J.* e201490009.

Safinia, N., Scotta, C., Vaikunthanathan, T., Lechler, R.I., and Lombardi, G. (2015). Regulatory T cells: serious contenders in the promise for immunological tolerance in transplantation. *Immunol. Toler.* 438.

Samelson, L.E. (2002). SIGNAL TRANSDUCTION MEDIATED BY THE T CELL ANTIGEN RECEPTOR: The Role of Adapter Proteins. *Annu. Rev. Immunol.* 20, 371–394.

Sano, Y., Inamura, K., Miyake, A., Mochizuki, S., Yokoi, H., Matsushime, H., and Furuichi, K. (2001). Immunocyte Ca^{2+} influx system mediated by LTRPC2. *Science* 293, 1327–1330.

Scheenen, W.J., Makings, L.R., Gross, L.R., Pozzan, T., and Tsien, R.Y. (1996). Photodegradation of indo-1 and its effect on apparent Ca^{2+} concentrations. *Chem. Biol.* 3, 765–774.

Schetelig, D., Wolf, I.M.A., Diercks, B.-P., Fliegert, R., Guse, A.H., Schlaefter, A., and Werner, R. (2015). A Modular Framework for Post-Processing and Analysis of Fluorescence Microscopy Image Sequences of Subcellular Calcium Dynamics. In *Bildver-*

arbeitung Für Die Medizin 2015, H. Handels, T.M. Deserno, H.-P. Meinzer, and T. Tolxdorff, eds. (Springer Berlin Heidelberg), pp. 401–406.

Schild, D., Jung, A., and Schultens, H.A. (1994). Localization of calcium entry through calcium channels in olfactory receptor neurones using a laser scanning microscope and the calcium indicator dyes Fluo-3 and Fura-Red. *Cell Calcium* 15, 341–348.

Schindelin, J., Arganda-Carreras, I., Frise, E., Kaynig, V., Longair, M., Pietzsch, T., Preibisch, S., Rueden, C., Saalfeld, S., Schmid, B., et al. (2012). Fiji: an open-source platform for biological-image analysis. *Nat. Methods* 9, 676–682.

Schmid, F., Bruhn, S., Weber, K., Mittrücker, H.-W., and Guse, A.H. (2011). CD38: a NAADP degrading enzyme. *FEBS Lett.* 585, 3544–3548.

Schmid, F., Fliegert, R., Westphal, T., Bauche, A., and Guse, A.H. (2012). Nicotinic acid adenine dinucleotide phosphate (NAADP) degradation by alkaline phosphatase. *J. Biol. Chem.* 287, 32525–32534.

Schuber, F., and Lund, F. (2004). Structure and Enzymology of ADP-ribosyl Cyclases: Conserved Enzymes that Produce Multiple Calcium Mobilizing Metabolites. *Curr. Mol. Med.* 4, 249–261.

Schwarz, E.C., Kummerow, C., Wenning, A.S., Wagner, K., Sappok, A., Waggershauer, K., Griesemer, D., Strauss, B., Wolfs, M.-J., Quintana, A., et al. (2007). Calcium dependence of T cell proliferation following focal stimulation. *Eur. J. Immunol.* 37, 2723–2733.

Schwarzmann, N., Kunerth, S., Weber, K., Mayr, G.W., and Guse, A.H. (2002). Knock-down of the type 3 ryanodine receptor impairs sustained Ca^{2+} signaling via the T cell receptor/CD3 complex. *J. Biol. Chem.* 277, 50636–50642.

Schwindling, C., Quintana, A., Krause, E., and Hoth, M. (2010). Mitochondria Positioning Controls Local Calcium Influx in T Cells. *J. Immunol.* 184, 184–190.

Sedarat, F., Lin, E., Moore, E.D.W., and Tibbits, G.F. (2004). Deconvolution of confocal images of dihydropyridine and ryanodine receptors in developing cardiomyocytes. *J. Appl. Physiol.* 97, 1098–1103.

Sei, Y., Gallagher, K.L., and Basile, A.S. (1999). Skeletal Muscle Type Ryanodine Receptor Is Involved in Calcium Signaling in Human B Lymphocytes. *J. Biol. Chem.* 274, 5995–6002.

Shaw, P.J., and Feske, S. (2012). Regulation of lymphocyte function by ORAI and STIM proteins in infection and autoimmunity. *J. Physiol.* 590, 4157–4167.

Shaw, P.J., Qu, B., Hoth, M., and Feske, S. (2013). Molecular regulation of CRAC channels and their role in lymphocyte function. *Cell. Mol. Life Sci. CMLS* 70, 2637–

2656.

Sherwood, M.W., Prior, I.A., Voronina, S.G., Barrow, S.L., Woodsmith, J.D., Gerasimenko, O.V., Petersen, O.H., and Tepikin, A.V. (2007). Activation of trypsinogen in large endocytic vacuoles of pancreatic acinar cells. *Proc. Natl. Acad. Sci.* *104*, 5674–5679.

Shkryl, V.M., and Blatter, L.A. (2013). Ca^{2+} Release Events in Cardiac Myocytes Up Close: Insights from Fast Confocal Imaging. *PLoS ONE* *8*, e61525.

Shrivastava, A., and Gupta, V. (2011). Methods for the determination of limit of detection and limit of quantitation of the analytical methods. *Chron. Young Sci.* *2*, 21.

Shuttleworth, T.J. (2012). Orai3 – the “exceptional” Orai? *J. Physiol.* *590*, 241–257.

Sibarita, J.-B. (2005). Deconvolution microscopy. *Adv. Biochem. Eng. Biotechnol.* *95*, 201–243.

da Silva, C.P., Schweitzer, K., Heyer, P., Malavasi, F., Mayr, G.W., and Guse, A.H. (1998). Ectocellular CD38-catalyzed synthesis and intracellular Ca^{2+} -signalling activity of cyclic ADP-ribose in T-lymphocytes are not functionally related. *FEBS Lett.* *439*, 291–296.

Slaugenhaupt, S.A. (2002). The molecular basis of mucopolidosis type IV. *Curr. Mol. Med.* *2*, 445–450.

Smith, I.F., and Parker, I. (2009). Imaging the quantal substructure of single IP_3R channel activity during Ca^{2+} puffs in intact mammalian cells. *Proc. Natl. Acad. Sci.* *106*, 6404–6409.

Smyth, J.W., and Shaw, R.M. (2008). Visualizing Ion Channel Dynamics at the Plasma Membrane. *Heart Rhythm Off. J. Heart Rhythm Soc.* *5*, S7–S11.

Smyth, J.T., DeHaven, W.I., Bird, G.S., and Putney, J.W. (2008). Ca^{2+} -store-dependent and -independent reversal of Stim1 localization and function. *J Cell Sci* *121*, 762–772.

Soares, S., Thompson, M., White, T., Isbell, A., Yamasaki, M., Prakash, Y., Lund, F.E., Galione, A., and Chini, E.N. (2007). NAADP as a second messenger: neither CD38 nor base-exchange reaction are necessary for in vivo generation of NAADP in myometrial cells. *Am. J. Physiol. Cell Physiol.* *292*, C227–C239.

Soboloff, J., Spassova, M.A., Hewavitharana, T., He, L.-P., Xu, W., Johnstone, L.S., Dziadek, M.A., and Gill, D.L. (2006). STIM2 Is an Inhibitor of STIM1-Mediated Store-Operated Ca^{2+} Entry. *Curr. Biol.* *16*, 1465–1470.

Soboloff, J., Rothberg, B.S., Madesh, M., and Gill, D.L. (2012). STIM proteins: dynamic calcium signal transducers. *Nat. Rev. Mol. Cell Biol.* *13*, 549–565.

- Song, E.-K., Lee, Y.-R., Kim, Y.-R., Yeom, J.-H., Yoo, C.-H., Kim, H.-K., Park, H.-M., Kang, H.-S., Kim, J.-S., Kim, U.-H., et al. (2012). NAADP mediates insulin-stimulated glucose uptake and insulin sensitization by PPAR γ in adipocytes. *Cell Rep.* 2, 1607–1619.
- Sonkusare, S.K., Bonev, A.D., Ledoux, J., Liedtke, W., Kotlikoff, M.I., Heppner, T.J., Hill-Eubanks, D.C., and Nelson, M.T. (2012). Elementary Ca²⁺ signals through endothelial TRPV4 channels regulate vascular function. *Science* 336, 597–601.
- Srikanth, S., and Gwack, Y. (2013). Orai1-NFAT Signalling Pathway Triggered by T Cell Receptor Stimulation. *Mol. Cells* 35, 182–194.
- Stathopoulos, P.B., Li, G.-Y., Plevin, M.J., Ames, J.B., and Ikura, M. (2006). Stored Ca²⁺ Depletion-induced Oligomerization of Stromal Interaction Molecule 1 (STIM1) via the EF-SAM Region AN INITIATION MECHANISM FOR CAPACITIVE Ca²⁺ ENTRY. *J. Biol. Chem.* 281, 35855–35862.
- Stathopoulos, P.B., Zheng, L., Li, G.-Y., Plevin, M.J., and Ikura, M. (2008). Structural and Mechanistic Insights into STIM1-Mediated Initiation of Store-Operated Calcium Entry. *Cell* 135, 110–122.
- Streb, H., Irvine, R.F., Berridge, M.J., and Schulz, I. (1983). Release of Ca²⁺ from a nonmitochondrial intracellular store in pancreatic acinar cells by inositol-1,4,5-trisphosphate. *Nature* 306, 67–69.
- Sumoza-Toledo, A., Lange, I., Cortado, H., Bhagat, H., Mori, Y., Fleig, A., Penner, R., and Partida-Sánchez, S. (2011). Dendritic cell maturation and chemotaxis is regulated by TRPM2-mediated lysosomal Ca²⁺ release. *FASEB J.* 25, 3529–3542.
- Sun, M., Goldin, E., Stahl, S., Falardeau, J.L., Kennedy, J.C., Acierno, J.S., Bove, C., Kaniski, C.R., Nagle, J., Bromley, M.C., et al. (2000). Mucopolipidosis type IV is caused by mutations in a gene encoding a novel transient receptor potential channel. *Hum. Mol. Genet.* 9, 2471–2478.
- Swedlow, J.R., and Platani, M. (2002). Live cell imaging using wide-field microscopy and deconvolution. *Cell Struct. Funct.* 27, 335–341.
- Tallini, Y.N., Ohkura, M., Choi, B.-R., Ji, G., Imoto, K., Doran, R., Lee, J., Plan, P., Wilson, J., Xin, H.-B., et al. (2006). Imaging cellular signals in the heart in vivo: Cardiac expression of the high-signal Ca²⁺ indicator GCaMP2. *Proc. Natl. Acad. Sci. U. S. A.* 103, 4753–4758.
- Taylor, C.W., and Konieczny, V. (2016). IP₃ receptors: Take four IP₃ to open. *Sci. Signal.* 9, pe1.
- Taylor, C.W., Genazzani, A.A., and Morris, S.A. (1999). Expression of inositol trisphosphate receptors. *Cell Calcium* 26, 237–251.

- Thakur, P., Dadsetan, S., and Fomina, A.F. (2012). Bidirectional Coupling between Ryanodine Receptors and Ca²⁺ Release-activated Ca²⁺ (CRAC) Channel Machinery Sustains Store-operated Ca²⁺ Entry in Human T Lymphocytes. *J. Biol. Chem.* *287*, 37233–37244.
- Thomas, D., Tovey, S.C., Collins, T.J., Bootman, M.D., Berridge, M.J., and Lipp, P. (2000). A comparison of fluorescent Ca²⁺ indicator properties and their use in measuring elementary and global Ca²⁺ signals. *Cell Calcium* *28*, 213–223.
- Tóth, B., and Csanády, L. (2010). Identification of direct and indirect effectors of the transient receptor potential melastatin 2 (TRPM2) cation channel. *J. Biol. Chem.* *285*, 30091–30102.
- Toth, B., Iordanov, I., and Csanady, L. (2015). Ruling out pyridine dinucleotides as true TRPM2 channel activators reveals novel direct agonist ADP-ribose-2'-phosphate. *J. Gen. Physiol.* *145*, 419–430.
- Tovey, S.C., de Smet, P., Lipp, P., Thomas, D., Young, K.W., Missiaen, L., De Smedt, H., Parys, J.B., Berridge, M.J., Thuring, J., et al. (2001). Calcium puffs are generic InsP(3)-activated elementary calcium signals and are downregulated by prolonged hormonal stimulation to inhibit cellular calcium responses. *J. Cell Sci.* *114*, 3979–3989.
- Toyoshima, C., and Nomura, H. (2002). Structural changes in the calcium pump accompanying the dissociation of calcium. *Nature* *418*, 605–611.
- Toyoshima, C., Nakasako, M., Nomura, H., and Ogawa, H. (2000). Crystal structure of the calcium pump of sarcoplasmic reticulum at 2.6 [[angst]] resolution. *Nature* *405*, 647–655.
- Tsien, R.Y. (1981). A non-disruptive technique for loading calcium buffers and indicators into cells. *Nature* *290*, 527–528.
- Tu, H., Wang, Z., and Bezprozvanny, I. (2005). Modulation of Mammalian Inositol 1,4,5-Trisphosphate Receptor Isoforms by Calcium: A Role of Calcium Sensor Region. *Biophys. J.* *88*, 1056–1069.
- Tugba Durlu-Kandilci, N., Ruas, M., Chuang, K.-T., Brading, A., Parrington, J., and Galione, A. (2010). TPC2 proteins mediate nicotinic acid adenine dinucleotide phosphate (NAADP)- and agonist-evoked contractions of smooth muscle. *J. Biol. Chem.* *285*, 24925–24932.
- Venkatachalam, K., Hofmann, T., and Montell, C. (2006). Lysosomal localization of TRPML3 depends on TRPML2 and the mucopolidiosis-associated protein TRPML1. *J. Biol. Chem.* *281*, 17517–17527.
- Venugopal, B., Browning, M.F., Curcio-Morelli, C., Varro, A., Michaud, N., Nant-hakumar, N., Walkley, S.U., Pickel, J., and Slaughaupt, S.A. (2007). Neurologic,

- Gastric, and Ophthalmologic Pathologies in a Murine Model of Mucopolysaccharidosis Type IV. *Am. J. Hum. Genet.* *81*, 1070–1083.
- Vicente, N.B., Zamboni, J.E.D., Adur, J.F., Paravani, E.V., and Casco, V.H. (2007). Photobleaching correction in fluorescence microscopy images. *J. Phys. Conf. Ser.* *90*, 012068.
- Vig, M., Peinelt, C., Beck, A., Koomoa, D.L., Rabah, D., Koblan-Huberson, M., Kraft, S., Turner, H., Fleig, A., Penner, R., et al. (2006). CRACM1 is a plasma membrane protein essential for store-operated Ca^{2+} entry. *Science* *312*, 1220–1223.
- Vig, M., DeHaven, W.I., Bird, G.S., Billingsley, J.M., Wang, H., Rao, P.E., Hutchings, A.B., Jouvin, M.-H., Putney, J.W., and Kinet, J.-P. (2008). Defective mast cell effector functions in mice lacking the CRACM1 pore subunit of store-operated calcium release-activated calcium channels. *Nat. Immunol.* *9*, 89–96.
- Wallace, W., Schaefer, L.H., and Swedlow, J.R. (2001). A workingperson's guide to deconvolution in light microscopy. *BioTechniques* *31*, 1076–1078, 1080, 1082 passim.
- Wang, Y. (2003). Computational Restoration of Fluorescence Images: Noise Reduction, Deconvolution, and Pattern Recognition. B.-M. in *C. Biology*, ed. (Academic Press), pp. 435–445.
- Wang, C.M., Ploia, C., Anselmi, F., Sarukhan, A., and Viola, A. (2014a). Adenosine triphosphate acts as a paracrine signaling molecule to reduce the motility of T cells. *EMBO J.* *33*, 1354–1364.
- Wang, X., Zhang, X., Dong, X.-P., Samie, M., Li, X., Cheng, X., Goschka, A., Shen, D., Zhou, Y., Harlow, J., et al. (2012). TPC proteins are phosphoinositide-activated sodium-selective ion channels in endosomes and lysosomes. *Cell* *151*, 372–383.
- Wang, X., Wang, Y., Zhou, Y., Hendron, E., Mancarella, S., Andrade, M.D., Rothberg, B.S., Soboloff, J., and Gill, D.L. (2014b). Distinct Orai-coupling domains in STIM1 and STIM2 define the Orai-activating site. *Nat. Commun.* *5*, 3183.
- Wang, Z., Tymianski, M., Jones, O.T., and Nedergaard, M. (1997). Impact of Cytoplasmic Calcium Buffering on the Spatial and Temporal Characteristics of Intercellular Calcium Signals in Astrocytes. *J. Neurosci.* *17*, 7359–7371.
- Wei, S.H., Safrina, O., Yu, Y., Garrod, K.R., Cahalan, M.D., and Parker, I. (2007). Ca^{2+} Signals in CD4^+ T Cells during Early Contacts with Antigen-Bearing Dendritic Cells in Lymph Node. *J. Immunol.* *179*, 1586–1594.
- Weisleder, N., Zhou, J., and Ma, J. (2012). Detection of calcium sparks in intact and permeabilized skeletal muscle fibers. *Methods Mol. Biol. Clifton NJ* *798*, 395–410.

- Wekerle, H., Kojima, K., Lannes-Vieira, J., Lassmann, H., and Linington, C. (1994). Animal models. *Ann. Neurol.* *36 Suppl*, S47–S53.
- Wenning, A.S., Neblung, K., Strauß, B., Wolfs, M.-J., Sappok, A., Hoth, M., and Schwarz, E.C. (2011). TRP expression pattern and the functional importance of TRPC3 in primary human T-cells. *Biochim. Biophys. Acta BBA - Mol. Cell Res.* *1813*, 412–423.
- Williams, R.T., Manji, S.S., Parker, N.J., Hancock, M.S., Van Stekelenburg, L., Eid, J.P., Senior, P.V., Kazenwadel, J.S., Shandala, T., Saint, R., et al. (2001). Identification and characterization of the STIM (stromal interaction molecule) gene family: coding for a novel class of transmembrane proteins. *Biochem. J.* *357*, 673–685.
- Wojcikiewicz, R.J., and He, Y. (1995). Type I, II and III inositol 1,4,5-trisphosphate receptor co-immunoprecipitation as evidence for the existence of heterotetrameric receptor complexes. *Biochem. Biophys. Res. Commun.* *213*, 334–341.
- Wolf, I.M.A., Diercks, B.-P., Gattkowsky, E., Czarniak, F., Kempinski, J., Werner, R., Schetelig, D., Mittrücker, H.-W., Schumacher, V., Osten, M. von, et al. (2015). Frontrunners of T cell activation: Initial, localized Ca²⁺ signals mediated by NAADP and the type 1 ryanodine receptor. *Sci Signal* *8*, ra102–ra102.
- Xiong, L., Zhang, J.-Z., He, R., and Hamilton, S.L. (2006). A Ca²⁺-Binding Domain in RyR1 that Interacts with the Calmodulin Binding Site and Modulates Channel Activity. *Biophys. J.* *90*, 173–182.
- Xu, H., Delling, M., Li, L., Dong, X., and Clapham, D.E. (2007). Activating mutation in a mucolipin transient receptor potential channel leads to melanocyte loss in varitint-waddler mice. *Proc. Natl. Acad. Sci. U. S. A.* *104*, 18321–18326.
- Yamada, M., Mizuguchi, M., Otsuka, N., Ikeda, K., and Takahashi, H. (1997). Ultrastructural localization of CD38 immunoreactivity in rat brain. *Brain Res.* *756*, 52–60.
- Yamaguchi, S., Jha, A., Li, Q., Soyombo, A.A., Dickinson, G.D., Churamani, D., Braioliu, E., Patel, S., and Muallem, S. (2011). Transient Receptor Potential Mucolipin 1 (TRPML1) and Two-pore Channels Are Functionally Independent Organellar Ion Channels. *J. Biol. Chem.* *286*, 22934–22942.
- Yamamoto, S., Shimizu, S., Kiyonaka, S., Takahashi, N., Wajima, T., Hara, Y., Negoro, T., Hiroi, T., Kiuchi, Y., Okada, T., et al. (2008). TRPM2-mediated Ca²⁺ influx induces chemokine production in monocytes that aggravates inflammatory neutrophil infiltration. *Nat Med* *14*, 738–747.
- Yamasaki, M., Thomas, J.M., Churchill, G.C., Garnham, C., Lewis, A.M., Cancela, J.-M., Patel, S., and Galione, A. (2005). Role of NAADP and cADPR in the induction and maintenance of agonist-evoked Ca²⁺ spiking in mouse pancreatic acinar cells. *Curr. Bi-*

ol. *CB 15*, 874–878.

Yáñez, M., Gil-Longo, J., and Campos-Toimil, M. (2012). Calcium binding proteins. *Adv. Exp. Med. Biol.* *740*, 461–482.

Yang, X., Jin, H., Cai, X., Li, S., and Shen, Y. (2012). Structural and mechanistic insights into the activation of Stromal interaction molecule 1 (STIM1). *Proc. Natl. Acad. Sci. U. S. A.* *109*, 5657–5662.

Yeromin, A.V., Zhang, S.L., Jiang, W., Yu, Y., Safrina, O., and Cahalan, M.D. (2006). Molecular identification of the CRAC channel by altered ion selectivity in a mutant of Orai. *Nature* *443*, 226–229.

Yuan, J.P., Zeng, W., Dorwart, M.R., Choi, Y.-J., Worley, P.F., and Muallem, S. (2009). SOAR and the polybasic STIM1 domains gate and regulate Orai channels. *Nat. Cell Biol.* *11*, 337–343.

Zalk, R., Lehnart, S.E., and Marks, A.R. (2007). Modulation of the Ryanodine Receptor and Intracellular Calcium. *Annu. Rev. Biochem.* *76*, 367–385.

Zalk, R., Clarke, O.B., des Georges, A., Grassucci, R.A., Reiken, S., Mancina, F., Hendrickson, W.A., Frank, J., and Marks, A.R. (2015). Structure of a mammalian ryanodine receptor. *Nature* *517*, 44–49.

Zeevi, D.A., Frumkin, A., Offen-Glasner, V., Kogot-Levin, A., and Bach, G. (2009). A potentially dynamic lysosomal role for the endogenous TRPML proteins. *J. Pathol.* *219*, 153–162.

Zhang, F., and Li, P.-L. (2007). Reconstitution and characterization of a nicotinic acid adenine dinucleotide phosphate (NAADP)-sensitive Ca^{2+} release channel from liver lysosomes of rats. *J. Biol. Chem.* *282*, 25259–25269.

Zhang, F., Jin, S., Yi, F., and Li, P.-L. (2009). TRP-ML1 functions as a lysosomal NAADP-sensitive Ca^{2+} release channel in coronary arterial myocytes. *J. Cell. Mol. Med.* *13*, 3174–3185.

Zhang, F., Xu, M., Han, W.-Q., and Li, P.-L. (2011). Reconstitution of lysosomal NAADP-TRP-ML1 signaling pathway and its function in TRP-ML1^{-/-} cells. *Am. J. Physiol. - Cell Physiol.* *301*, C421–C430.

Zhang, G.Q., Wei, H., Lu, J., Wong, P., and Shim, W. (2013). Identification and Characterization of Calcium Sparks in Cardiomyocytes Derived from Human Induced Pluripotent Stem Cells. *PLoS ONE* *8*, e55266.

Zhang, S.L., Yeromin, A.V., Zhang, X.H.-F., Yu, Y., Safrina, O., Penna, A., Roos, J., Stauderman, K.A., and Cahalan, M.D. (2006). Genome-wide RNAi screen of Ca^{2+} influx identifies genes that regulate Ca^{2+} release-activated Ca^{2+} channel activity. *Proc.*

Natl. Acad. Sci. *103*, 9357–9362.

Zhao, Y.J., Lam, C.M.C., and Lee, H.C. (2012). The membrane-bound enzyme CD38 exists in two opposing orientations. *Sci. Signal.* *5*, ra67.

Zheng, L., Stathopoulos, P.B., Li, G.-Y., and Ikura, M. (2008). Biophysical characterization of the EF-hand and SAM domain containing Ca^{2+} sensory region of STIM1 and STIM2. *Biochem. Biophys. Res. Commun.* *369*, 240–246.

Zhou, Y., Ramachandran, S., Oh-hora, M., Rao, A., and Hogan, P.G. (2010). Pore architecture of the ORAI1 store-operated calcium channel. *Proc. Natl. Acad. Sci. U. S. A.* *107*, 4896–4901.

Zong, X., Schieder, M., Cuny, H., Fenske, S., Gruner, C., Rötzer, K., Griesbeck, O., Harz, H., Biel, M., and Wahl-Schott, C. (2009). The two-pore channel TPCN2 mediates NAADP-dependent Ca^{2+} -release from lysosomal stores. *Pflüg. Arch. Eur. J. Physiol.* *458*, 891–899.

Zweifach, A., and Lewis, R.S. (1995). Rapid inactivation of depletion-activated calcium current (ICRAC) due to local calcium feedback. *J. Gen. Physiol.* *105*, 209–226.

Figure Index

| | |
|---|----|
| FIG. 1 SIMPLIFIED MODEL OF THE INTRACELLULAR SIGNALING PATHWAYS INITIATED AFTER T LYMPHOCYTE ACTIVATION THROUGH THE TCR | 2 |
| FIG. 2 CONCENTRATION OF Ca^{2+} MOBILIZING SECOND MESSENGERS AFTER T LYMPHOCYTE STIMULATION WITH ANTI-CD3 ANTIBODIES (OKT3) | 5 |
| FIG. 3 MODEL OF STIM1 ACTIVATION AND THE ORAI1 COUPLING PROCESS | 8 |
| FIG. 4 ATOMIC STRUCTURE OF NICOTINIC ACID ADENINE DINUCLEOTIDE PHOSPHATE (NAADP) | 10 |
| FIG. 5 MODEL OF PROPOSED NAADP RECEPTORS IN T LYMPHOCYTES | 12 |
| FIG. 6 MODELS OF TPC ACTIVATION | 16 |
| FIG. 7 SCHEMATIC MEMBRANE TOPOLOGY OF TRPM2 | 17 |
| FIG. 8 SCHEMATIC LOADING OF AM ESTERIFIED Ca^{2+} INDICATORS INTO CELLS | 20 |
| FIG. 9 COMPARISON OF THE $[Ca^{2+}]_i$ CALIBRATION FROM JURKAT AND PRIMARY T LYMPHOCYTES USING THE ONE- AND THE DOUBLE-K_D MODEL | 33 |
| FIG. 10 COMPARISON OF THE POST-PROCESSING WORKFLOWS | 37 |
| FIG. 11 IMPACT OF DIFFERENT DECONVOLUTION ALGORITHMS ON IMAGE QUALITY | 40 |
| FIG. 12 COMPARISON OF THE MULTIPLICATIVE AND ADDITIVE BI-EXPONENTIAL BLEACHING CORRECTION OF FURA RED IN WT T LYMPHOCYTES | 41 |
| FIG. 13 COMPARISON OF THE FRAME-BY-FRAME ELEVATION USING ADDITIVE AND MULTIPLICATIVE APPROACHES | 42 |
| FIG. 14 Ca^{2+} MICRODOMAINS IN PRIMARY T LYMPHOCYTES AFTER STIMULATION WITH IGG-COATED BEADS | 46 |
| FIG. 15 INITIAL Ca^{2+} MICRODOMAINS IN PRIMARY WT AND RYR3-KO T LYMPHOCYTES | 51 |
| FIG. 16 SUMMARY OF THE OBTAINED RESULTS AND OPEN QUESTIONS | 57 |

Publications, awards, talks and poster presentations

Publications

Insa M.A. Wolf*, **Björn-P. Diercks***, Ellen Gattkowsky, Frederik Czarniak, Jan Kemp-ski, René Werner, Daniel Schetelig, Hans-Willi Mittrücker, Valeá Schumacher, Manuel von Osten, Dimitri Lodygin, Alexander Flügel, Andreas Guse 2015 „ Frontrunners of T cell activation: Initial, localized Ca²⁺ signals mediated by NAADP and the type 1 ryanodine receptor“. *Science Signaling* **8** (398), ra102. [doi: 10.1126/scisignal.aab0863].

* These authors contributed equally to this work.

Daniel Schetelig, Insa M.A. Wolf, **Björn-P. Diercks**, Ralf Fliegert, Andreas H. Guse, Alexander Schlaefer, René Werner 2015 „A Modular Framework for Post-Processing and Analysis of Fluorescence Microscopy Image Sequences of Subcellular Calcium Dynamics“. DOI: 10.1007/978-3-662-46224-9_69 Conference: *Bildverarbeitung für die Medizin* 2015, At Lübeck, Volume: Informatik aktuell

Diercks Björn-P., Hauschildt Inga, Stäb Franz, Wenck Horst, Döring Olaf, Peters Nils 2012 „IL-10 Promotes Secretion of S100A8/A) from Human Monocytes Trough an Inclusion in Plasma Membranes“. *Scandinavian Journal of Immunology* 77(2):169-70. doi: 10.1111/sji.12015

Awards

UKE Paper of the Month December 2015

Insa M.A. Wolf*, **Björn-P. Diercks***, Ellen Gattkowsky, Frederik Czarniak, Jan Kemp-ski, René Werner, Daniel Schetelig, Hans-Willi Mittrücker, Valeá Schumacher, Manuel von Osten, Dimitri Lodygin, Alexander Flügel, Andreas Guse 2015 „ Frontrunners of T cell activation: Initial, localized Ca²⁺ signals mediated by NAADP and the type 1 ryanodine receptor“. *Science Signaling* **8** (398), ra102. [doi: 10.1126/scisignal.aab0863].

* These authors contributed equally to this work.

Talks

Björn-P. Diercks, Insa M.A. Wolf, Ellen Gattkowsky, Frederik Czarniak, Jan Kemp-ski, René Werner, Daniel Schetelig, Hans-Willi Mittrücker, Valeá Schumacher, Manuel van Osten, Dimitri Lodygin, Alexander Flügel, Andreas Guse (2015) “Frontrunners of T cell

activation: Initial short-lived localized Ca^{2+} signals". *FASEB Science Research Conference on NAD Metabolism and Signaling* August 09 – 14, Timmendorfer Strand, Germany

Björn-Philipp Diercks (2015) "Subzelluläre Calcium-Signale in der Immunologischen Synapse – Funktion von sekundären Botenstoffen und Calcium-Kanälen". *12. Studententagung Hamburg zur Innovativen Medizin- und Biotechnologie*, 28. April 2015 in Hamburg, Germany

Insa M.A. Wolf, **Björn-Philipp Diercks**, Ellen Gattkowsky, Ralf Fliegert, René Werner, Daniel Schetelig, Manuel von Osten, Alexander Flügel, Andreas H. Guse (2014) „Elementary Ca^{2+} signaling events: contribution of NAADP and RyR“. Meeting of the *Biochemical Society Calcium Signaling: the next generation*, 9. to 10. Oktober 2014 in London, UK

Insa M.A. Wolf, **Björn-Philipp Diercks**, Ellen Gattkowsky, Ralf Fliegert, René Werner, Daniel Schetelig, Manuel von Osten, Stefan Feske, Alexander Flügel, Andreas H. Guse (2014) „Fast subcellular Ca^{2+} signals in T cell signaling“. *13th International Meeting of the European Calcium Society (ECS)*, 13. to 17. September 2014 in Aix-on-Provence, France

Poster presentations

Björn-P. Diercks, Insa M.A. Wolf, Ellen Gattkowsky, Frederik Czarniak, Jan Kempfski, René Werner, Daniel Schetelig, Hans-Willi Mittrücker, Valeá Schumacher, Manuel von Osten, Dimitri Lodygin, Alexander Flügel, Andreas Guse (2015) Frontrunners of T cell activation: Initial, localized Ca^{2+} signals mediated by NAADP and the type 1 ryanodine receptor. *Seeing is Believing – Imaging the Processes of Life*, October 06 – 10, EMBL Heidelberg, Germany

Ellen Gattkowsky, **Björn-Philipp Diercks**, Andreas H. Guse, Insa M.A. Wolf (2014) Analyse subzellulärer Calciumsignale in T-Lymphozyten. *12. Studententagung Hamburg zur Innovativen Medizin- und Biotechnologie*, 28. April 2015 in Hamburg, Germany

Björn-Philipp Diercks, Ralf Fliegert, Daniel Schetelig, Rene Werner, Andreas H. Guse, Insa M.A. Wolf (2014) High-spatio-temporal resolution Ca^{2+} Imaging in T cells during immune synapse formation. *13th International Meeting of the European Calcium Society (ECS)*, 13. to 17. September 2014 in Aix-on-Provence, France

Ellen Gattkowsky, **Björn-Philipp Diercks**, Andreas H. Guse, Insa M.A. Wolf (2014) Analysis of elementary Ca^{2+} signals in T-Lymphocytes evoked by microinjection of NAADP. *13th International Meeting of the European Calcium Society (ECS)*, 13. to 17. September 2014 in Aix-on-Provence, France

Björn-Philipp Diercks, Insa M.A. Wolf, Andreas H. Guse (2013) NAADP Mediated Calcium Signalling and Arrhythmias in the Heart Evoked by β -Adrenergic Stimulation. *43rd Annual Meeting German Society for Immunology (DGfI)*, 11. – 14. September 2013 in Mainz, Germany

Eidesstattliche Versicherung

Name: Diercks

Vorname: Björn-Philipp

Hiermit erkläre ich an Eides statt, dass ich die vorliegende Dissertationsschrift selbst verfasst und keine anderen als die angegebenen Quellen und Hilfsmittel benutzt habe.

Ort, Datum

Unterschrift

Acknowledgment

First of all, my special thanks go to Prof. Dr. Andreas H. Guse for providing the exciting project, his constant enthusiasm and for guiding me throughout the work of this thesis. Furthermore, I gratefully thank Dr. Insa Wolf for the superb supervision, advice and proofreading of my thesis.

I would like to thank Prof. Dr. Arp Schnittger for the evaluation of my thesis on behalf of the Department of Biology.

Special thanks go to Dr. René Werner and Daniel Schetelig for the Matlab implementation of our analysis-workflow (..that saved a hell lot of time!!) and for the always nice meetings.

Moreover, I would like to thank our collaboration partners from the lab of Prof. Alexander Flügel for the provision of RYR-KO T lymphocytes and for teaching me the isolation of primary T lymphocytes.

Furthermore, I would like to thank the whole Calcium Signaling Group for the enjoyable and motivating work environment, but especially Ralf Fliegert, Anette Rosche, Ellen Gattkowski und Jan Kempinski for their support.

Last but not least I would like to thank my Family for the constant support and patience throughout my thesis and particularly Anne, my soul mate, for the never-ending encouragement.